# POST-PUNCHING RESPONSE OF FLAT PLATE SLAB-COLUMN CONNECTIONS

Erin D. Redl



Department of Civil Engineering and Applied Mechanics

McGill University

Montréal, Québec, Canada

February 2009

A thesis submitted to McGill
University in partial fulfilment of the requirements
for the degree of Master of Engineering

© Copyright Redl 2009. All rights reserved.

#### **Abstract**

The post-punching failure response of reinforced concrete flat plate slab-column connections is investigated. The first part of this thesis discusses previous research on the tensile membrane action of reinforced concrete slabs and the use of structural integrity reinforcement to prevent progressive collapse after punching failure of slab-column connections. The second part of this thesis describes the design of a flat plate slab system that is the basis for slab-column connection test specimens. Two specimens were constructed and tested to determine punching failure resistance and post-punching failure resistance. The parameter investigated was the detailing of structural integrity reinforcement.

Observations from testing contributed to the understanding of the post-punching resisting mechanism that developed. Three failure modes observed during testing were the yielding of reinforcing steel, concrete failure similar to the breakout of embedments, and pullout bond failure. The test results were compared to the predicted resistance of structural integrity reinforcement by CSA A23.3-04 (2004). The test specimens achieved 98% and 104% of the predicted resistance. Test results were also used to evaluate the equation proposed by Melo and Regan (1998) for concrete failure similar to the breakout of embedments, and the equation was found to underestimate the post-punching resistance of flat plate slab-column connections.

### Résumé

La réponse après-poinçonnement d'assemblages dalle-poteau de béton armé a été étudiée. Cette thèse constitue de deux parties dont la première discute les recherches précédentes sur l'effet des membranes en traction en plus de l'utilisation d'armature d'intégrité structurale de façon à éviter l'effondrement progressif après avoir subit un poinçonnement en cisaillement d'assemblage dalle-poteau. La deuxième partie décrit la conception d'un système formant d'une dalle plate qui sera la base des modèles d'assemblage dalle-poteau de cette recherche. Deux modèles ont été construits et testés à déterminer la résistance de poinçonnement en cisaillement et la résistance après-poinçonnement pour étudier le paramètre d'armature d'intégrité structurale.

Les résultats expérimentaux obtenus ont contribués aux connaissances du mécanisme de résistance après-poinçonnement et trois modes de rupture ont été observés : le fluage de l'acier, la rupture du béton similaire aux brisures des ancrages, et l'échec du lien de retirement. Les résultats ont été comparés aux prédictions de la résistance d'armature intégrité structurale du CSA A23.3-04 (2004) et les modèles conçus ont obtenus 98% et 104% de la résistance prévue. De plus, ses résultats ont été utilisés pour évaluer l'équation proposée par Melo et Regan (1998) pour la rupture du béton similaire aux brisures des ancrages et cette équation a été déterminée à sous-estimer la résistance après-poinçonnement des assemblages dalle-poteau.

# Acknowledgements

The author would like to give her sincere thanks to Professor Denis Mitchell and to Dr. William Cook for their supervision and guidance, and for sharing their knowledge throughout her graduate studies. For the work completed in the Jamieson Structures Laboratory, the author thanks Ron Sheppard, John Bartczak, Marek Przykorski, and Damien Kiperchuk. Without their generous assistance and technical expertise, this project would not have been possible. Also, thanks go to Lesley Wake, Ting Peng, and most especially Michael Egberts for the hard and diligent work and the enjoyable company throughout the summer of laboratory work.

Acknowledgement is given to NSERC and McGill University for the financial support that made this research program possible.

Finally, the author expresses her gratitude to her family and friends for their continual encouragement and support. Special thanks go to Tom Skinner and Sarah Johnson, and especially to Dr. Scott Alexander for his encouragement and guidance.

Erin Redl February 2009 Montréal

# **Table of Contents**

Abstract	i
Résumé	ii
Acknowledgements	iii
Table of Contents	
List of Figures	
List of Tables	
List of Symbols	
Chapter 1	
Introduction and Literature Review	1
1.1 Introduction	1
1.2 Previous Research on Membrane Action in Flat Plate Structures	2
1.2.1 Park (1964)	2
1.2.2 Hawkins and Mitchell (1979)	4
1.2.3 Cook (1982)	6
1.3 Previous Research on Structural Integrity Reinforcing Steel	7
1.3.1 Mitchell and Cook (1984)	7
1.3.2 Pan and Moehle (1992)	8
1.3.3 Mitchell (1993)	9
1.3.4 Melo and Regan (1998)	10
1.3.5 Ghannoum (1998)	11
1.4 Current Design Provisions	12
1.4.1 CSA A23.3-04	12
1.4.2 ACI 318M-08	13
1.5 Research Objectives	15
Chantar 2	
Chapter 2	
Experimental Program	16
2.1 Introduction	16

2.2 Prototype Structure	16
2.3 Details of Test Specimen	17
2.4 Material Properties	21
2.4.1 Reinforcing steel	21
2.4.2 Concrete	22
2.5 Test Set-Up	24
2.6 Instrumentation	26
2.7 Test Procedure	27
Chapter 3	
Post-punching Response of Slab-Column Connections	30
3.1 Introduction	30
3.2 Specimen S1	31
3.2.1 Test description	31
3.2.2 Concrete cracking and strains	33
3.2.3 Reinforcement strains	33
3.3 Specimen S2	42
3.3.1 Test description	42
3.3.2 Concrete cracking and strains	
3.3.3 Reinforcement strains	45
Chapter 4	
Comparison of Test Results and Predictions	56
4.1 Introduction	56
4.2 Comparison of Test Results of Specimens S1 and S2	56
4.2.1 Load-deflection response	
4.2.2 Punching failure	58
4.2.3 Post-punching response	58
4.2.4 Tensile membrane action	61
4.2.5 Contribution of top reinforcing steel	62
4.3 Comparison with Predictions of Design Standard CSA A23.3-04	67
4.3.1 Punching shear failure	67
4.2.2 Peak post-punching shear	68

4.4 Comparison with Predictions of Melo and Regan (1998)	71
4.4.1 Concrete failure	71
4.4.2 Reinforcement failure	72
4.4.3 Discussion of experimental program reported by Melo and Regan (1998)	73
4.5 Comparison with Experimental Results of Ghannoum (1998)	75
Chapter 5	_
Conclusions	77
References	 80
Appendix A: Design of Prototype Structure and Test Specimens	_
Appendix B: Post-Punching Failure Resistance Governed by "Concre Failure"	— ete

# **List of Figures**

experiencing membrane action (from Park 1964)	2
Figure 1.2 Bottom reinforcement through a column minimizes the "tearing out" of top reinforcement (from Hawkins and Mitchell 1979)	5
Figure 1.3 Permissible details to achieve effectively continuous bottom reinforcement (from Explanatory Notes on CSA A23.3-04)	. 13
Figure 2.1 Slab test specimen	18
Figure 2.2 Reinforcing steel layout	19
Figure 2.3 Structural integrity reinforcing steel layout	19
Figure 2.4 Photo of reinforcing steel layout in specimen S1	20
Figure 2.5 Photo of reinforcing steel layout in specimen S2	21
Figure 2.6 Typical stress-strain curve of reinforcing steel	. 22
Figure 2.7 Typical compressive stress-strain curve of concrete 22 days after casting	24
Figure 2.8 Loading locations and test set-up	25
Figure 2.9 Photo of loading locations and test set-up	26
Figure 2.10 Strain gauge locations	28
Figure 2.11 Location of deflection measurement.	29
Figure 2.12 Location of surface targets to measure concrete strain and crack width on specimen S2	. 29
Figure 3.1 Shear-displacement behaviour of specimen S1	31
Figure 3.2 Load stage 11 of test S1. Punching shear failure has occurred.	35
Figure 3.3 Load stage 16 of test S1. Concrete around column breaks up.	36
Figure 3.4 Completion of test S1. Concrete has been removed.	. 37
Figure 3.5 Maximum crack width versus displacement for specimen S1 of interior cracks (near column) and exterior cracks (near outer edges of specimen)	
Figure 3.6 Strain-displacement behaviour of bottom reinforcing steel of gauges B1-B5 in specimen S1	. 39
Figure 3.7 Stain-displacement behaviour of bottom reinforcing steel of gauges B6-B10 in specimen S1	. 39
Figure 3.8 Stain-displacement behaviour of top reinforcing steel of gauges T1-T4 in specimen S1	40

Figure 3.9 Stain-displacement behaviour of top reinforcing steel of gauges T5-T8 in specimen S1	40
Figure 3.10 Stain-displacement behaviour of structural integrity reinforcing steel of gauges S1-S4 in specimen S1	41
Figure 3.11 Stain-displacement behaviour of structural integrity reinforcing steel of gauges S5-S8 in	41
Figure 3.12 Shear-displacement behaviour of specimen S2	44
Figure 3.13 Load stage 9 of test S2. Cracking around column is characteristic of punching shear.	46
Figure 3.14 Load stage 14 of test S2. Punching shear failure.	47
Figure 3.15 Load stage 16 of test S2. Before removal of concrete.	48
Figure 3.16 Load stage 16 of test S2. After removal of concrete.	49
Figure 3.17 Completion of test S2. E-W top reinforcement nearly completely ripped out	50
Figure 3.18 Completion of test S2. Column crushed.	50
Figure 3.19 Angle of structural integrity reinforcement. Perpendicular bar caused chang in angle.	
Figure 3.20 Maximum crack width versus displacement for specimen S2 of interior cracks (near column) and exterior cracks (near outer edges of specimen)	52
Figure 3.21 Strain-displacement diagram of concrete at slab edges in specimen S2	52
Figure 3.22 Strain-displacement behaviour of bottom reinforcing steel of gauges B1-B5 in specimen S2	
Figure 3.23 Strain-displacement behaviour of bottom reinforcing steel of gauges B6-B1 in specimen S2	0 53
Figure 3.24 Strain-displacement behaviour of top reinforcing steel of gauges T1-T4 in specimen S2	54
Figure 3.25 Strain-displacement behaviour of top reinforcing steel of gauges T5-T8 in specimen S2	54
Figure 3.26 Strain-displacement behaviour of structural integrity reinforcing steel of gauges S0-S4 in specimen S2	55
Figure 3.27 Strain-displacement behaviour of structural integrity reinforcing steel of gauges S5a-S8 in specimen S2	55
Figure 4.1 Shear-displacement behaviour of specimens S1 and S2	57
Figure 4.2 Breakout failure of reinforcement extends further from column in S2 than in S1 at similar deflection and lower shear value.	61
Figure 4.3 Reinforced concrete slab with unrestrained edges develops tensile membrane action	62

Figure 4.4 Top reinforcement exterior to the column reduced the tear-out of perpendicular underlying reinforcement	65
Figure 4.5 Top centre reinforcement, which was not restrained by perpendicular top reinforcement, tore out of the slab nearly completely	66
Figure 4.6 Contribution of top reinforcing steel.	66
Figure 4.7 Locations where concrete resists breakout failure is at the ends of all bars transferring significant load into the column	67
Figure 4.8 Area A <sub>CH</sub> determined from cone-shaped failure surface for breakout failure embedments (Adapted from Melo and Regan 1998)	

# **List of Tables**

Table 1.1	Comparison of requirements for structural integrity in current design standards.	14
Table 2.1	Reinforcing steel properties	22
Table 2.2	Concrete mix design	23
Table 2.3	Concrete characteristics	23
Table 2.4	Average concrete material properties	23
Table 3.1	Summary of key load stages in test of specimen S1	32
Table 3.2	Angle below the horizontal structural integrity reinforcing steel near the column face (Specimen S1).	38
Table 3.3	Summary of key load stages in test of specimen S2	44
Table 3.4	Angle below the horizontal of top and structural integrity reinforcing steel near the column face (Specimen S2).	51
Table 4.1	Summary of shear-displacement behaviour of specimens S1 and S2	57
Table 4.2	Calculated stress of structural integrity reinforcement of specimen S2	59
Table 4.3	Angle below the horizontal of reinforcing steel of specimen S2 at peak post-punching shear	64
Table 4.4	Predicted and experimental values for punching shear failure	68
Table 4.5	Predicted and experimental values for post-punching failure peak load	69
Table 4.6	Comparison of punching failure, post-punching failure, and design service loads	70
Table 4.7	Comparison of experimental results with post-punching failure resistance predicted by Melo and Regan (1998)	73
Table 4.8	Comparison of experimental results with post-punching failure resistance predicted by Melo and Regan (1998) accounting for contribution of top reinforcement	73
Table 4.9	Post-punching failure resistance of test specimens reported by Melo and Regan (1998)	74
Table 4.1	O Comparison of post-punching failure resistance to test specimens reported by Ghannoum (1998)	76
Table 4.1	1 Post-punching failure resistance of test specimens by Ghannoum (1998), as predicted by Melo and Regan (1998)	76

# **List of Symbols**

$A_{CH}$	area of horizontal projection of conical failure surface for breakout concrete
	failure
$A_s$	area of structural integrity reinforcing steel
$A_s'$	area of all bottom reinforcement passing through column
$A_{sb}$	area of bottom reinforcement passing through column, often referred to as
	structural integrity reinforcing steel; the minimum area of effectively
	continuous bottom reinforcement in the direction $l_n$ placed through the reaction
4	area of supports
$A_{sbt}$	total area of effectively continuous bottom steel protruding from all sides of a
h	column  norimeter of critical section for shear in slabs
$egin{array}{c} b_o \ d \end{array}$	perimeter of critical section for shear in slabs effective depth of slab
f <sub>c</sub> '	specified compressive strength of concrete
$f_{ct}$	splitting tensile strength of concrete
$f_r$	modulus of rupture of concrete
$f_s$	calculated yield stress of reinforcing steel
$f_y$	specified yield strength of reinforcing steel; specified yield strength of non-
- /	prestressed reinforcement
$F_u$	ultimate tensile strength of structural integrity reinforcement
$l_d$	tension development length of reinforcement
$l_n$	clear span, in the direction being considered, measured face-to-face of supports
$l_2$	distance measured from the centreline of the panel on one side of the catenary
	to the centerline of the panel on the other side of the catenary
$L_x$ , $L_y$	span lengths of the slab in the x and y directions, with $L_x > L_y$ ; span lengths in
D	the short and long directions, respectively
P	post-punching resistance defined by fracture of reinforcement
$P_u$	post-punching resistance defined by breakout concrete failure
$T_x$ , $T_y$	yield forces of the reinforcement in the x and y directions; tension per unit length in the x and y directions
$V_n$	nominal punching shear resistance
$V_{se}$	post-punching resistance predicted by CSA A23.3-04; design service load
<b>'</b> se	specified as shear transmitted to column due to specified loads, but not less
	than shear corresponding to twice the self-weight of the slab
$V_{exp}$	experimental punching or post-punching resistance of test specimen
$V_{pred}$	predicted punching or post-punching resistance of test specimen
W	uniformly distributed load per unit area of slab
$W_S$	load to be carried after initial failure
$\varepsilon_x$ , $\varepsilon_y$	membrane strains in the x and y directions
Δ	maximum value of deflection
arphi	capacity reduction factor, 0.9 for tension

## Chapter 1

### **Introduction and Literature Review**

#### 1.1 Introduction

Overloading during construction and severe seismic loading have resulted in a number of punching shear failures in flat plate structures. As the slab suffers a punching shear failure, the load carried by the slab connection must be redistributed to adjacent supports. The adjacent slab-column connections will likely be overloaded, and hence fail in punching shear. This would result in collapse of the floor onto the slab below, thereby propagating the collapse both horizontally and vertically. Progressive collapse is extremely undesirable, as costs and chances of injury and death are high.

Some examples of progressive collapse in flat plate structures include: 2000 Commonwealth Avenue in Boston in 1971 (King and Delatte 2004); Bailey Crossroads in 1973 (Leyendecker and Fattal 1973); a condominium collapse in Cocoa Beach, Florida in 1981 (Lew, Carino and Fattal 1982); and a number of collapses during the Mexico City earthquake of 1985. These collapses gave impetus to research on the post-punching failure behaviour of flat plate structures and resulted in an addition to the CSA Standard A23.3-84 *Design of Concrete Structures for Buildings* (CSA 1984). The new clauses were introduced as "minimum bottom reinforcement requirements for structural integrity," where the provision of continuous bottom reinforcement through the column or support provides an alternative load path and, thus, prevents progressive collapse.

The objectives of this research program were to investigate the behaviour of flat plate structures after punching shear failure and to investigate the required detailing of bottom reinforcement to provide structural integrity after punching shear failure.

This chapter will provide a background on the behaviour of reinforced concrete slabs and will provide a brief overview of previous research on flat plate structures, progressive collapse, and bottom reinforcement for structural integrity. The requirements of current design standards are also presented.

#### 1.2 Previous Research on Membrane Action in Flat Plate Structures

#### 1.2.1 Park (1964)

A paper by Park (1964) presented his work on membrane action of uniformly loaded rectangular slabs where all edges are laterally restrained. He stated that reinforced concrete slabs may benefit from "membrane action," a behaviour which increases the capacity of a slab under gravity loads. Membrane forces, either compressive or tensile develop in the slab because of its boundary conditions and the geometry of its deformations.

A typical load-central deflection curve of a slab subjected to uniform load is shown in Figure 1.1. At point B, the slab reaches its ultimate load, where failure occurs due to shear or flexure and where the capacity is enhanced by compressive membrane action. Compressive membrane action occurs because, as the slab is loaded, small cracks develop that increase the length of the slab. If the edges of the slab are laterally restrained (either by adjacent slab panels or by edge beams), forces will develop as the edges try to move outward.

At point C, the membrane forces change from compressive to tensile as the deflections of the slab are large enough to pull the edges of the slab inward. Again, if the edges are laterally restrained, forces will develop. Catenary action of the reinforcing

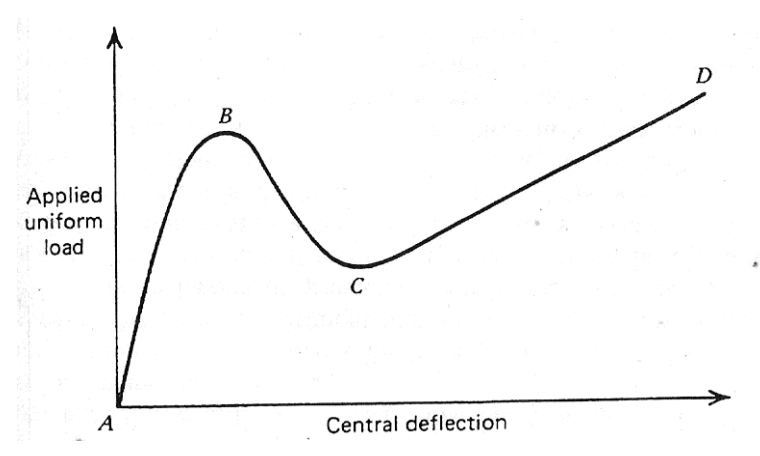


Figure 1.1 Typical load-central deflection behaviour of a reinforced concrete slab experiencing membrane action (from Park 1964)

steel develops, and the slab behaves like a 'hanging net' where the entire load is carried by the reinforcing steel in tension.

The load carried by the slab can increase with increasing deflection until the reinforcement fractures or other failure occurs at point D. For tensile membrane action to be significant, the reinforcing bars must be adequately anchored.

Park attempted to develop theory for the behaviour of slabs in the region between C and D (Fig. 1.1) and to support this theory with experimental work by himself and Powell. Based on equilibrium of forces on a differential rectangular element of slab and based on a solution by Timoshenko for the boundary conditions of laterally restrained edges, Park proposed the equation:

$$\frac{wL_{x}^{2}}{T_{x}\Delta} = \frac{\pi^{3}}{4\sum_{n=1,3,5...}^{\infty} \frac{1}{n^{3}} (-1)^{\frac{n-1}{2}} \left(1 - \frac{1}{\cosh\left(\frac{n\pi L_{y}}{2L_{x}}\sqrt{\frac{T_{x}}{T_{y}}}\right)}\right)}$$
(Eq. 1.1)

where w is the uniformly distributed load per unit area of the slab;  $L_x$  and  $L_y$  are the span lengths of the slab, with  $L_x \ge L_y$ ;  $T_x$  and  $T_y$  are the yield forces of the reinforcement in the x and y directions, per unit width; and  $\Delta$  is the maximum value of deflection.

The equation provides a linear relation for slab behaviour between C and D (Fig. 1.1). Three assumptions inherent to the equation are:

- 1. concrete is cracked through the full depth of the slab and cannot carry any load;
- 2. all reinforcement has reached yield stress; and,
- 3. strain hardening of steel does not occur.

Also, it is noted that the behaviour of the slab as it approaches point D (Fig. 1.1) is limited by the ductility of the reinforcing steel.

When compared to experimental load-deflection curves of uniformly loaded rectangular slabs on beams, the equation was conservative. Park attributed the conservatisms to the following observations:

- 1. pure membrane action did not occur, as the slab was not fully cracked at the peak load carried by tensile membrane action;
- 2. the assumption of no strain hardening is likely inaccurate, although conservative; and,
- 3. top steel at the edges of the slab contributes to the tensile membrane action, but is not accounted for by the equation because it is not continuous through the slab.

Park and Powell suggested a safe value for the central deflection of the slab -0.1 times the length of the short span - such that reinforcing steel will not fracture in tension. Using the suggested value of central deflection, Park compared the ultimate flexural strength of the slab (point B, Fig. 1.1) to the capacity of the slab given by Eq. 1.1. For many typical reinforced concrete slabs, the load-carrying capacity due to tensile membrane action will exceed the ultimate flexural strength.

Park acknowledged the practical application of the behaviour depicted in Figure 1.1. If a slab fails under gravity loading, the slab will drop suddenly but may be "caught" by the reinforcing steel if its strength in tensile membrane action is sufficient.

#### 1.2.2 Hawkins and Mitchell (1979)

Hawkins and Mitchell (1979) discussed the susceptibility of flat plate structures to progressive collapse and the possibilities for defence against progressive collapse. An analysis of tributary areas illustrated that an unreasonable factor of safety is required for progressive collapse to be arrested at an adjacent column. So, Hawkins and Mitchell encouraged the provision of bottom reinforcement or the intentional development of tensile membrane action.

Tests performed at the University of Washington included continuous bottom reinforcing steel in all tests. Some also included shear reinforcement. All slab specimens developed a shear capacity greater than  $0.5A_s'f_y$  where  $A_s'$  is the area of all bottom reinforcing steel passing through the column. Hawkins and Mitchell described the greater reliability of bottom versus top reinforcing steel, because top reinforcing steel rips out as load increases, but the presence of bottom reinforcing steel minimized the

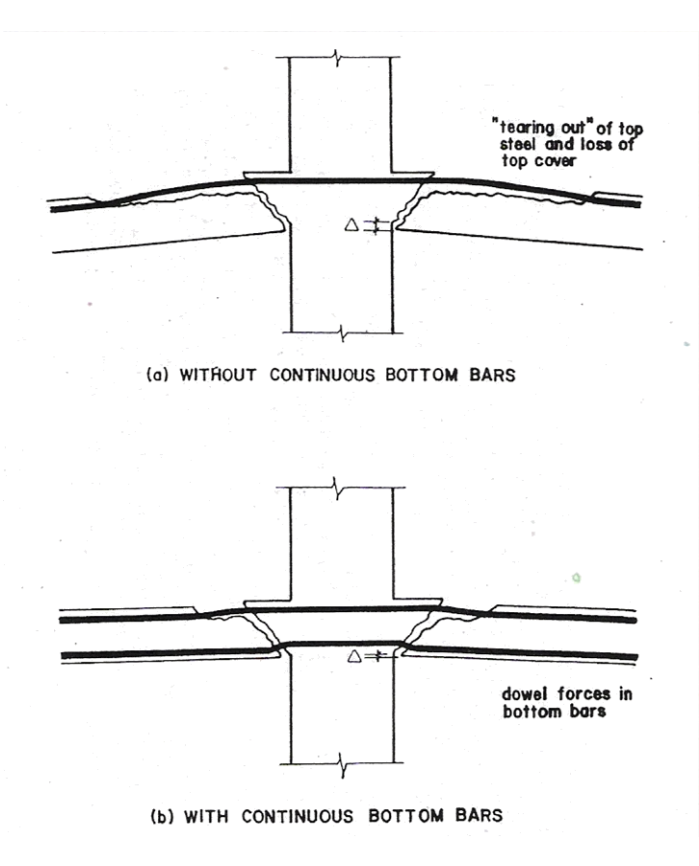


Figure 1.2 Bottom reinforcement through a column minimizes the "tearing out" of top reinforcement (from Hawkins and Mitchell 1979)

tearing action (Fig. 1.2). A post-punching shear capacity of  $0.5A_s'f_y$  was suggested, but it was noted that, if moment transfer is required at the column, shear capacity will be reduced.

Additionally, an equation was presented to predict the load-deflection response of a rectangular slab with uniform load and restrained edges, developing tensile membrane action. Assuming the membrane takes a circular deformed shape,

$$w = \frac{2T_x \sin \sqrt{6\varepsilon_x}}{L_x} = \frac{2T_y \sin \sqrt{6\varepsilon_y}}{L_y}$$
(Eq. 1.2)

where w is the uniform load;  $T_x$  and  $T_y$  are the tension per unit length for the x and y directions, respectively;  $\varepsilon_x$  and  $\varepsilon_y$  are the membrane strains in the x and y directions, respectively; and  $L_x$  and  $L_y$  are the span lengths of the slab in the short and long directions, respectively.

When compared with experimental results of other researchers, Hawkins and Mitchell found a reasonable agreement between experimental and theoretical results. It is noted that, to achieve tensile membrane action, bottom reinforcement must be continuous so as to develop the full tensile strength of the reinforcing steel within a splice or anchorage length. Therefore, detailing must exceed the requirements of ACI 318-77.

#### 1.2.3 Cook (1982)

At McGill University, Cook (1982) developed a three-dimensional computer program intended to predict the response of reinforced concrete panels in tensile membrane action with fully restrained edges. In a comparison of the program's predictions to experimental results from tests by Park, Brotchie and Holley, Black, Keenan, and Huff, the program was consistently conservative. The conservatism is attributed to assumptions of the program that neglect the following:

- 1. the contribution of concrete through bending action, particularly at panel corners;
- 2. "tension stiffening" effects; i.e. the effect of concrete between the cracks on the development of strain in the reinforcement; and
- 3. the contribution of discontinuous top reinforcement at panel edges to tensile membrane action.

In support of the third effect, Cook reported that, although theoretical predictions were close to parallel to experimental results, there was often a constant offset. However, the best correspondence between results existed with Brotchie and Holley's tests in which there was only bottom reinforcement; there was no top reinforcement to contribute to the tensile membrane action.

Cook also constructed and tested two single panel flat plate specimens, supported by four columns and with no in-plane edge restraint. The specimens were ¼ scale models of a prototype panel with 6 m column spacings, 190 mm slab thickness, and 400 mm square columns, and were loaded at 9 points to simulate uniform loading. The first specimen included enhanced detailing to provide anchorage of bottom reinforcement at

panel edges to allow tensile membrane action to develop. The second specimen was detailed to meet CSA A23.3-M77 minimum requirements.

While the theory predicted that tensile membrane action could not develop in a slab lacking in-plane edge restraint, the tests show that some tensile membrane action occurred in the central regions of the slab. Cook concluded that a compressive ring forms around the edges of the slab, anchoring the reinforcement in tension and providing its own in-plane restraint through compressive arching action. The development of tensile membrane action in the tests ended when the corner concrete crushed.

#### 1.3 Previous Research on Structural Integrity Reinforcing Steel

#### 1.3.1 Mitchell and Cook (1984)

A research program at McGill University investigated the prevention of progressive collapse in slab structures through the development of tensile membrane action (Mitchell and Cook 1984). A number of slab structures were designed according to the CSA Code A23.3-M77 or the ACI Standard 318-77, but the detailing of bottom reinforcement was improved. At least 50 percent of the bottom reinforcement was extended to the panel edges and hooked or lapped with bottom reinforcement of the adjacent panels to achieve continuity of reinforcement and to allow the development of tensile forces necessary for tensile membrane action.

Mitchell and Cook recommended the equation

$$A_{sb} = \frac{0.5 w_s l_n l_2}{\varphi f_V}$$
 (Eq. 1.3)

where  $A_{sb}$  is the minimum area of effectively continuous bottom reinforcement in the direction  $l_n$  placed through the reaction area of supports;  $w_s$  is the load to be carried after initial failure;  $l_n$  is clear span, in the direction being considered, measured face-to-face of supports;  $l_2$  is distance measured from the centerline of the panel on one side of the catenary to the centerline of the panel on the other side of the catenary;  $f_y$  is specified yield strength of non-prestressed reinforcement; and  $\varphi$  is capacity reduction factor, 0.9 for tension.

Mitchell and Cook reported that top reinforcement rips out of the top surface of the slab during punching shear and becomes ineffective in supporting the slab. But, the provision of bottom reinforcement  $A_{sb}$  through the support provides some post-punching resistance by dowel action if the bars are well-anchored. And, if the bottom reinforcement is effectively continuous, it acts in tension at large deflections to allow the slab to hang from the supports and to prevent progressive collapse.

In the derivation of the equation, a limiting deflection of  $0.15l_n$  was used for the one-way catenary. Also, limits were placed on the loading  $w_sl_nl_2$ : the loading may not be less than the total unfactored design service loading, nor less than twice the slab dead load, which is a typical load level during construction. It was emphasized that, if a significant portion of the slab system is grossly overloaded, the provision of  $A_{sb}$  is not expected to prevent progressive collapse, because a slab panel would not have sufficient edge support and restraint to allow for the development of tensile membrane action.

To achieve the continuity of bottom reinforcement that is critical to postpunching resistance, Mitchell and Cook permitted three details: (1) a lap splice of minimum length  $l_d$  in the support reaction area; (2) a lap splice of minimum length  $2l_d$ immediately outside of the support reaction area, but within a region containing top reinforcement; or (3) bends or hooks at discontinuous edges that develop the full yield stress of the reinforcement by the face of the support.

The second permissible detail – a lap splice of minimum length  $2l_d$  – satisfied a request of practicing engineers by attempting to achieve effective continuity without causing excessive congestion in the column or support reaction area. An additional bar, which is lap spliced with the reinforcement on either side of the column, was placed through the column; therefore, no splices were required inside the column. The length  $2l_d$  was based on reasonable assumptions of reinforcement behaviour and bond length.

Mitchell and Cook also indicated that, away from the column face where top reinforcement had not ripped out of the concrete, top reinforcement participated in the transfer of tension to the overlapping bottom reinforcement.

#### 1.3.2 Pan and Moehle (1992)

An experimental study performed by Pan and Moehle (1992) tested four slabcolumn connections under combined gravity and uniaxial or biaxial lateral loading. Test specimens were constructed at a 60 percent scale of a prototype slab system. The prototype was designed with 203 mm slab thickness, 6.1 m spans, and 457 mm square columns. Along with uniform bottom reinforcement and banded top reinforcement designed for flexural loads, continuous bottom reinforcement was provided through the column to prevent progressive collapse. Only approximately 1/3 of the value of continuous bottom reinforcement required by Mitchell and Cook's equation was included in the slab.

After complete punching failure occurred due to a combination of gravity and lateral loads, the slabs were subjected to gravity loads only to evaluate the residual strength of the slab. Pan and Moehle reported that all slabs were capable of supporting the total simulated dead and live design loads during post-punching testing. Analysis of the test results show that the residual strength of the slab was greater than that predicted by Mitchell and Cook's equation (Eq. 1.3), even when taking the resistance factor  $\varphi$  equal to 1.0 and  $f_y$  equal to the measured yield stress. Consequently, Pan and Moehle attributed the slab's additional post-punching resistance to the top reinforcement passing through the column, also acting in tension.

#### 1.3.3 Mitchell (1993)

Mitchell (1993) emphasized the need for careful detailing of slab-column connections as part of the Thomas Paulay Symposium in 1993. He reported that, after a number of failures during the Mexico City Earthquake of 1985, flat-plate slab structures were undeniably susceptible to punching failure and progressive collapse under seismic loading. To prevent progressive collapse, slab-column connections should be carefully detailed to provide alternative load paths. Bottom bars that are well-anchored and effectively continuous may provide an alternative load path by allowing tensile membrane action within the slab.

Mitchell presented a modified form of the design equation found in the 1984 paper by Mitchell and Cook and in the 1984 edition of the Canadian design standard A23.3. The new equation read:

$$A_{sbt} = \frac{2V_s}{\varphi f_y} \tag{Eq. 1.4}$$

where  $A_{sbt}$  is the total area of effectively continuous bottom steel protruding from all sides of a column,  $V_s$  is the likely service load shear on the slab column joint,  $\varphi$  is the capacity reduction factor for tension (0.9), and  $f_y$  is the specified yield strength of the bottom bars.

The likely service load shear  $V_s$  replaced the load  $w_s l_n l_2$  in the 1984 equation, such that the calculation of bottom reinforcement no longer required a consideration of each span direction. The residual shear capacity  $V_s$  of a slab after punching failure was calculated as  $0.5\varphi A_{sbt}f_y$ , and inherently assumed that only the bottom reinforcement provided capacity and that the bottom reinforcement deformed to a 60 degree angle with the vertical column.

Mitchell's specifications for achieving effective continuity of bottom reinforcement and for appropriate values of loading remained the same as those presented by Mitchell and Cook in 1984.

#### 1.3.4 Melo and Regan (1998)

Melo and Regan (1998) presented a report of tests on structural integrity reinforcement intended to identify the type of failure and to calculate post-punching resistance. In a first set of tests, the post-punching behaviour of a slab surrounding a square column suggested that the limit of resistance was due to the disintegration of concrete around the structural integrity reinforcement. A formula based on the breakout resistance of an embedment was adapted from the ACI code for nuclear safety-related structures (349-76). Melo and Regan suggested that an estimation of the resistance provided by bottom reinforcement is

$$P_u = 0.33\sqrt{f_c'} \frac{\pi d^2}{2}$$
 (Eq. 1.5)

where  $0.33\sqrt{f_c'}$  represents the average tensile strength of the concrete, and  $\frac{\pi d^2}{2}$  is the horizontal projection of a conical failure surface with d equal to the effective depth of the of the concrete slab. When bars are spaced closely, the overlap of the failure area is accounted for.

A second set of tests showed that, at post-punching failure, small bars (10 or 12mm) failed by fracture of the bar. Melo and Regan proposed the equation:

$$P = 0.44 \sum A_s F_u$$
 (Eq. 1.6)

where  $A_s$  is the area of structural integrity reinforcement  $F_u$  is the ultimate tensile strength of the structural integrity reinforcement, and 0.44 is a coefficient representative of the bend angle of the structural integrity reinforcement at failure.

This equation is similar to Eq. 1.3 proposed by Mitchell and Cook, except that the bend angle of the structural integrity reinforcement at failure is estimated from experimental results as approximately 26 degrees. Mitchell and Cook assumed a failure angle of 30 degrees, which provides a less conservative estimation of capacity. Also, Melo and Regan's equation allows fracture of the bars, while Mitchell and Cook allow only yielding of the bars, this time providing a more conservative estimate of capacity.

Specimens with larger bars exhibited anchorage failure when the bars were short and crushing of concrete when the bars were long enough to be fully anchored. Melo and Regan stated that the development of the forces in the recommended equations requires sufficient length to properly anchor the bottom bars within intact concrete, i.e. starting at a distance approximately 2d away from the face of the concrete, where d is the effective depth of the concrete.

#### 1.3.5 Ghannoum (1998)

Six tests on slab-column connections were performed at McGill University by Ghannoum in 1998. While the intention of the research program was to study the effect of concrete strength on punching failure, the tests were continued beyond the initial punching failure, and the behaviour of the slabs was recorded.

Based on a prototype flat plate structure with 4.5 m bays, test specimens were 2.3 m by 2.3 m and 150 mm thick. The slab surrounded a 225 mm square column stub extending 300 mm above and below the surface of the slab. Top and bottom flexural reinforcement was designed according to CSA A23.3-94 and for loads specified in NBCC 1995. One half of the specimens had banded top reinforcement, and one half had uniform top reinforcement. The concrete strengths of the specimens were 37.2, 57.1, or 67.1 MPa.

The total required area of structural integrity reinforcement was calculated in accordance with Clause 13.11.5 in A23.3-94 as 1170 mm<sup>2</sup>. In addition to the one 10M

bottom reinforcing bar passing through the column, two 10M bars were placed each way for a total of 1200 mm<sup>2</sup> of structural integrity reinforcement. All bars providing "structural integrity" were continuous and were the full length of the slab specimen (i.e. 2.3 m, less cover).

Observations included that all slab specimens carried a post-punching peak load greater than the design service load. Ghannoum reported that "top reinforcing bars ripped out of the top surface of the slab" during the post-punching reloading.

### 1.4 Current Design Provisions

#### 1.4.1 CSA A23.3-04

The concept of providing "structural integrity reinforcement" in flat plate structures to prevent progressive collapse first appeared in the 1984 publication of the CSA Standard *Design of Concrete Structures for Buildings*. Based strictly on the conclusions presented by Mitchell and Cook (1984), a minimum area of bottom reinforcement was required to pass through the column or support reaction area, and three permissible ways of providing effectively continuous bottom reinforcement were provided (Fig. 1.3). Slight modifications to the structural integrity clauses appeared in the 1995 edition of the standard after the suggestions of Mitchell at the Thomas Paulay Symposium. The resistance factor  $\varphi$  was also removed from the design equation, as the failure leading to progressive collapse was deemed a rare loading event, and the variability allowed for by the resistance factor was deemed unnecessary. The current design standard A23.3-04 (CSA 2004) includes the following provisions:

 a minimum area of bottom reinforcement must connect the slab, drop panel, or slab band to the column or column capital. ΣA<sub>sb</sub> is the summation of the area of bottom reinforcement on all sides of the column or column capital, and it is calculated as:

$$\sum A_s \ge \frac{2V_s}{f_y}$$
 (Eq. 1.7)

where  $V_{se}$  is the shear transmitted to a column or column capital due to specified

- loads, but not less than the shear corresponding to twice the self-weight of the slab, and  $f_v$  is the specified yield strength of the reinforcement.
- at least two bars or tendons must be provided in each direction through the column or column capital.
- if bottom reinforcement is not continuous at an interior column or column capital, effective continuity may be achieved by (1) a Class A tension lap splice over the column or column capital, or (2) additional reinforcement passing through the column, lapped with the bottom reinforcement in adjacent spans with a splice length greater than  $2l_d$ .

Other provisions are made for edges and prestressing steel.

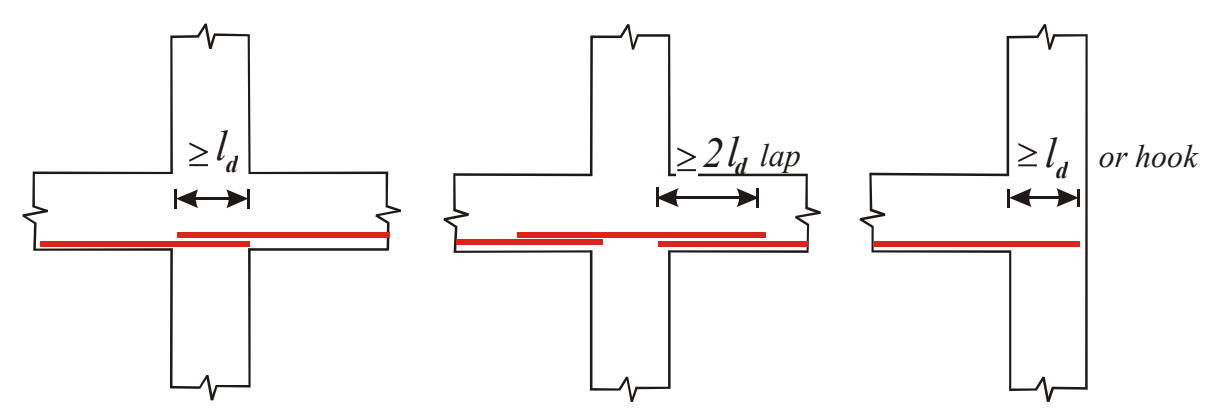


Figure 1.3 Permissible details to achieve effectively continuous bottom reinforcement (from Explanatory Notes on CSA A23.3-04)

#### 1.4.2 ACI 318M-08

The ACI Standard *Building Code Requirements for Structural Concrete and Commentary* (ACI 318M-08) acknowledges the concept and purpose of structural integrity reinforcement, citing research by Mitchell and Cook (1984) in its commentary notes. However, the design recommendations of Mitchell and Cook have not been adopted by the design standard. Clause 13.3.8.5 states that at least 2 bottom bars or wires must pass through the column in each direction, but a minimum area of steel is not required.

Similar to A23.3-04, if the bottom bars are not actually continuous through the column, continuity may be achieved by splices. The splices are permitted within a larger region  $-0.3l_n$  around the column for slabs without drop panels or  $0.33l_n$  for slabs with drop panels – than that allowed by A23.3-04. ACI 318M-08 permits tension, mechanical or welded splices, while A23.3-04 specifies only Class A tension splices.

To assist the development of tensile membrane action and a "hanging net" of reinforcement, all other bottom bars or wires within the column strip must be continuous or spliced. A23.3-04 requires only 50% of bottom bars to be continuous within the column strip.

The differences between the detailing requirements providing structural integrity in current CSA and ACI design standards are summarized in Table 1.1

Table 1.1 Comparison of requirements for structural integrity in current design standards

	CSA A23.3-04	ACI 318M-08
REQUIRED AREA OF BOTTOM REINFORCEMENT	2 bars each direction with minimum $\sum A_s \ge \frac{2V_s}{f_y}^e$	2 bars each direction
SPLICE REGION	within column	within $0.3l_n$ (slabs w/o drop panels) or $0.33l_n$ (slabs with drop panels)
PERMISSIBLE SPLICES	Class A tension	Class A tension mechanical or welded
OTHER BOTTOM REINFORCEMENT WITHIN COLUMN STRIP	50% effectively continuous	100% effectively continuous

# 1.5 Research Objectives

A research program was developed at McGill University to observe the performance of structural integrity steel and the prevention of progressive collapse through the experimental testing and analysis of flat plate slab-column connections. The objectives of this program were to:

- 1. investigate the behaviour of flat plate structures and the development of a post-punching failure response mechanism after punching failure;
- 2. evaluate the ability to achieve "effective continuity" by detailing structural integrity reinforcement to the requirements of CSA A23.3-04 versus enhanced detailing;
- 3. predict a failure load for post-punching failure of flat plate structures with structural integrity reinforcement.

# **Chapter 2**

# **Experimental Program**

#### 2.1 Introduction

The purpose of this experimental program is to investigate the post-punching failure behaviour of reinforced concrete slabs containing structural integrity reinforcing steel. A flat-plate reinforced concrete slab system was designed to meet the minimum requirements of CSA A23.3-04 (2004) and ACI 318M-08 (2008). Then, two full-scale interior slab-column connections were constructed in the Structures Laboratory of the Department of Civil Engineering and Applied Mechanics of McGill University and tested for punching failure and post-punching failure behaviour.

#### 2.2 Prototype Structure

A prototype structure was designed with 4.75 m by 4.75 m bays and for assembly area use, as specified by the National Building Code of Canada (NBCC 2005). The design loads included a superimposed dead load of 1.2 kPa and a live load of 4.8 kPa. The load combinations under consideration were: (1) dead load only, with a load factor of 1.4, or (2) dead load and live load, with load factors of 1.25 and 1.5, respectively. Design assumptions included concrete compressive strength of 30 MPa and reinforcing steel yield strength of 400 MPa.

Based on these design criteria, the prototype structure had a slab thickness of 150 mm and a column of 250 mm by 250 mm. The column was slightly under-designed, according to CSA A23.3-04, so as to ensure punching shear failure even at nominal resistance. The design also provides equal and sufficient flexural resistance both ways to ensure that punching shear failure will result. Design notes and calculations are provided in Appendix A.

#### 2.3 Details of Test Specimen

As shown in Figure 2.1, the test specimen was a flat plate 150 mm thick and 3.4 m by 3.4 m. A central column stub was 250 mm square and extended 300 mm above and below the slab. The column reinforcement consists of 4-15M vertical bars and 4-10M hoops spaced at 300 mm. Concrete cover was 25 mm at the top and bottom of the slab.

The layout of top, bottom, and structural integrity reinforcing steel is shown in Figures 2.2 and 2.3. The top reinforcing steel in both specimens consisted of 11-15M bars on the outermost layer and 13-15M bars on the innermost layer. The bottom reinforcing steel consisted of 11-10M bars in each direction. The reinforcing steel was distributed uniformly throughout the slab, so as to provide the minimum resistance allowed by ACI 318-08. Bar lengths and cut-off locations were in accordance with CSA A23.3-04. In addition, the bottom reinforcing steel was hooked at the exterior edge of the slab to fully anchor the bottom steel, as if the specimen were a portion of a flat-plate system. The 180° hooks lie flat, so as to not interfere with the typical transfer of forces from the top reinforcing steel to the bottom reinforcing steel and to the surrounding concrete.

In specimen S1, the structural integrity reinforcing steel fulfilled the requirements of CSA A23.3-04. The design equation for the summation of the area of bottom reinforcing steel connecting the slab to the column on all faces is:

$$\sum A_s \ge \frac{2V_s}{f_v} e \tag{Eq. 2.1}$$

 $V_{se}$  is the shear transmitted to a column due to the specified loads, equal to 215 kN. This is greater than the shear corresponding to twice the self-weight of the slab, equal to 79 kN. Consequently, both specimens contained two 15M bars in each direction, for a total area of 1600 mm<sup>2</sup>.

CSA A23.3-04 also requires that the structural integrity reinforcing steel is effectively continuous through the column. Specimen S1 was detailed as shown in Figure 1.3, such that the bars overlapped the bottom reinforcing steel by twice the development length  $(2l_d)$  outside the column face, equal to 780 mm. In specimen S2, the length of the structural integrity reinforcing steel was  $2l_d + 2d$ , equal to 1000 mm outside

the column face. A distance of twice the effective depth of the slab (2d) was estimated as the radius of the area of disintegrated concrete around the column in post-punching behaviour, based on the research of Melo and Regan (1998).

Photos of the specimens are provided in Figures 2.4 and 2.5.

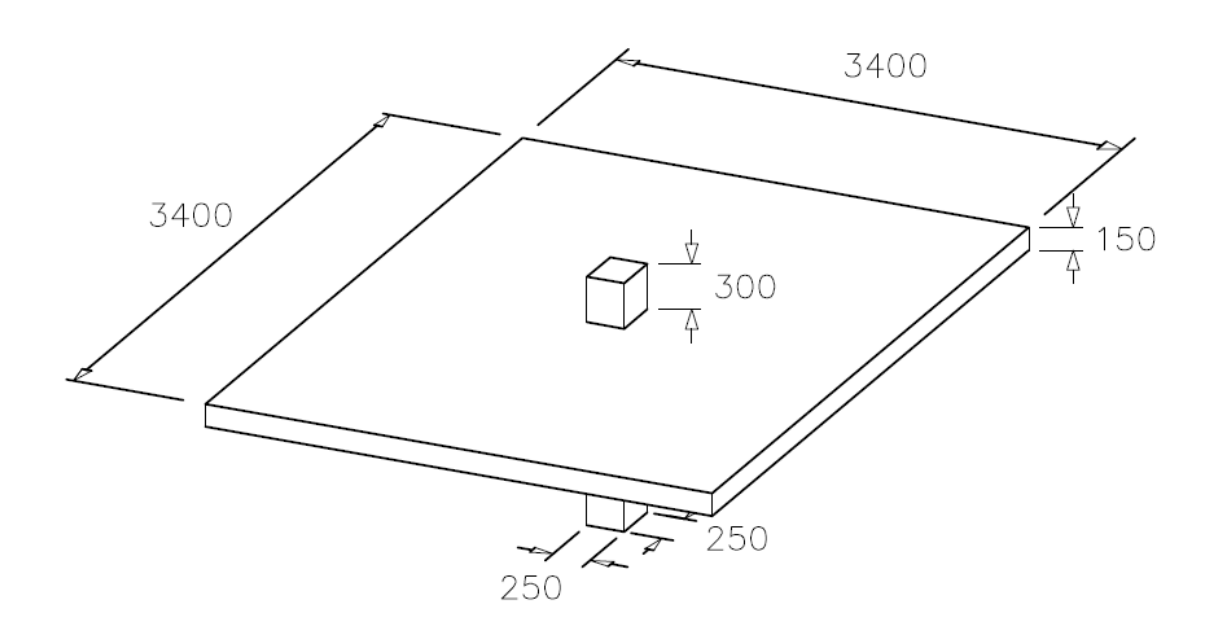


Figure 2.1 Slab test specimen

Note: Dimensions provided in millimetres.

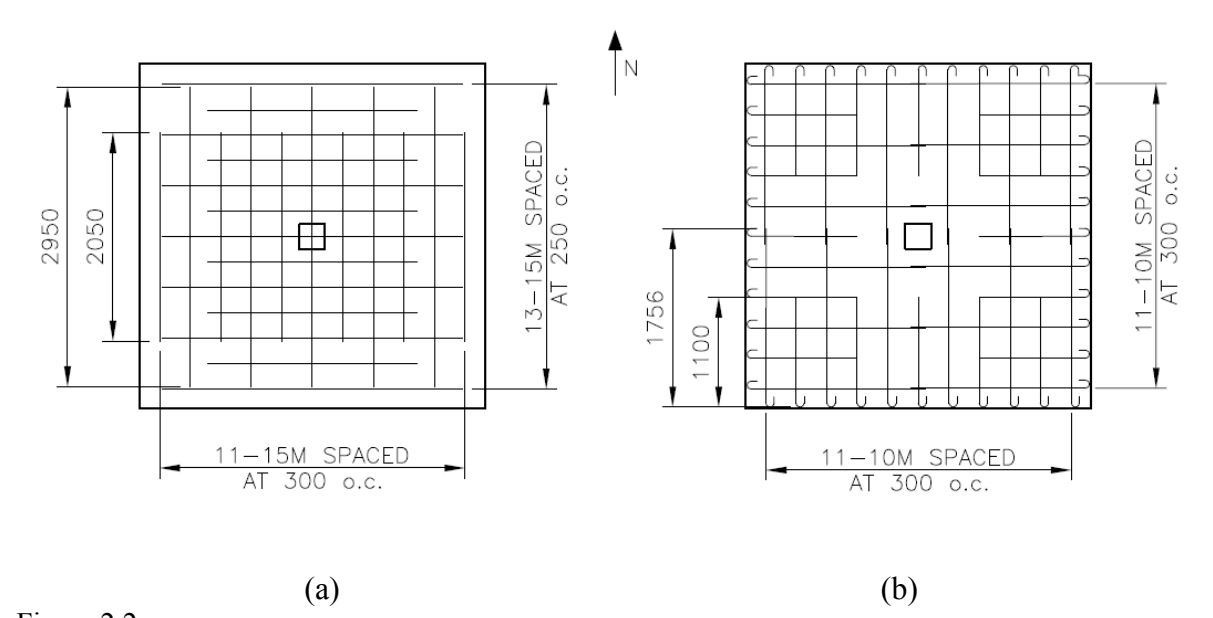


Figure 2.2
Reinforcing steel layout
(a) Top reinforcing steel; (b) Bottom reinforcing steel

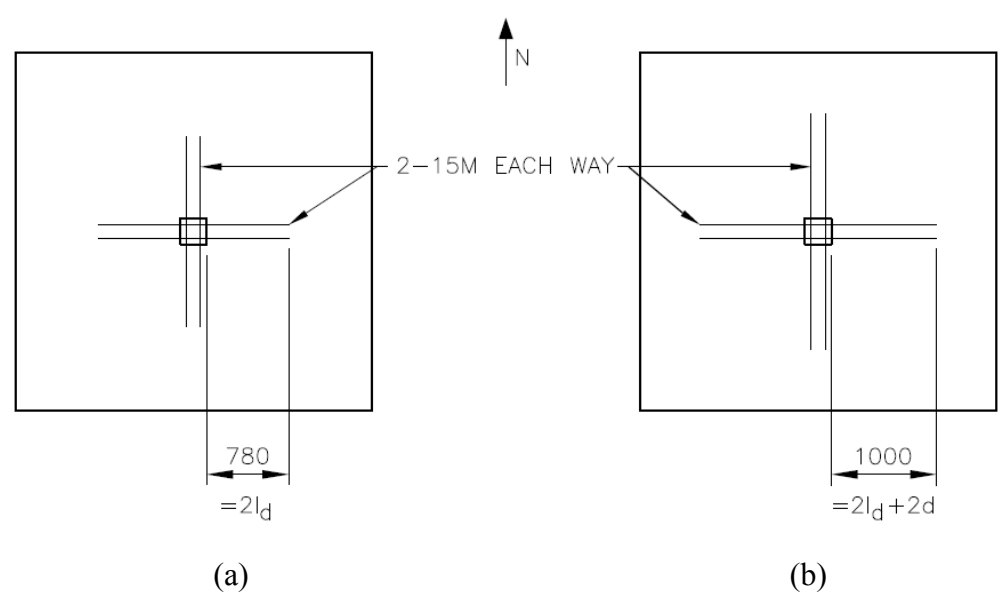
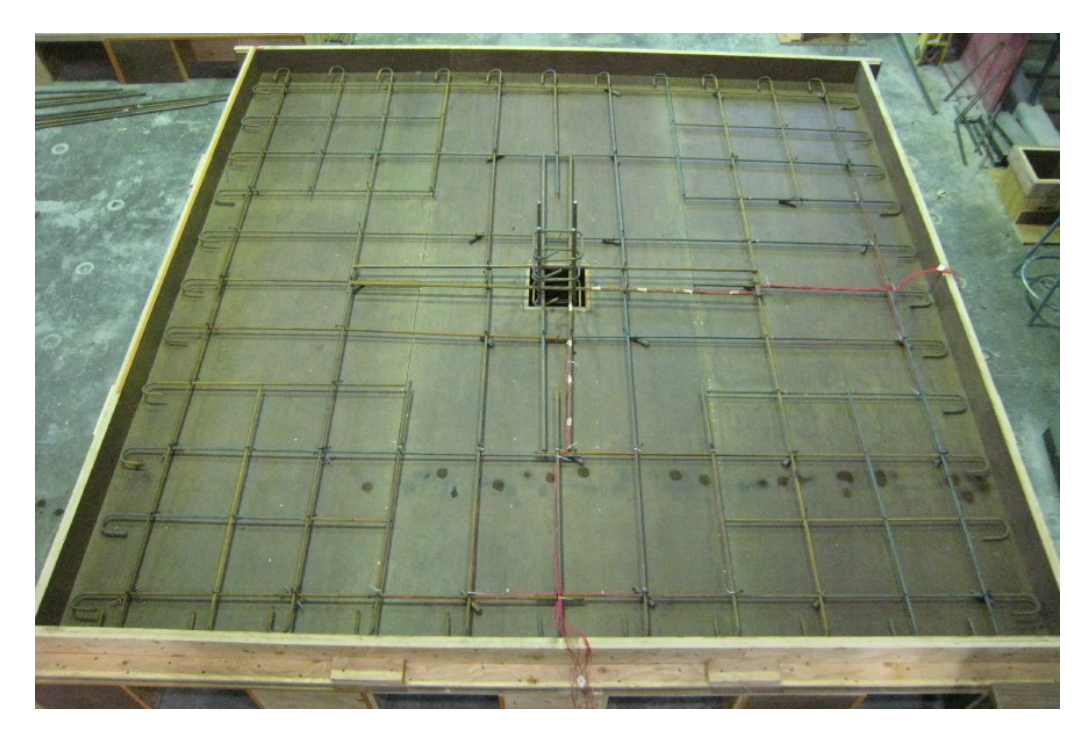
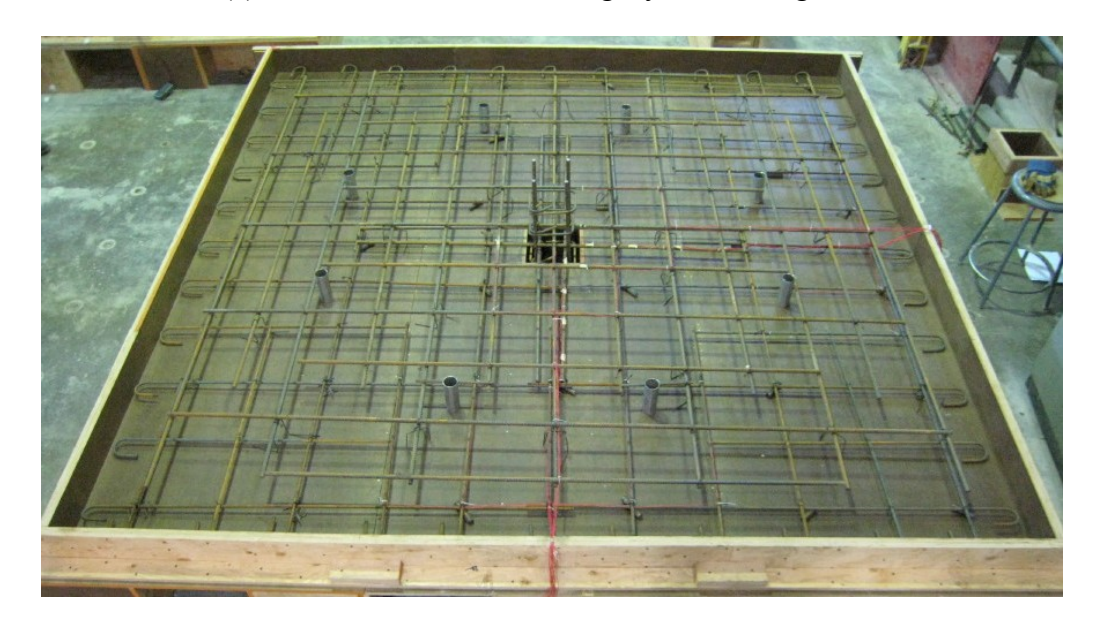


Figure 2.3 Structural integrity reinforcing steel layout (a)Specimen S1; (b) Specimen S2

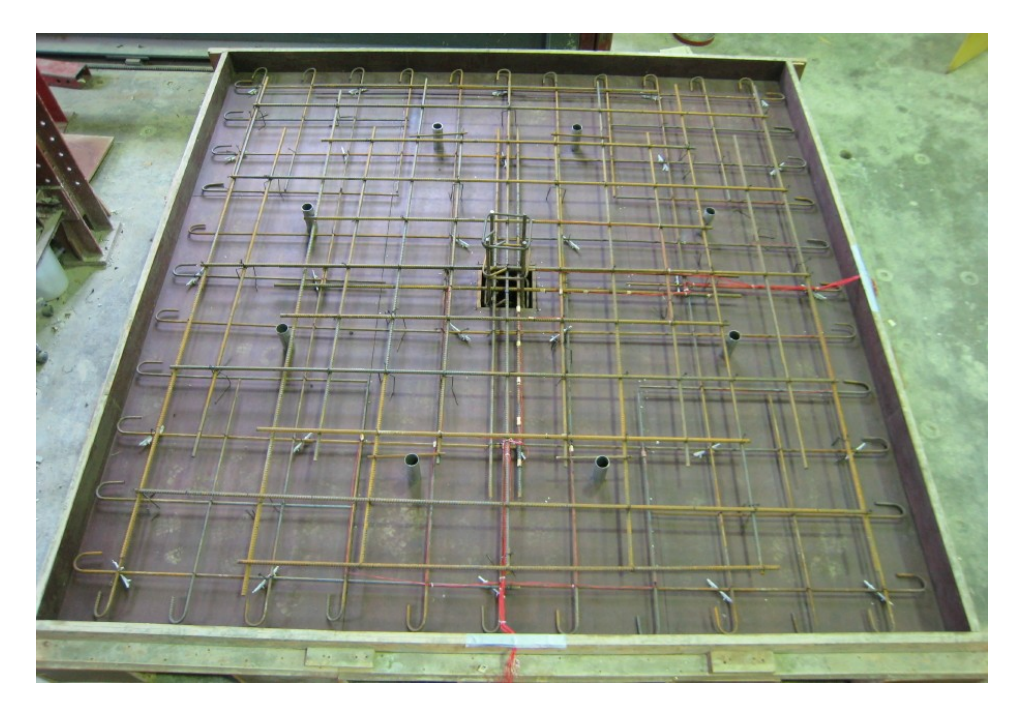


(a) Bottom and structural integrity reinforcing steel



(b) Top, bottom, and structural integrity reinforcing steel

Figure 2.4 Photo of reinforcing steel layout in specimen S1



(a) Top, bottom, and structural integrity reinforcing steel

Figure 2.5 Photo of reinforcing steel layout in specimen S2

# 2.4 Material Properties

#### 2.4.1 Reinforcing steel

The reinforcing steel used in all test specimens was hot-rolled deformed bars of minimum specified yield strength equal to 400 MPa. Table 2.1 provides the material properties of the reinforcing steel based on the average values of tests performed on three samples. Tension tests were performed to determine values of yield strength, ultimate strength, yield strain, and the strain at strain hardening. A typical stress-strain response of the reinforcing steel is shown in Figure 2.6.

Table 2.1 Reinforcing steel properties

Size Designation	Area (mm²)	(	f <sub>y</sub> (MPa)		f <sub>u</sub> (MPa)	ε <sub>y</sub> (%)	ε <sub>sh</sub> (%)	Use
		Avg.	Std. Dev.	Avg.	Std. Dev.			
10M	100	455	4.2	578	3.6	0.23	2.43	bottom flexural reinf.
								column hoops
15M	200	457	3.7	594	1.4	0.23	1.84	top flexural reinf.
								structural integrity reinf.
								vertical column bars

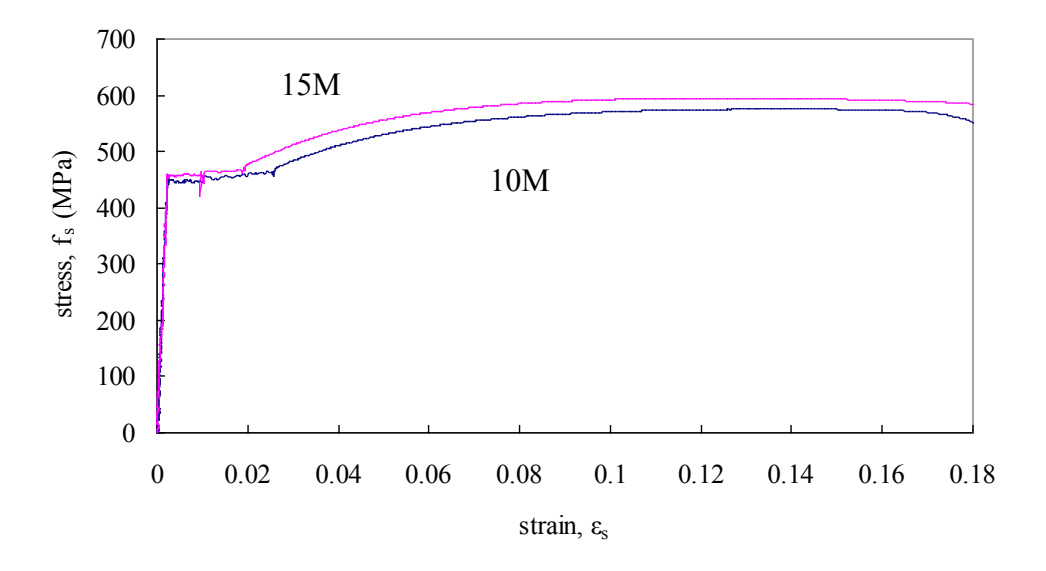


Figure 2.6 Typical stress-strain curve of reinforcing steel

#### 2.4.2 Concrete

The test specimens were made of normal-weight concrete with target compressive strength of 30 MPa. The ready mix concrete was obtained from a local supplier, and the mix design is provided in Table 2.2. Measured slump and air content are given in Table 2.3.

Standard material tests were performed at the time of slab testing (i.e. 22 days after casting), including: uniaxial compression tests on cylinders 100 mm in diameter and 200 mm in length to determine compressive strength,  $f_c$ '; split-cylinder tensile

strength tests on cylinders 100 mm in diameter and 200 mm in length to determine splitting tensile strength,  $f_{sp}$ ; and, third-point bending tests on beams 100 mm by 100 mm by 400 mm to determine modulus of rupture,  $f_r$ , over a span of 300 mm. All cylinders and beam specimens were moist-cured until material testing was performed. Table 2.4 provides material properties based on average values of each test performed on 3 samples. Figure 2.7 shows a typical stress-strain curve of the concrete of specimen S2.

Table 2.2 Concrete mix design

Components	Quantity
Cement, Type 10	289 kg/m³
SCM, Type F Fly Ash	73 kg/m <sup>3</sup>
Sand	812 kg/m³
Coarse aggregate, 20 mm max.	$635 \text{ kg/m}^3$
Coarse aggregate, 14 mm max.	$343 \text{ kg/m}^3$
Water	165 L/m³
Air-entraining agent	0.12 L/m <sup>3</sup>
Retarding agent	-
Accelerating agent (Pozzutec 20+)	$0.36 \text{ L/m}^3$
Water-reducing agent (Ployheed 997)	1.27 L/m <sup>3</sup>

Table 2.3 Concrete characteristics

Characteristics	S1	S2
Slump	105 mm	128 mm
Air content	6.75%	6.40%

Table 2.4 Average concrete material properties

Test Specimen	f <sub>c</sub> ' (MPa)		$\varepsilon_c'$ (x 10 <sup>-6</sup> )		$f_{sp}$ (MPa)		f <sub>r</sub> (MPa)	
	Avg.	Std. Dev.	Avg.	Std. Dev.	Avg.	Std. Dev.	Avg.	Std. Dev.
<b>S1</b>	28.0	0.1	1043	174	3.2	0.1	5.3	0.2
S2	29.8	1.4	1800	615	3.8	0.1	3.8	0.3

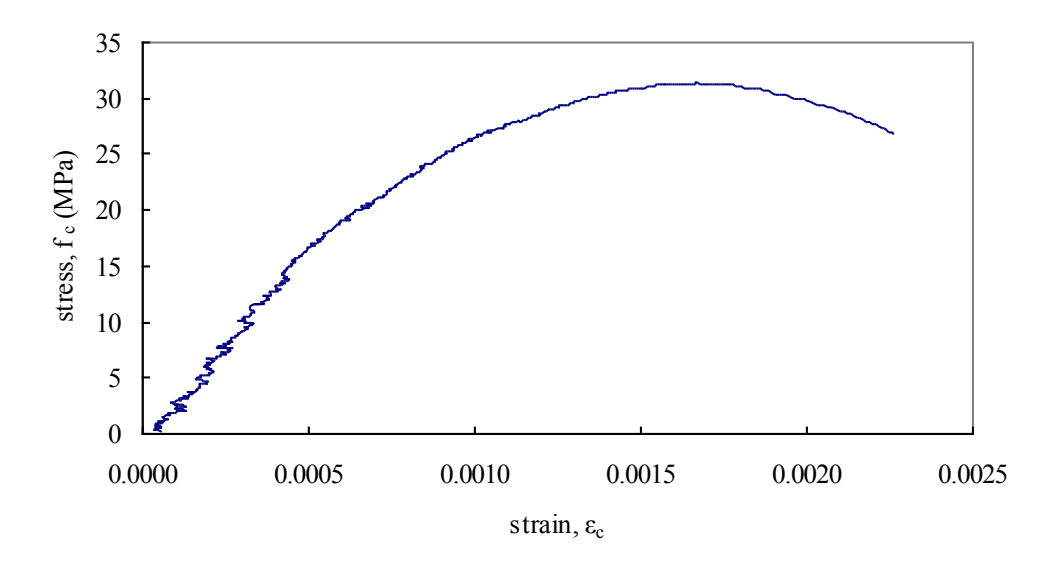


Figure 2.7
Typical compressive stress-strain curve of S2 concrete 22 days after casting

### 2.5 Test Set-Up

The lower column stub was placed on a steel pedestal, and the slab was loaded with eight equal concentrated loads around the column stub. The loading locations, as shown in Figure 2.8, were chosen at approximately the point of inflection as determined though the analysis of the prototype structure; the set-up was intended to simulate a uniformly distributed load on the slab.

Threaded rods passed through the slab, through steel distribution beams, and through the laboratory's strong floor, as shown in Figure 2.8. The steel distribution beams spanned 750 mm between adjacent loading points and spread the load that was applied from four hydraulic jacks. The four identical hydraulic jacks were connected to a single hydraulic pump to ensure that eight equal loads were applied to the slab. Four load cells were placed under the hydraulic jacks to measure the load applied by each jack and to provide a check on the uniformity of loading.

The holes in the slab at the loading locations were 50 mm in diameter to ensure that rotation of the slab at large deflections during testing would not result in the threaded rod bearing on the side of the hole and creating an undesired applied moment. Also, steel plates 19 mm thick and 100 mm square were used to provide a larger bearing area on the slab surface at loading locations, and roller bearings were used to allow the threaded rods to remain vertical as the slab deflected.

Photos of the test set-up are provided in Figure 2.9.

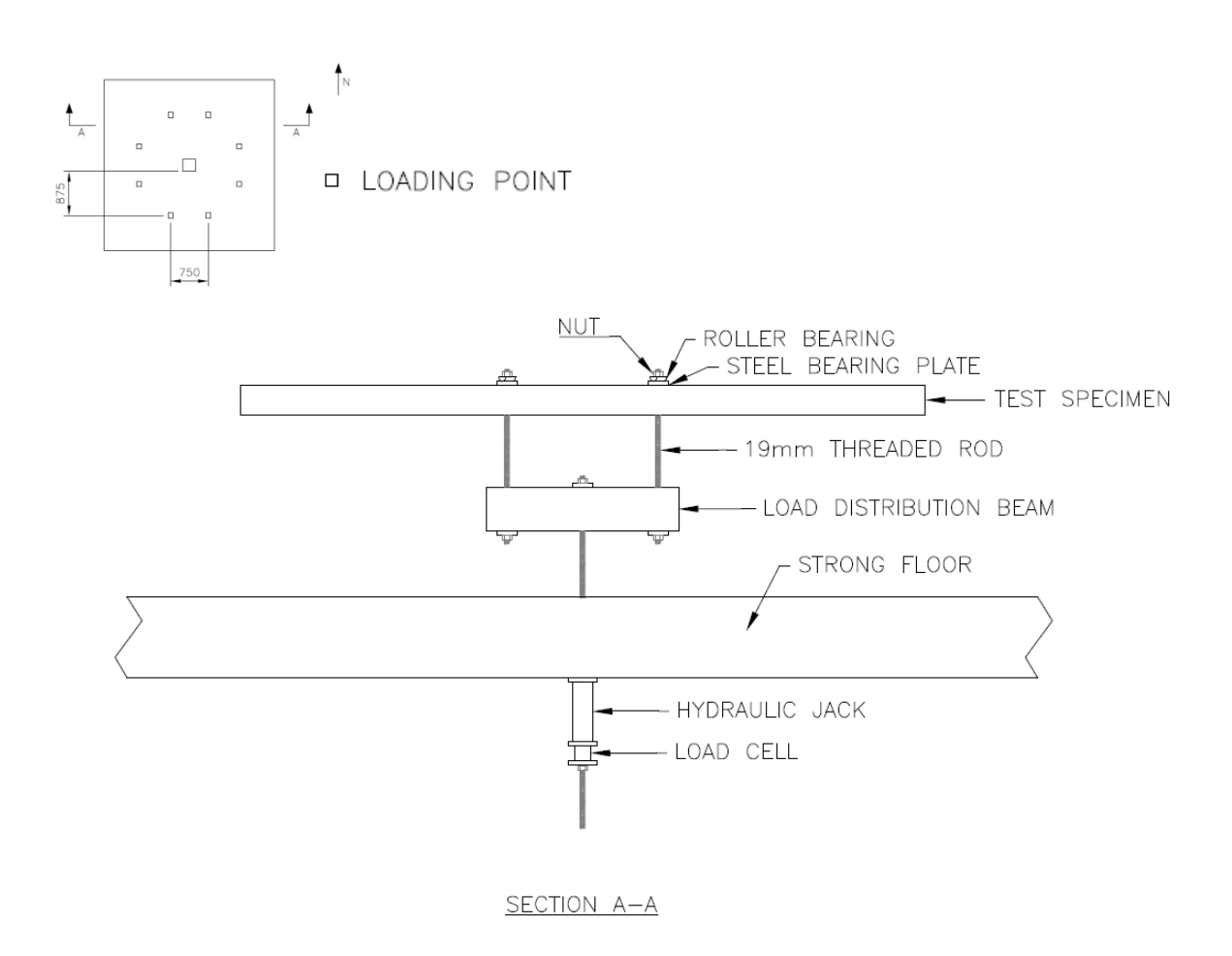


Figure 2.8 Loading locations and test set-up

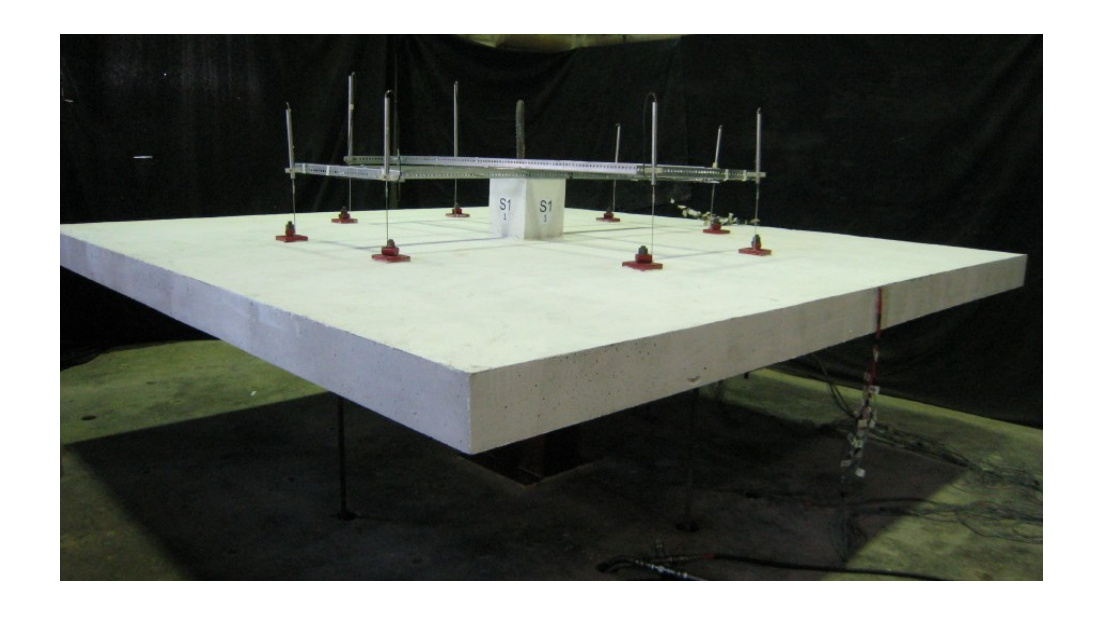




Figure 2.9 Photo of loading locations and test set-up

# 2.6 Instrumentation

In test specimens S1 and S2, 26 and 28 electrical resistance strain gauges were used, respectively, to monitor the development and distribution of strain in the top, bottom, and structural integrity reinforcing steel. Gauges had an electrical resistance of 120 ohms and were 5 mm in length. Gauges were placed on top reinforcing steel at the face of the column. Gauges were placed on top and bottom reinforcing steel at the

location corresponding to the end of the structural integrity reinforcing steel in specimen S1. And, gauges were placed along the length of the structural integrity reinforcing steel, spaced at 200 mm. Locations of all gauges are shown in Figure 2.10.

Linear voltage differential transformers (LVDTs) were located at each of the 8 loading points on the slab to measure deflection during testing. A surveyor's level and scale were also used to measure deflection at the 8 loading points and at 8 points on the edge of the test specimen. These locations are shown in Figure 2.12.

Strain gauges and LVDTs were connected to the computer system which automatically recorded strain and deflection for the entire testing duration.

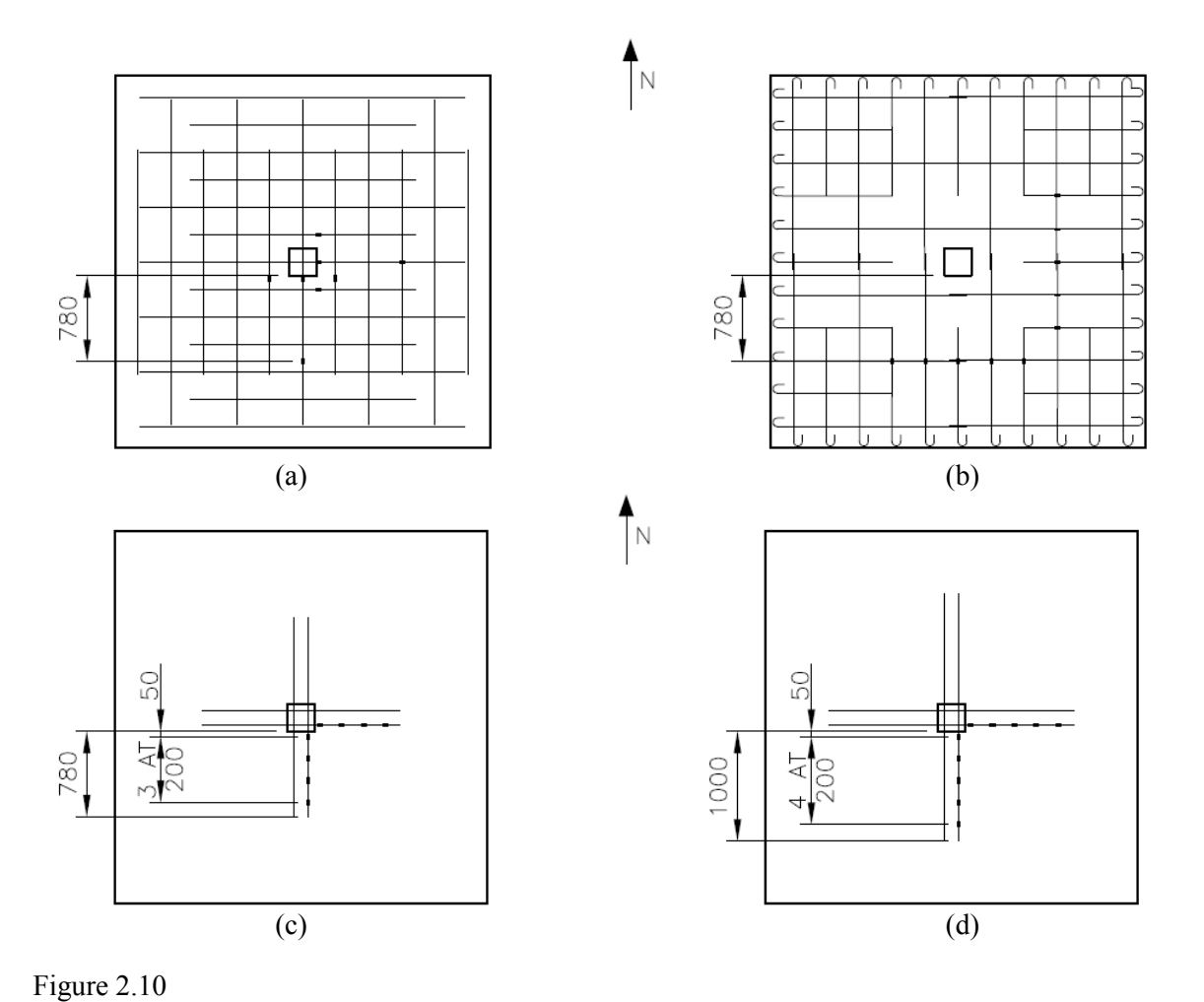
Targets were glued on the surface of specimen S2 at a gauge length of 203 mm to monitor the change in concrete strain and the change in crack width near its edges. Measurements were taken with a mechanical extensometer. Locations of the targets are shown in Figure 2.12.

#### 2.7 Test Procedure

Load was applied in increments of approximately 20 kN until punching failure. At each of these load stages, deflections were measured with the surveyor's level and scale. Also, crack development was marked on the surface of the slab, crack widths were measured, and photos were taken.

Due to the large deflections of the slab during the post-punching response, the slab was unloaded and reloaded so that the hydraulic jacks could be reset to allow for sufficient stroke of the jack for the remainder of the test.

In specimen S2, before achieving the peak post-punching resistance, spalled and broken concrete was removed from the top of the slab to expose the length of debonded reinforcing steel. The length and angle below the horizontal of the exposed reinforcing steel were measured.



Strain gauge locations
(a) Top reinforcing steel; (b) Bottom reinforcing steel; (c) Structural integrity reinforcing steel in specimen S1; (d) Structural integrity reinforcing steel in specimen S2

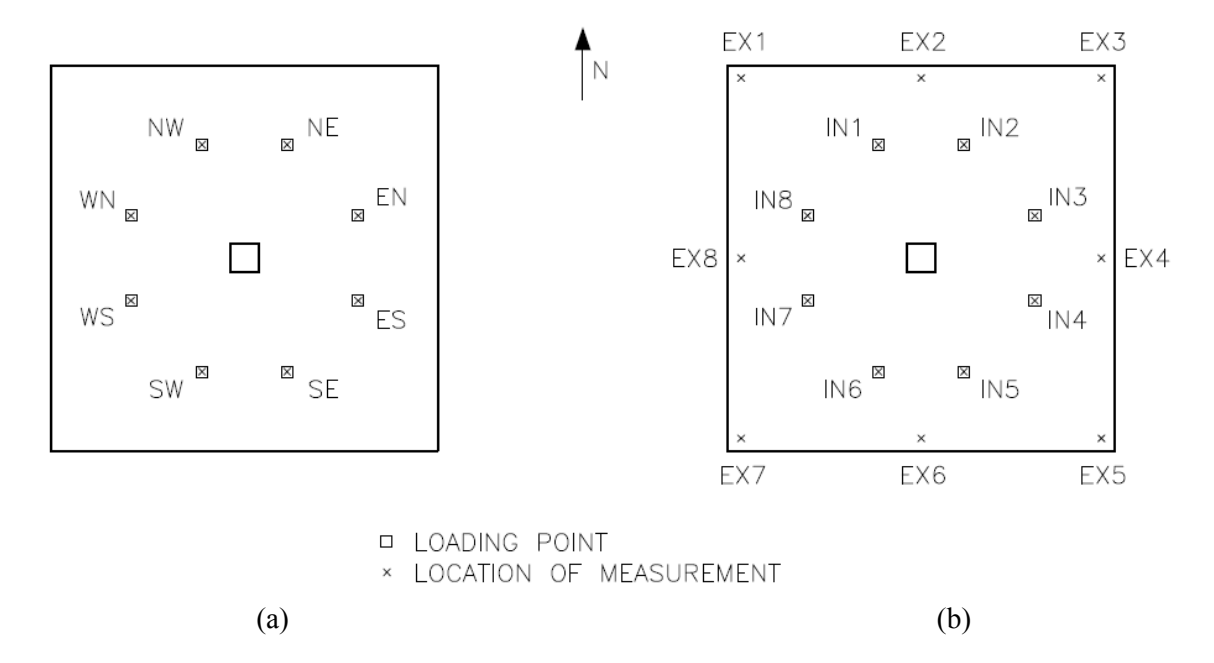


Figure 2.11 Location of deflection measurement (a) LVDT location; (b) Surveyor's level and scale

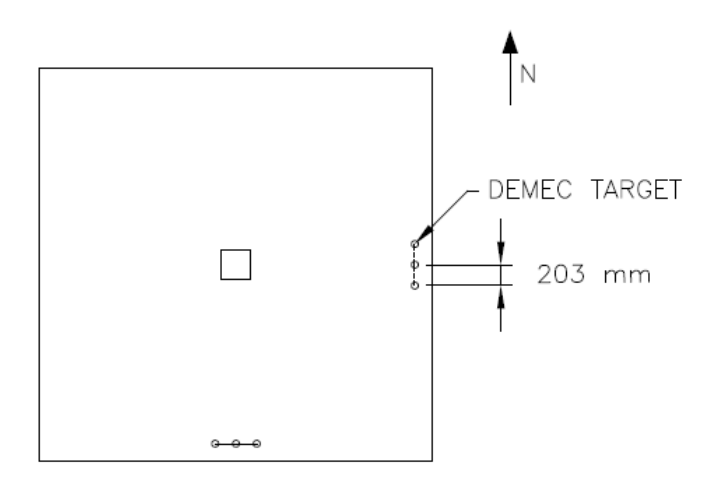


Figure 2.12 Location of surface targets to measure concrete strain and crack width on specimen S2

# **Chapter 3**

# **Post-punching Response of Slab-Column Connections**

### 3.1 Introduction

The two full-scale slab-column connection specimens were tested in the laboratory for punching failure and post-punching failure behaviour. Observations of the specimens' experimental behaviour are presented in this chapter. These observations include the development of cracks, the deflection of the specimen, the strain of reinforcing steel, and the corresponding applied shears. Important stages in the loading of the specimen are first cracking, yielding of reinforcing steel, punching failure, and post-punching failure peak shear.

The shear values presented are the sum of the loads applied by the four hydraulic jacks and the self-weight of the specimen and testing apparatus. The deflection values presented are the average values of deflections measured at all eight loading points.

The nominal shear resistance of the specimen at punching failure, as predicted by CSA A23.3-04, was 277 kN. The post-punching failure resistance, based on the development of tensile membrane action by the structural integrity reinforcing steel, was 320 kN. The post-punching failure resistance was calculated from the equation

$$\sum A_s \ge \frac{2V_s}{f_y} e \tag{Eq. 3.1}$$

This equation assumes that only structural integrity reinforcing steel contributes to the resistance and that the structural integrity reinforcing steel bends to an angle of 30 degrees below the horizontal at the face of the column.

## 3.2 Specimen S1

#### 3.2.1 Test description

The complete shear-displacement behaviour of the specimen is shown in Figure 3.1, and a summary of key load stages during the test is provided in Table 3.1. The behaviour closely follows the typical load-deflection diagram of reinforced concrete slabs experiencing membrane action, as the peak shear value at punching failure was followed by a sudden drop in shear and a significant increase in deflection. Then, the shear carried by the specimen increased as deflection increased.

At load stage 4, hairline cracking at the corners of the column was observed, indicating the presence of punching shear stresses. Cracks along the centerline of the specimen extended the full width of the specimen in all four directions by load stage 5. The shear-displacement curve (Fig. 3.1) shows the change in stiffness as cracking developed.

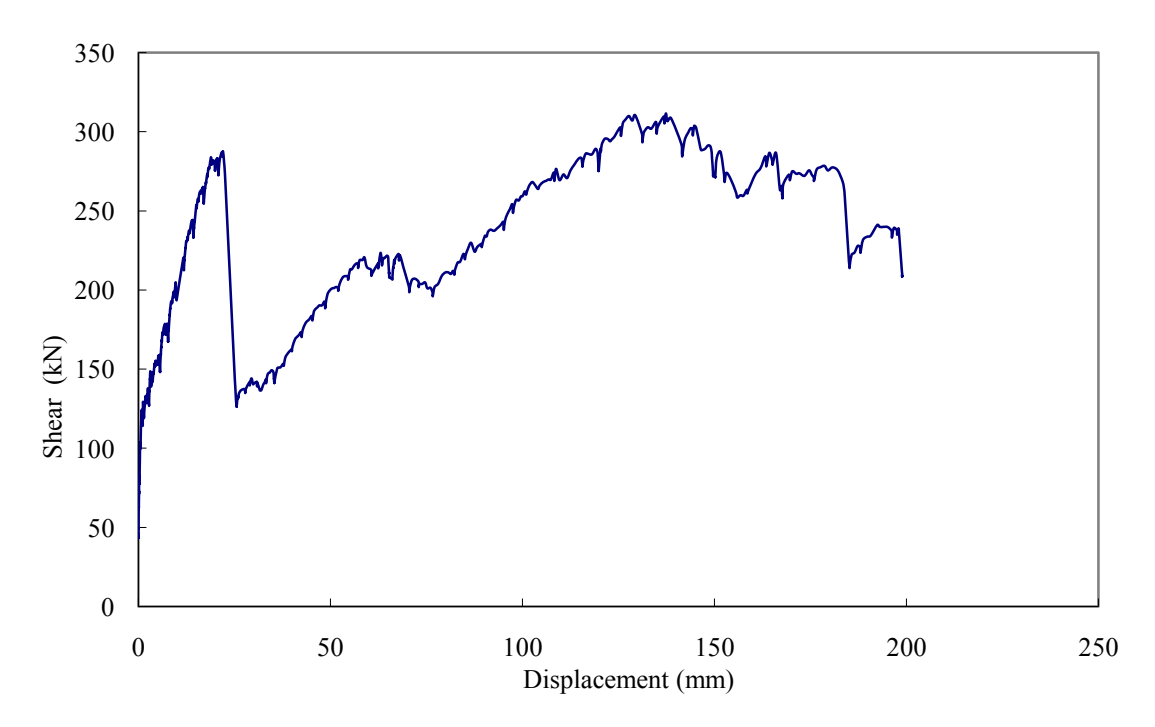


Figure 3.1 Shear-displacement behaviour of specimen S1

Table 3.1 Summary of key load stages in test of specimen S1

	Shear (kN)	Deflection (mm)
First Cracking	123	0.9
First Yield (Top Reinforcement)	193	9
First Yield (S.I. Reinforcement)	219	12
Punching Failure	289	22
Post-Punching Peak Shear	314	138

By load stage 8, data from strain gauges showed that top reinforcing steel was yielding near the column, and cracking around the column was extensive, forming a ring that is characteristic of punching shear failure. By load stage 9, structural integrity steel was yielding near the column.

At load stage 12, the upcoming punching shear failure was evident, as there was a slight depression at the cracking at the northeast corner of column. Punching shear failure occurred at load stage 13 at a peak shear of 289 kN. Figure 3.2 shows the characteristic cone failure around the column. The failure resulted in a sudden drop in shear to 128 kN and an increase in deflection from 22 mm to 26 mm.

Loading continued after punching shear failure. The significant loss in stiffness compared to the initial loading response was evident, as deflection of the specimen increased. The concrete around the column and within the punching shear cone broke up as further load was applied (Fig. 3.3). The top reinforcing steel ripped out of the top surface of the slab, with this tearing out progressing relatively equally in the N-S and E-W directions.

The peak shear during the post-punching failure response was 314 kN at a deflection of 138 mm. Testing was stopped when the structural integrity reinforcing steel

was observed to pull out of the slab, indicating that higher strains could not be developed in the steel.

After testing was completed, loose concrete was removed from around the column to expose the structural integrity reinforcing steel (Fig. 3.4). The angle below the horizontal of structural integrity reinforcing steel was measured. Angles varied between 23 and 40 degrees (Table 3.2).

Finally, bars were manually examined for loss of bond by twisting them with a vice grip. Structural integrity reinforcing steel on the south and west sides of the column were determined to have lost all bond, as the bars rotated relatively easily.

#### 3.2.2 Concrete cracking and strains

Figure 3.5 shows the maximum crack widths near the column and near the specimen edges for the duration of the test. Cracks near the column widened as the specimen was loaded and failed in punching shear. During the post-punching response, the crack widths near the column were not measured because the top concrete was loose. Cracks near the outside edge of the specimen were initially larger than the interior cracks, probably due to a lack of flexural reinforcement near the edges of the specimen. The exterior cracks were widest (0.5 mm) at punching failure. After punching failure, which corresponds with a displacement of 22 mm, the exterior cracks closed slightly to 0.4 mm and then remained constant in width. The closure of these cracks during the post-punching failure loading suggested that the edges of the specimen were in compression.

#### 3.2.3 Reinforcement strains

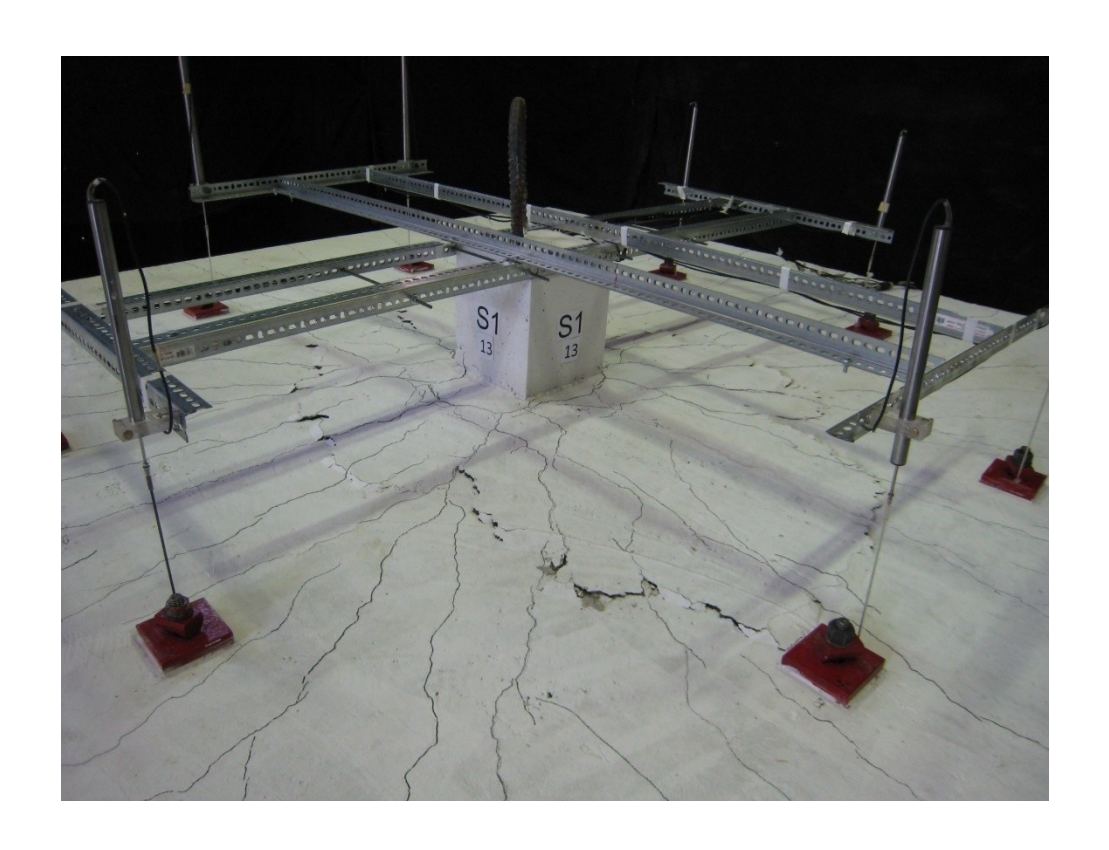
Figures 3.6 to 3.11 present the data collected from the strain gauges placed on top, bottom, and structural integrity reinforcing steel. Where no data is presented, the strain gauge was broken either during casting of the concrete or during testing.

The strain-displacement curves of the bottom reinforcement (Figs. 3.6 and 3.7) closely resemble the shape of the shear-displacement curve (Fig. 3.1). The strains peaked at the time of punching failure and then dropped off. Throughout the post-

punching response, the strains in the bottom reinforcement were less than the yield strain of the steel, except for the centremost bar.

The six strain gauges on the top reinforcement near the column face – T1, T2, T3, T5, T6, T7 – were ineffective after punching failure, as the concrete around the column broke up (Figs. 3.8 and 3.9). Strain gauges T4 and T8, near the ends of the centre bar, measured high strains during the post-punching response. Gauge T8, on the uppermost layer of top reinforcing steel, stopped working before gauge T4, on the innermost layer of top reinforcing steel. This was because the uppermost layer of top reinforcing steel tore out of the top surface of slab sooner than the innermost layer of top reinforcing steel.

Strain-displacement curves are shown in Figures 3.10 and 3.11 for the structural integrity reinforcement. The strain gauges closest to the column face – S4 and S8 – yielded before punching failure due to the significant bending moments at the column face. The measurements at all other locations along the structural integrity reinforcement achieved strains greater than the yield strain of steel during the post-punching response.



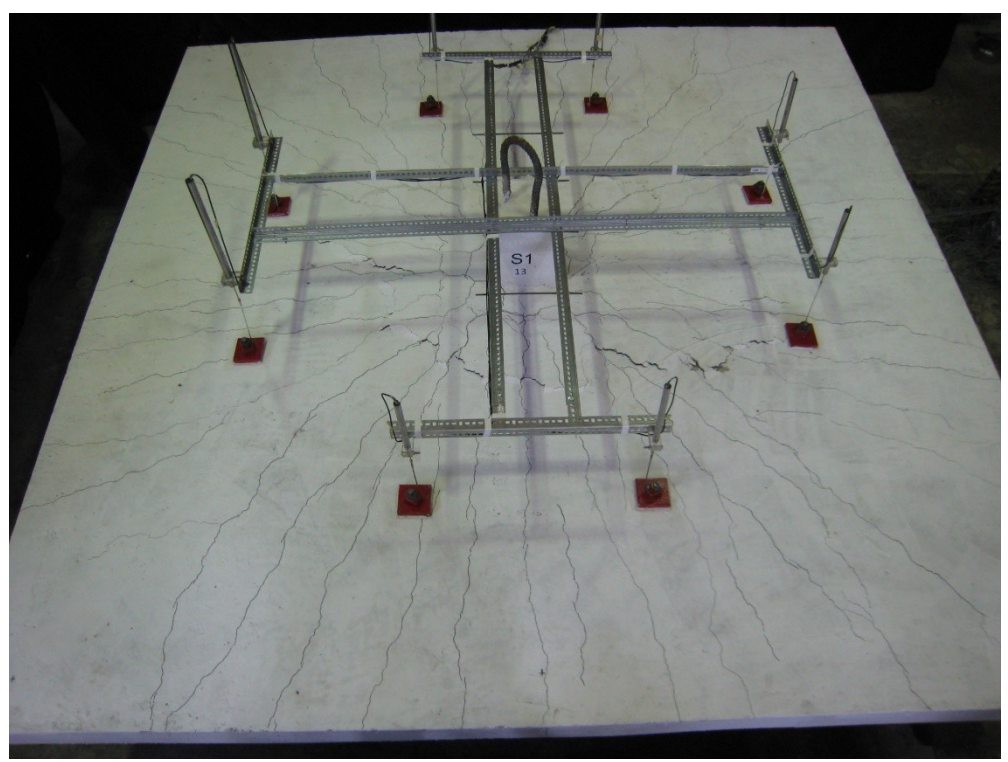
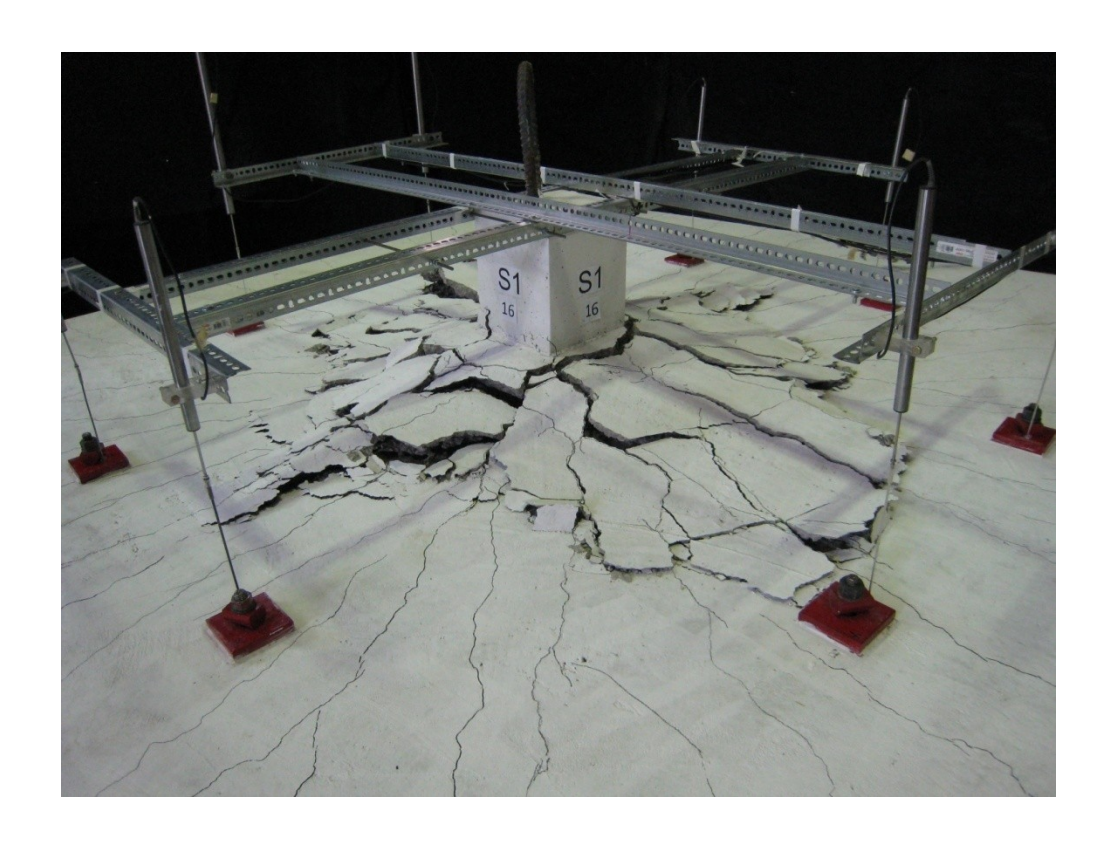


Figure 3.2 Load stage 13 of test S1. Punching shear failure has occurred.



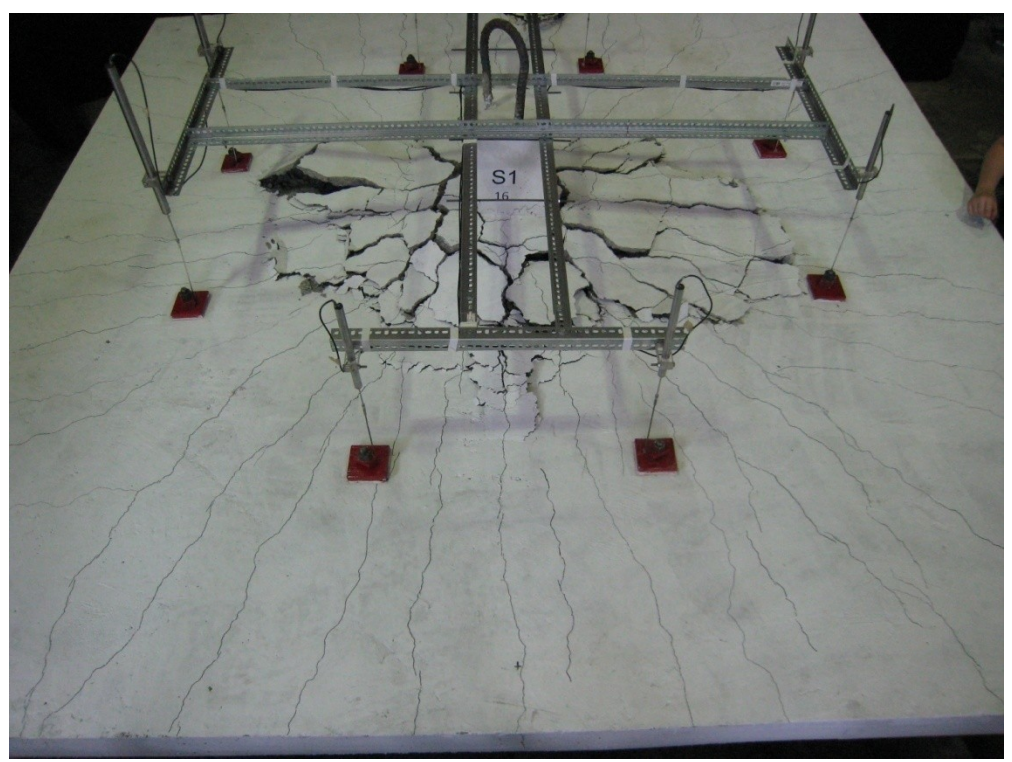


Figure 3.3 Load stage 16 of test S1. Concrete around column breaks up.



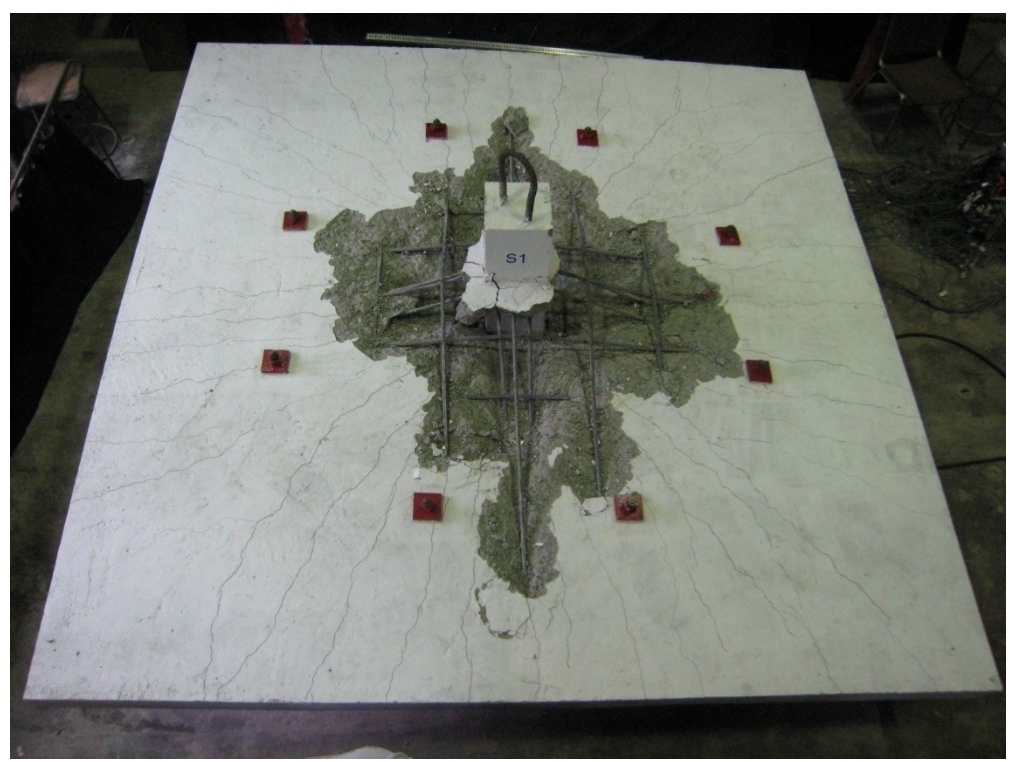


Figure 3.4 Completion of test S1. Concrete has been removed.

Table 3.2 Angle below the horizontal structural integrity reinforcing steel near the column face (Specimen S1).

		Load Stage
		21
	NW	23
	NE	23
	EN	37
Structural	ES	40
Integrity	SE	29
Reinforcing Steel	SW	28   32
	WS	34
	WN	31

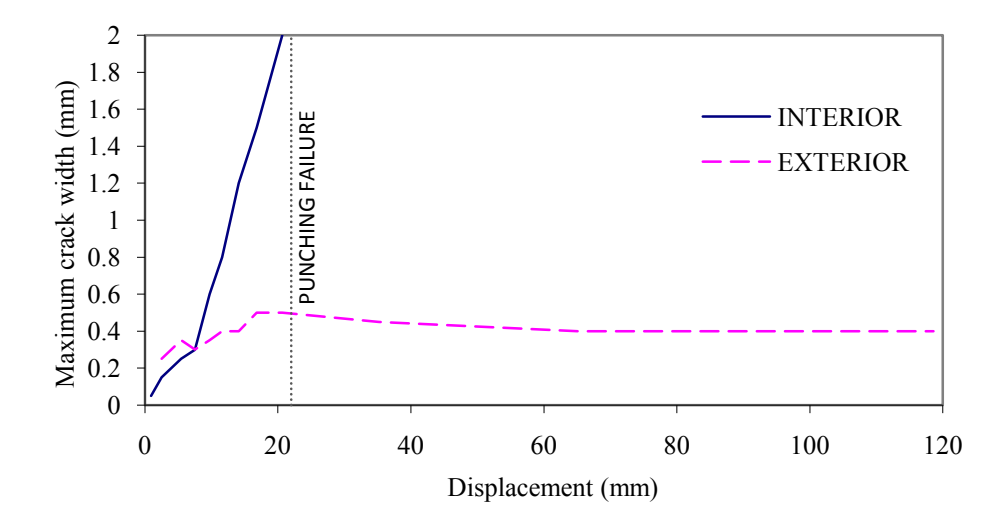


Figure 3.5 Maximum crack width versus displacement for specimen S1 of interior cracks (near column) and exterior cracks (near outer edges of specimen)

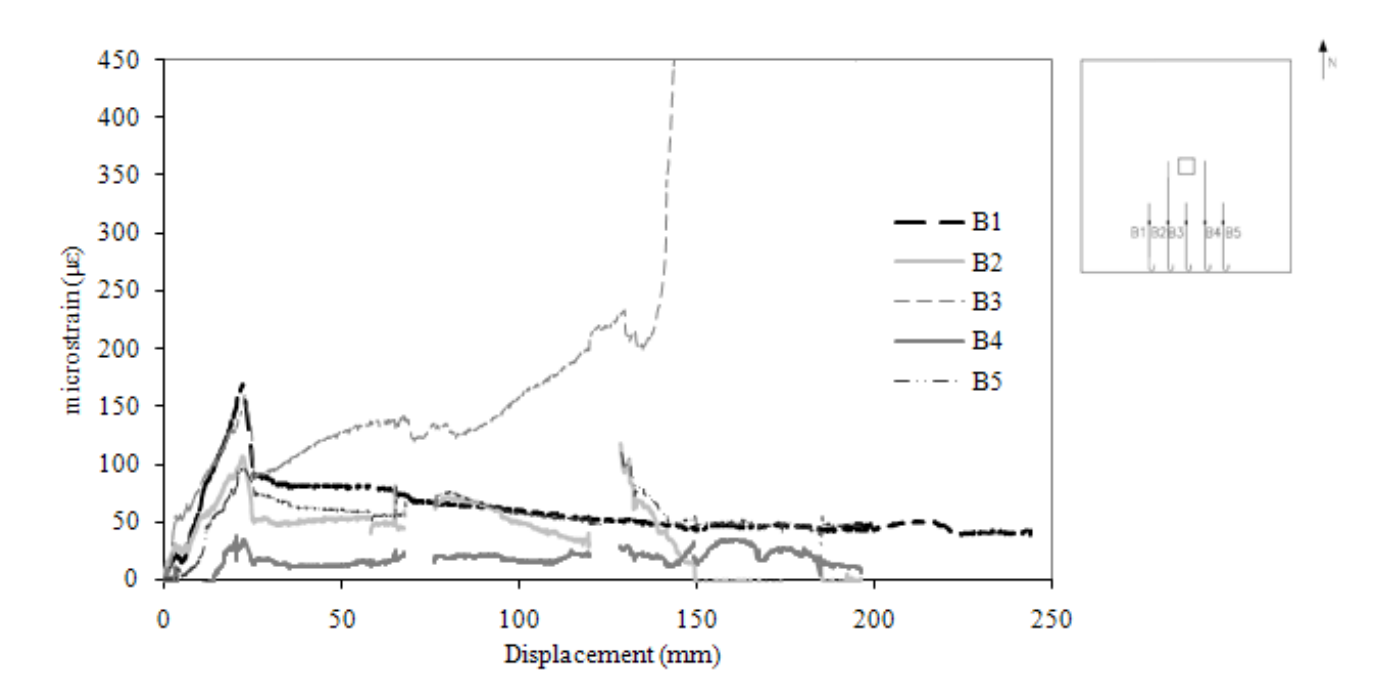


Figure 3.6 Strain-displacement behaviour of bottom reinforcing steel of gauges B1-B5 in specimen S1

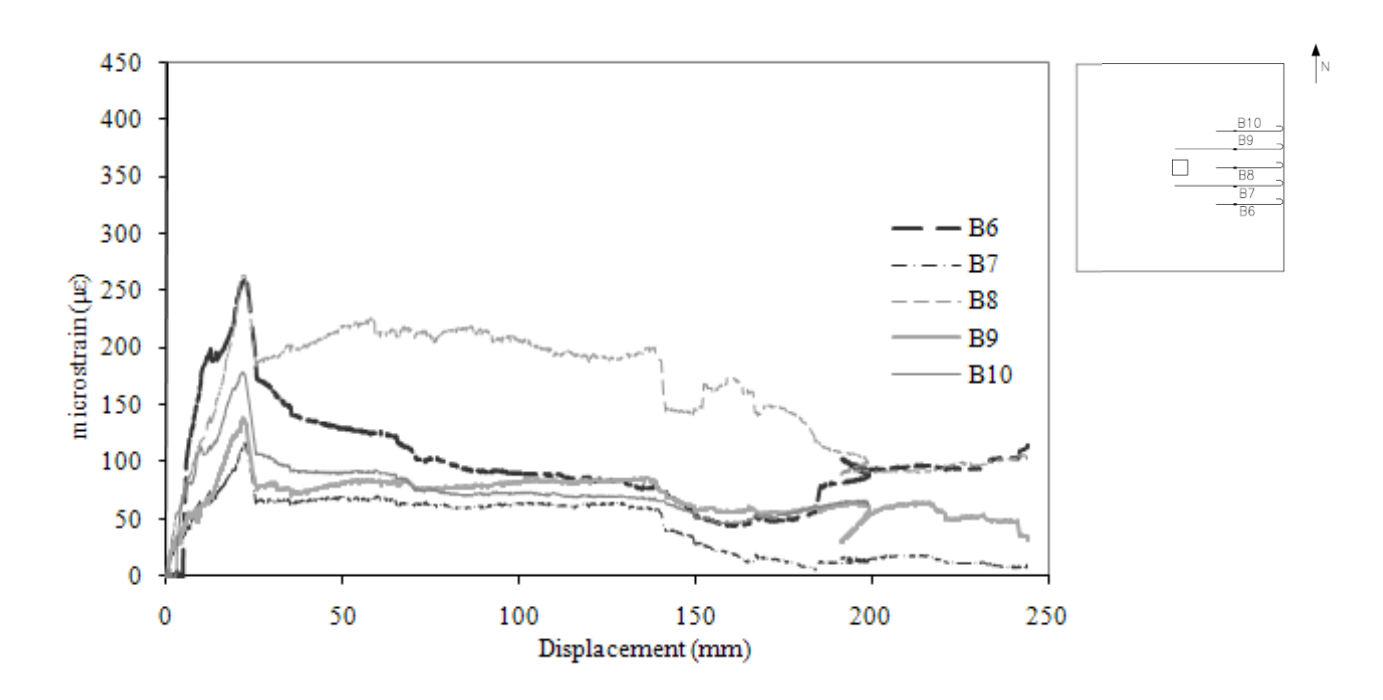


Figure 3.7 Stain-displacement behaviour of bottom reinforcing steel of gauges B6-B10 in specimen S1

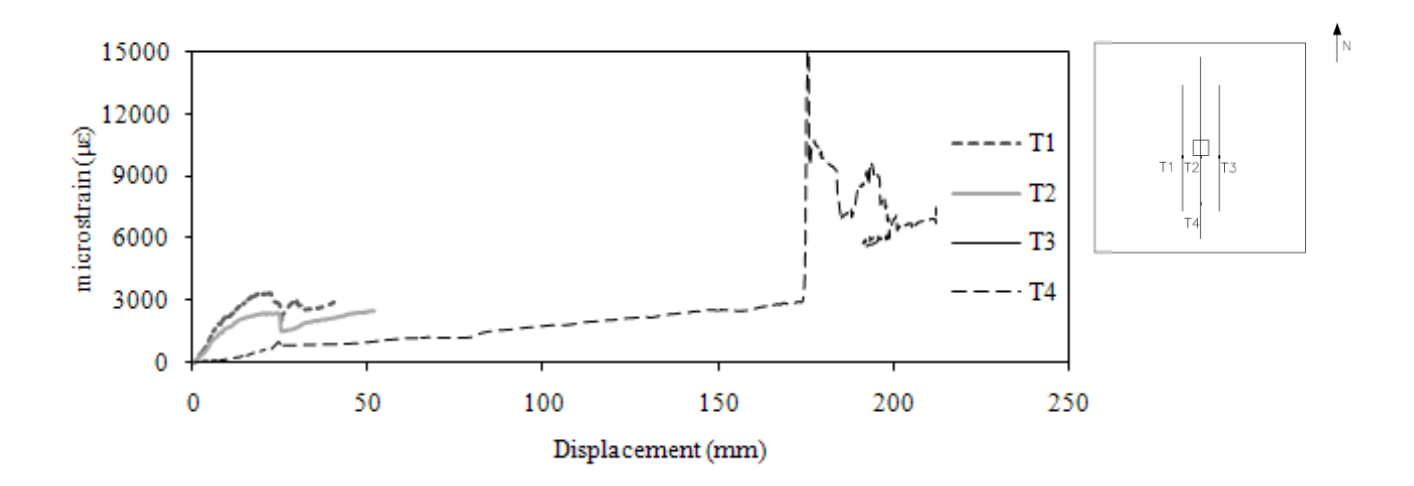


Figure 3.8 Stain-displacement behaviour of top reinforcing steel of gauges T1-T4 in specimen S1

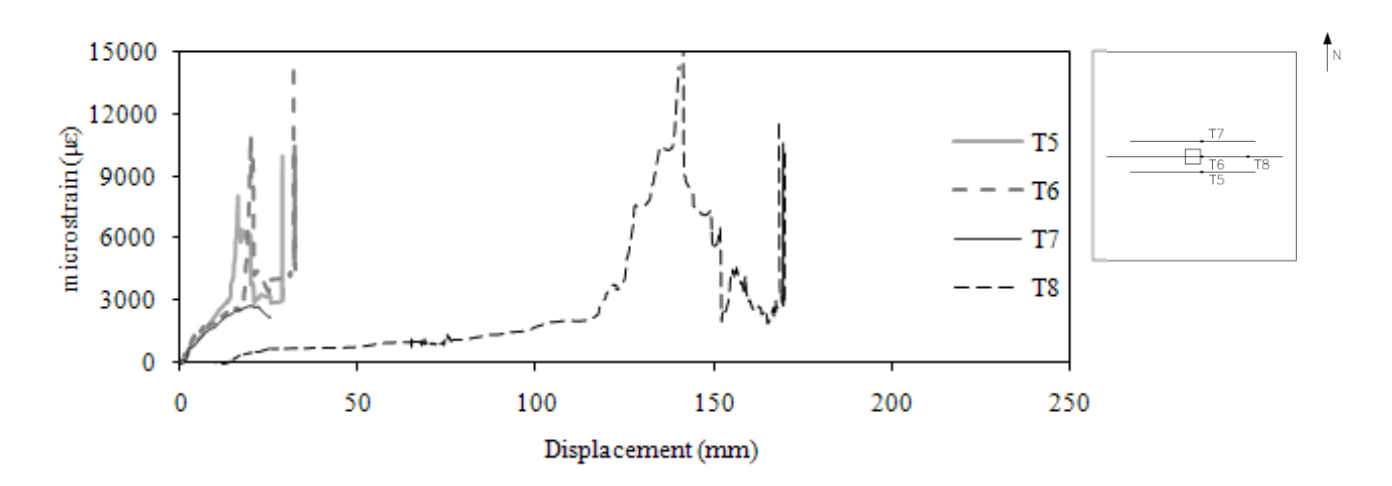


Figure 3.9 Stain-displacement behaviour of top reinforcing steel of gauges T5-T8 in specimen S1

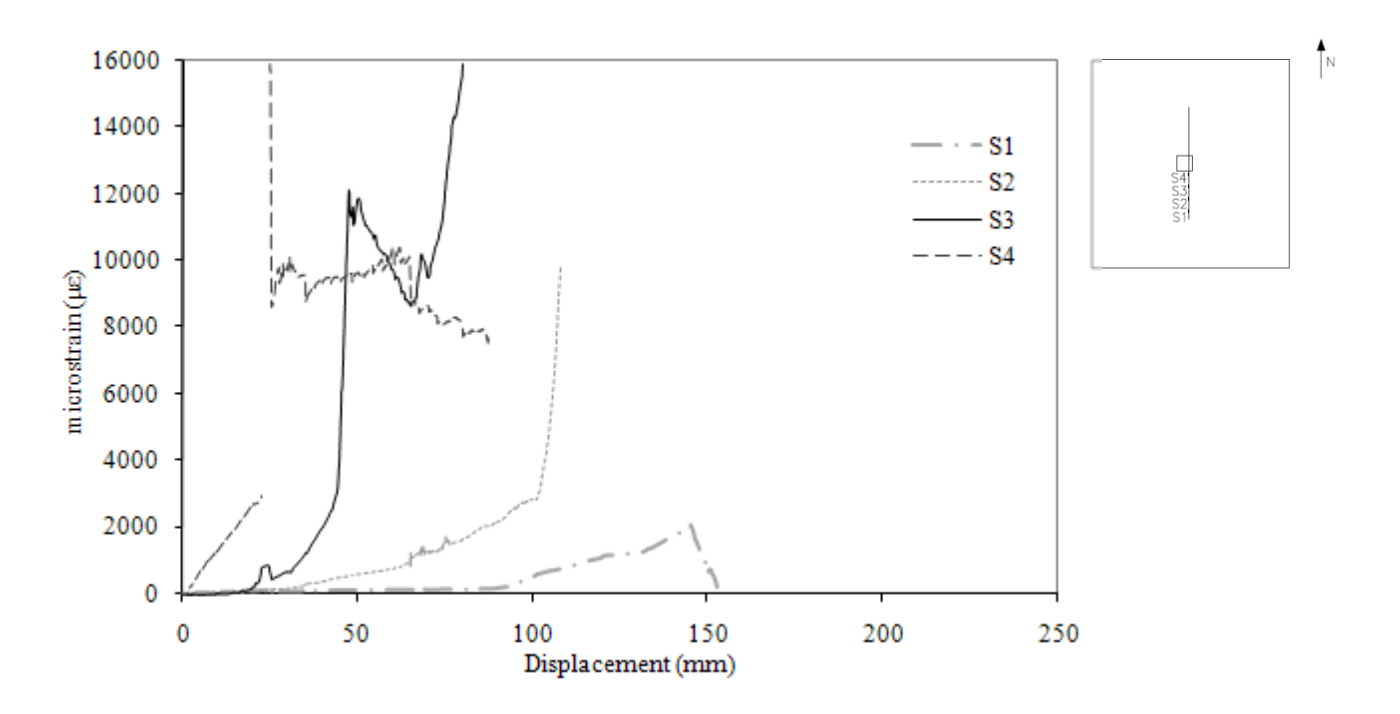


Figure 3.10 Stain-displacement behaviour of structural integrity reinforcing steel of gauges S1-S4 in specimen S1

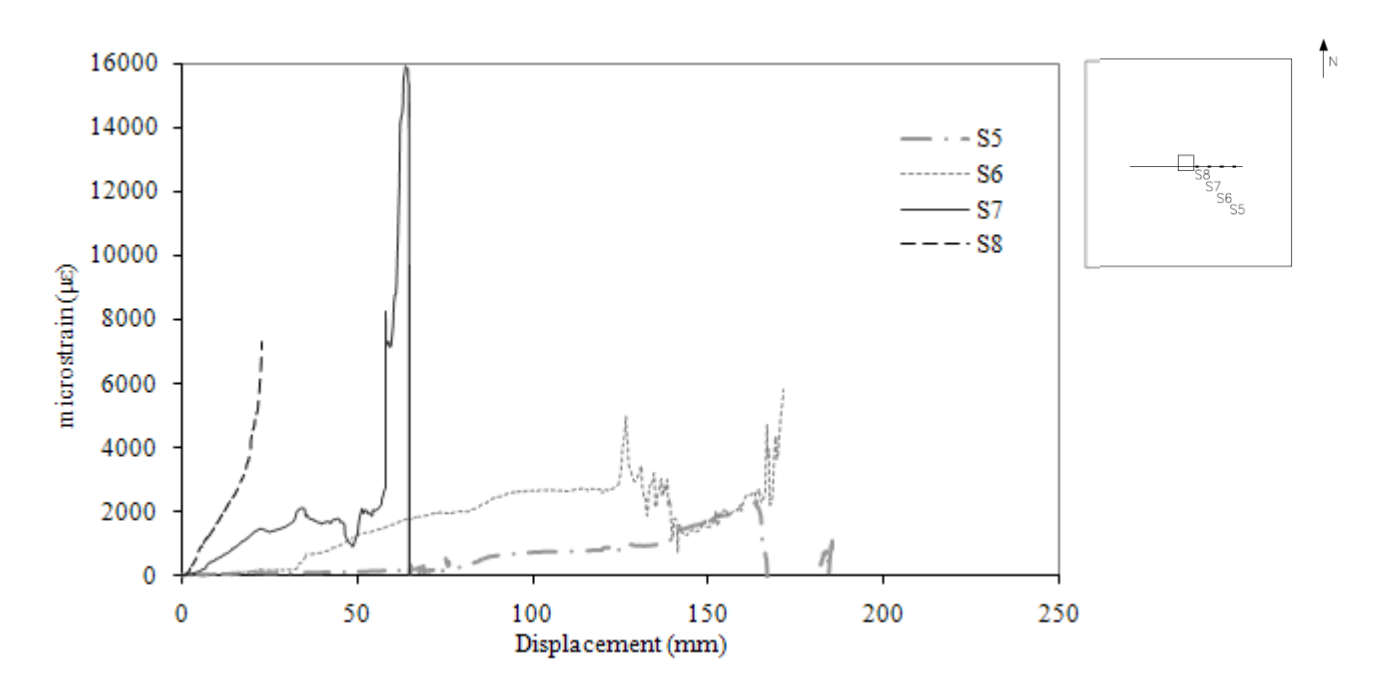


Figure 3.11 Stain-displacement behaviour of structural integrity reinforcing steel of gauges S5-S8 in specimen S1

## 3.3 Specimen S2

### 3.3.1 Test description

The complete shear-displacement behaviour of the specimen is shown in Figure 3.12, and a summary of key load stages in the test is provided in Table 3.3. The behaviour closely follows the typical load-displacement diagram of reinforced concrete slabs experiencing membrane action, as the peak shear value at punching failure was followed by a sudden drop in shear and a significant increase in deflection. Then, the shear carried by the specimen increased as deflection increased.

At load stage 3, hairline cracking at the corners of the column was observed, indicating the presence of punching shear stresses. Cracks along the centerline of the specimen extended the full width of the specimen in all four directions by load stage 4. The shear-displacement curve (Fig. 3.12) shows the change in stiffness of the specimen as cracking developed.

By load stage 9, data from strain gauges showed that top reinforcing steel was yielding near the column, and cracking around the column was extensive, forming a ring that is characteristic of punching shear failure (Fig. 3.13). By load stage 11, structural integrity reinforcing steel was yielding near the column.

At load stage 13, the upcoming punching shear failure was evident, as there was a slight depression at the cracking at the northwest corner of column. Punching shear failure occurred at load stage 14 at a peak shear of 314 kN. Figure 3.14 shows the characteristic cone failure around the column. The failure resulted in a sudden drop in shear to 117 kN and an increase in deflection from 22 mm to 26 mm.

Loading continued after punching shear failure. The significant loss in stiffness compared to the initial loading response was evident, as deflection of the specimen increased. By load stage 16, the concrete around the column and within the punching shear cone broke up (Fig. 3.15). Loose concrete was removed from around the column to expose the structural integrity reinforcing steel. The uppermost (E-W) top reinforcing steel had ripped out of the top surface of the slab to a greater extent than the underlying (N-S) top reinforcing steel (Fig. 3.16).

At load stage 17, the centre uppermost (E-W) top reinforcing steel pulled out suddenly and nearly completely. This was followed by significant tear-out of the uppermost (E-W) top reinforcing steel on each side of centre at load stage 18, then followed by tear-out of the centre underlying (N-S) top reinforcing steel (Fig. 3.17). At load stage 19, the shear dropped suddenly as the column split locally under the bars passing through the column (Fig. 3.18).

The peak shear carried during the post-punching failure response was 333 kN at a deflection of 228 mm. Testing was completed when the shear carried by the specimen was no longer increasing as deflection increased.

After concrete was removed from around the column, the angle below the horizontal of top and structural integrity reinforcing steel was measured. Table 3.4 provides the angles of the top and structural integrity reinforcing steel for the final 6 load stages. On the east and west sides of the column, structural integrity reinforcing steel was held down by top reinforcing steel extending in the perpendicular (N-S) direction. At the location of this perpendicular reinforcing steel, there was a distinct change in the angle of the structural integrity reinforcing steel (Fig. 3.19); two values of angles are given in Table 3.4.

Finally, bars were manually examined for loss of bond by twisting them with a vice grip. The structural integrity reinforcing bars showed no evidence of pullout bond failure.

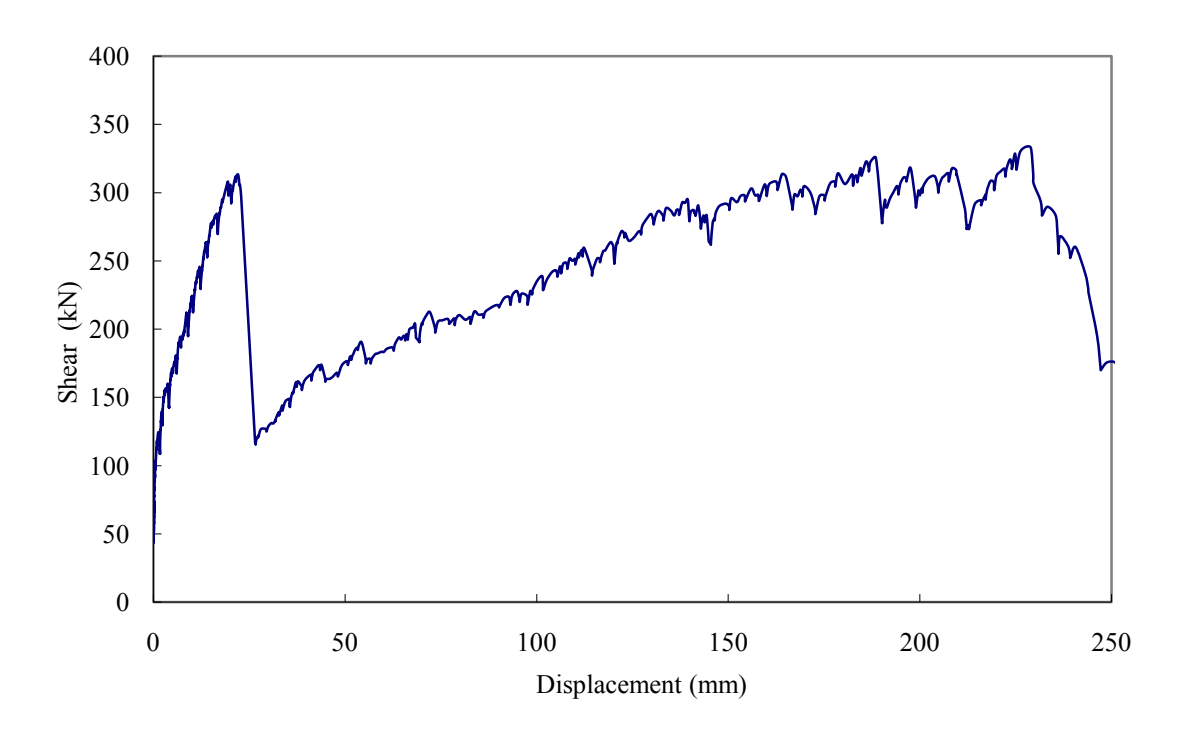


Figure 3.12 Shear-displacement behaviour of specimen S2

Table 3.3 Summary of key load stages in test of specimen S2

	Shear (kN)	Deflection (mm)
First Cracking	103	0.2
First Yield (Top Reinforcement)	212	9
First Yield (S.I. Reinforcement)	275	15
Punching Failure	314	22
Post-Punching Peak Shear	333	228

#### 3.3.2 Concrete cracking and strains

Figure 3.20 shows the maximum crack widths near the column and near the specimen edges for the duration of the test. Cracks near the column widened quickly as the specimen was loaded and failed in punching shear. During the post-punching response, the crack widths near the column were not measured because the top concrete was loose. Cracks near the outside edge of the specimen were initially larger than the interior cracks, probably due to a lack of flexural reinforcement near the edges of the specimen. The exterior cracks were widest (0.5 mm) at punching failure. After punching failure, which corresponds with a displacement of 22 mm, the exterior cracks closed slightly to 0.4 mm and then remained constant in width.

To confirm the behaviour of the exterior cracks, four pairs of targets were glued to the surface of the slab, and readings were taken with a mechanical extensometer. Figure 3.21 presents the strain-displacement behaviour for the four pairs of targets. Cracks passed between the SE and ES targets; consequently, significant changes in distance between the two targets at each of these locations occurred during the test. Most importantly, the distance between the targets increased with increasing shear up to punching failure, decreased suddenly as shear dropped, and then remained small as shear increased during the post-punching response. The closure of these cracks throughout the post-punching response suggested that the edges of the specimen were in compression.

### 3.3.3 Reinforcement strains

Figures 3.22 to 3.27 present the data collected from the strain gauges placed on top, bottom, and structural integrity reinforcing steel. Where no data is presented, the strain gauge was broken either during casting of the concrete or during testing.

The strain-displacement curves of the bottom reinforcement (Figs. 3.22 and 3.23) closely resemble the shape of the shear-displacement curve (Fig. 3.12). The strains peaked at the time of punching failure and then dropped off. Throughout the post-punching response, the strains in the bottom reinforcement were less than the yield strain of the steel, except for the centremost bar.

The six strain gauges on the top reinforcement near the column face – T1, T2, T3, T5, T6, T7 – were ineffective after punching failure, as the concrete around the column broke up (Figs. 3.24 and 3.25). Strain gauges T4 and T8, near the ends of the centre bar, measured high strains during the post-punching response. Gauge T8, on the uppermost layer of top reinforcing steel, stopped working before gauge T4, on the innermost layer of top reinforcing steel. This was because the uppermost layer of top reinforcing steel tore out of the top surface of slab sooner than the innermost layer of top reinforcing steel.

Strain-displacement curves are shown in Figures 3.26 and 3.27 for the structural integrity reinforcement. The strain gauges closest to the column face – S4 and S8 – yielded before punching failure due to significant bending moments at the column face. The measurements at all other locations along the structural integrity reinforcement achieved strains greater than the yield strain of steel during the post-punching response.

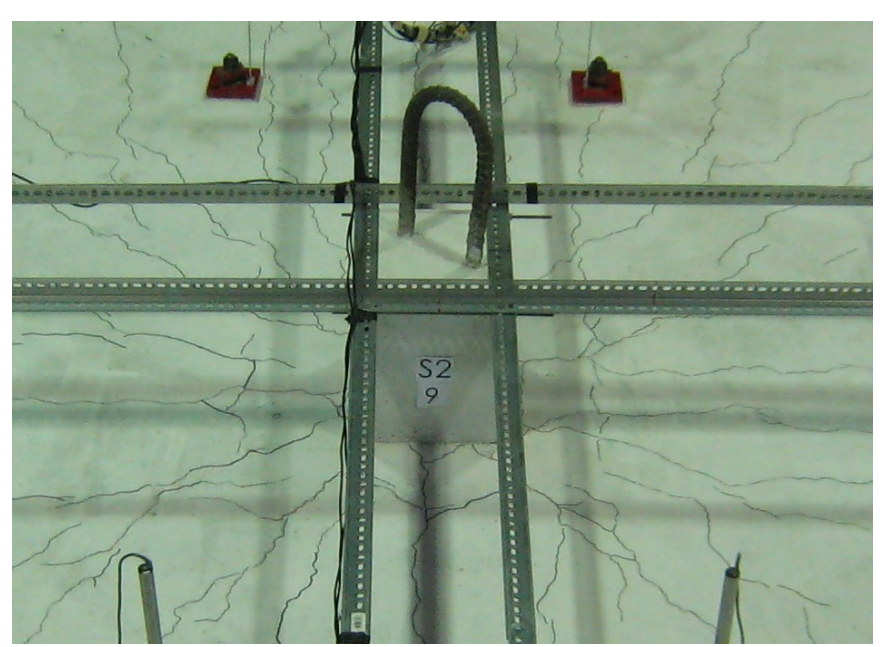


Figure 3.13 Load stage 9 of test S2. Cracking around column is characteristic of punching shear.

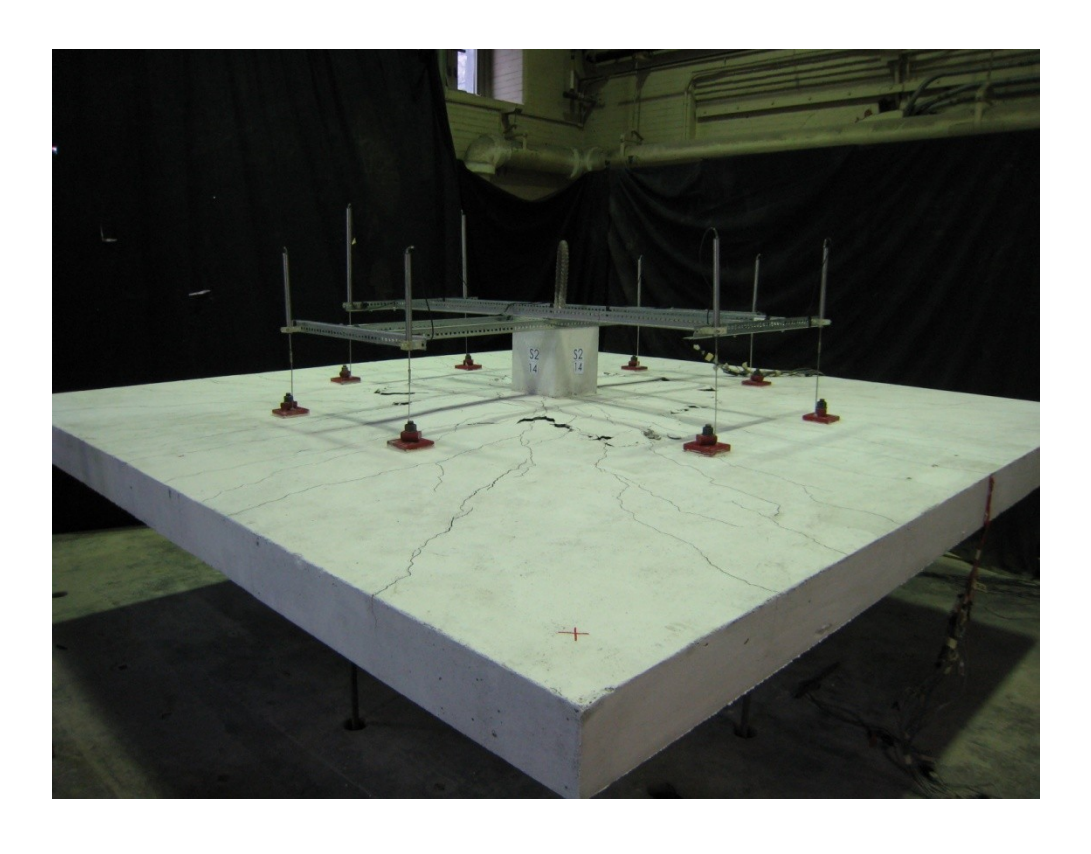
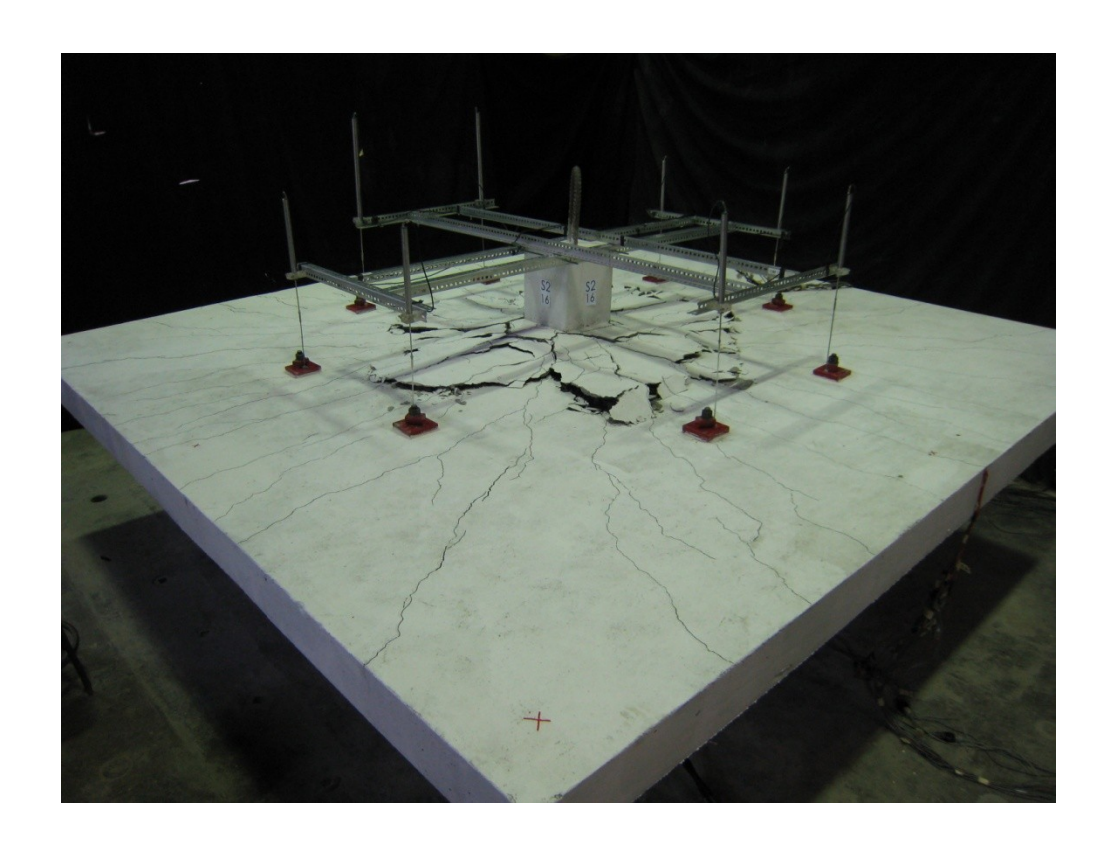




Figure 3.14 Load stage 14 of test S2. Punching shear failure.



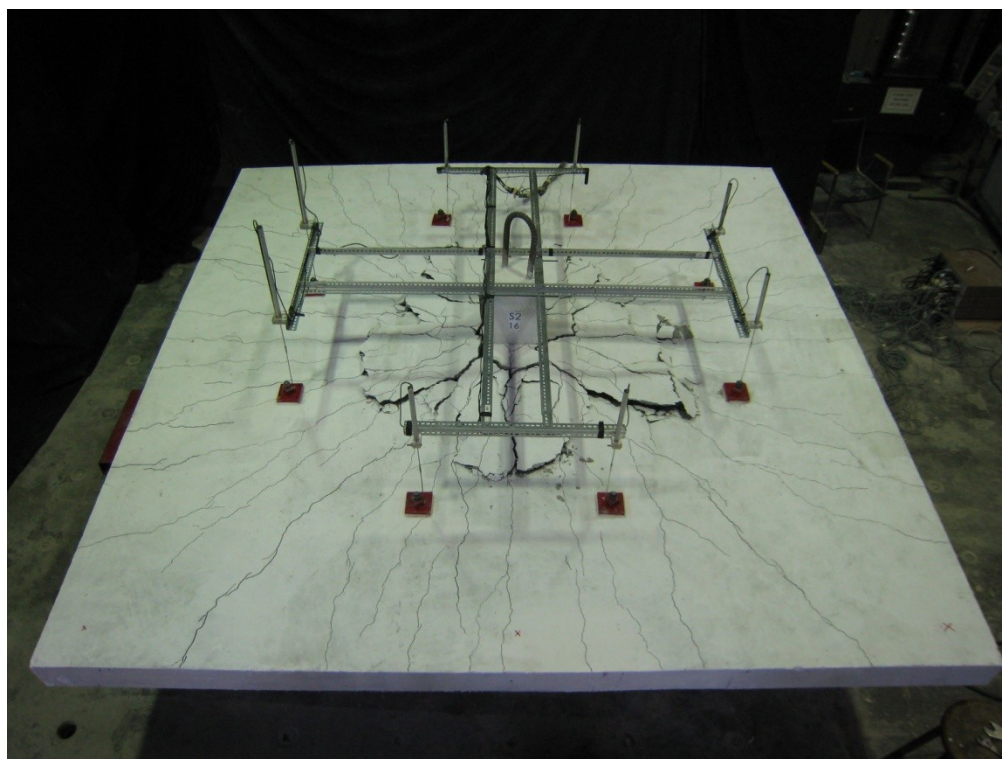


Figure 3.15 Load stage 16 of test S2. Before removal of concrete.



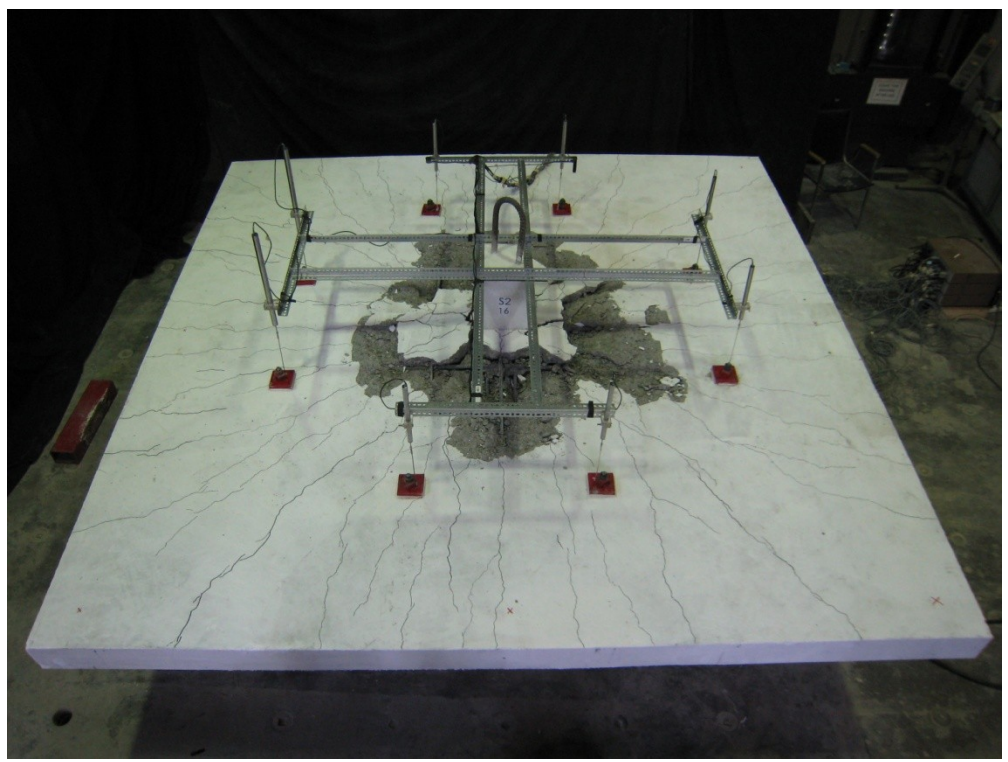


Figure 3.16 Load stage 16 of test S2. After removal of concrete.

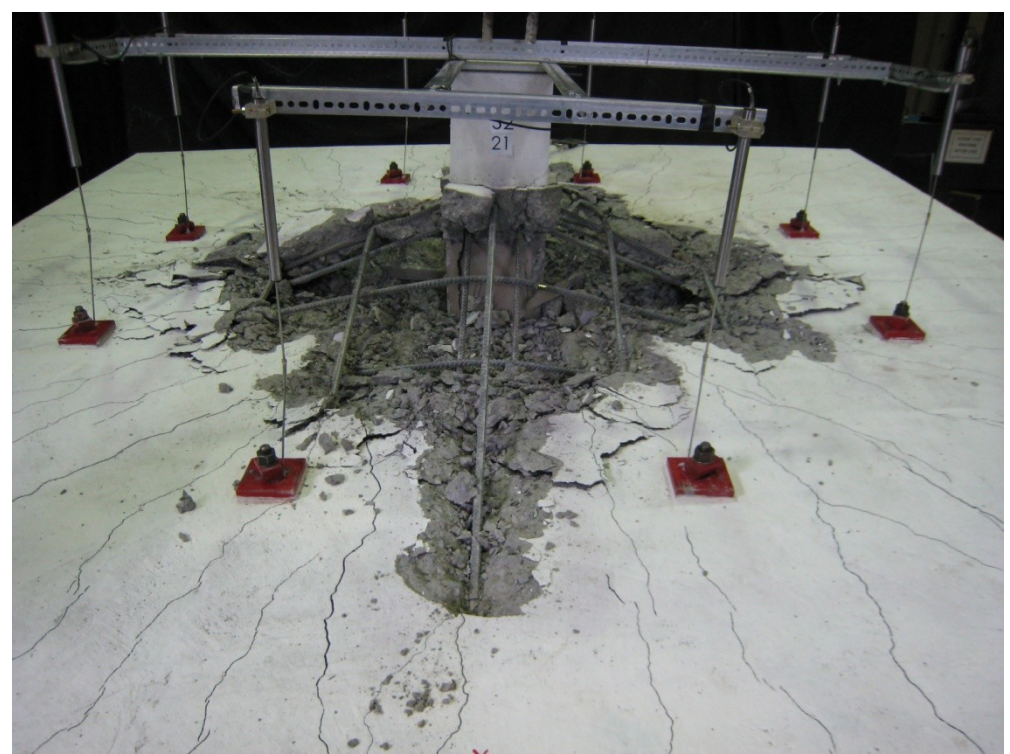


Figure 3.17 Completion of test S2. E-W top reinforcement nearly completely ripped out.

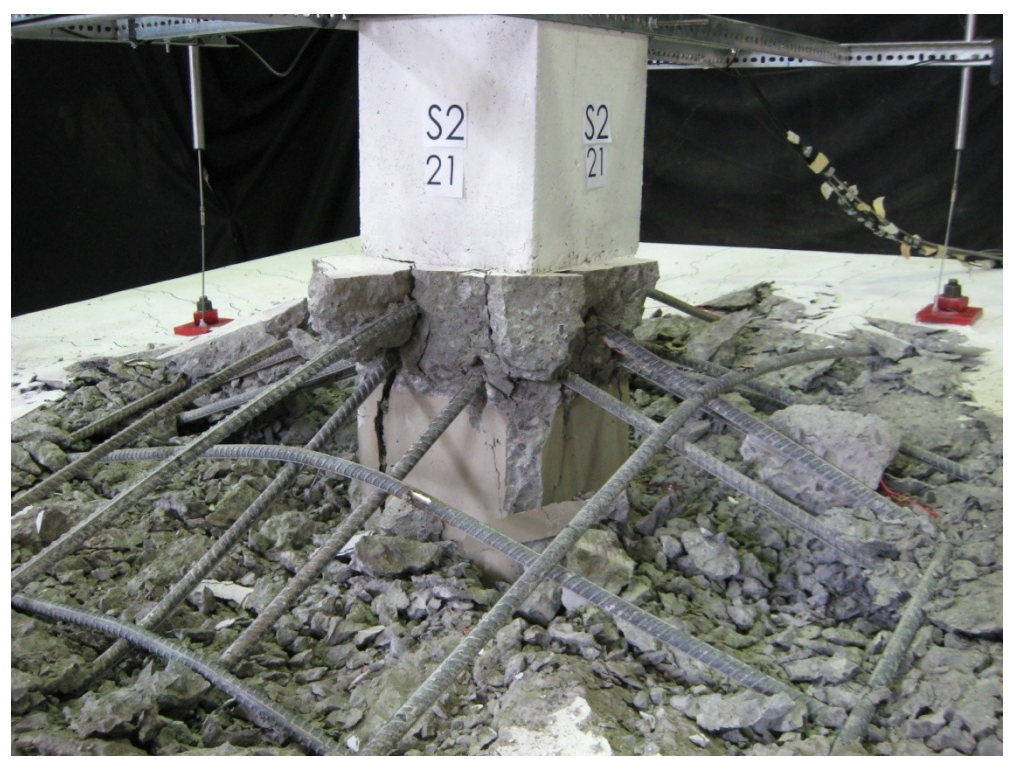


Figure 3.18 Completion of test S2. Column split.



Figure 3.19
Angle of structural integrity reinforcement. Perpendicular bar caused change in angle.

Table 3.4 Angle below the horizontal of top and structural integrity reinforcing steel near the column face (Specimen S2).

		Load Stage					
		16	17	18	19	20	21
	NW				18	18	22
	NE			18	20	21	26
	EN	9	17/12	18/14	18/17	19/17	24/24
Structural	ES		15/11	17/12	22/19	22/16	22/22
Integrity Reinforcing Steel	SE			17	17	18	19
Kemioreing Steel	SW			15	16	20	20
	WS	11	15	19/15	21/20	27/24	32/27
	WN	13	18/15	20/14	22/21	26/24	33/31
	N				20/16	19	23
Ton	Е			8	10	9	15
Top Reinforcing Steel	S			18/12	20/16	19/18	25/20
remioreing seed	W			10	12	15	21

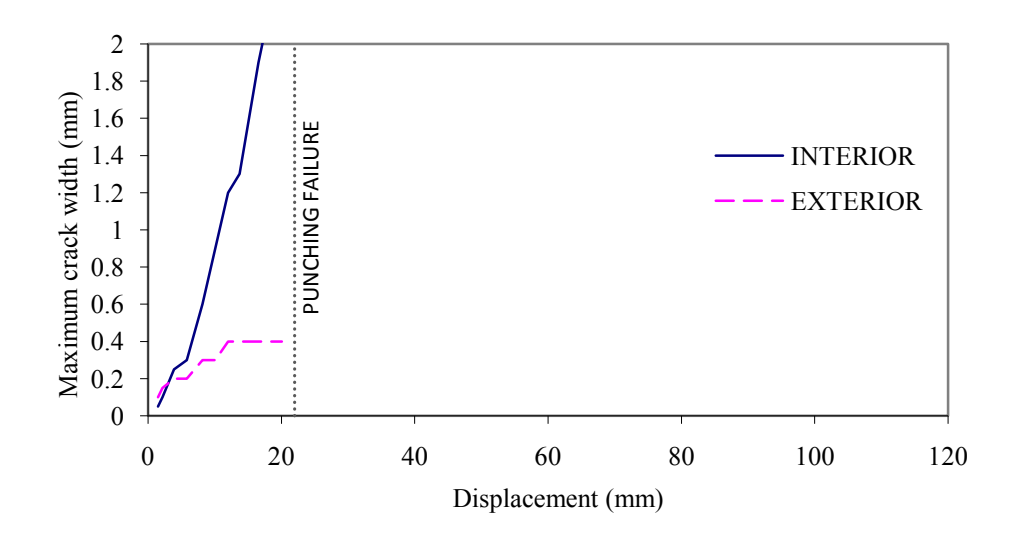


Figure 3.20 Maximum crack width versus displacement for specimen S2 of interior cracks (near column) and exterior cracks (near outer edges of specimen).

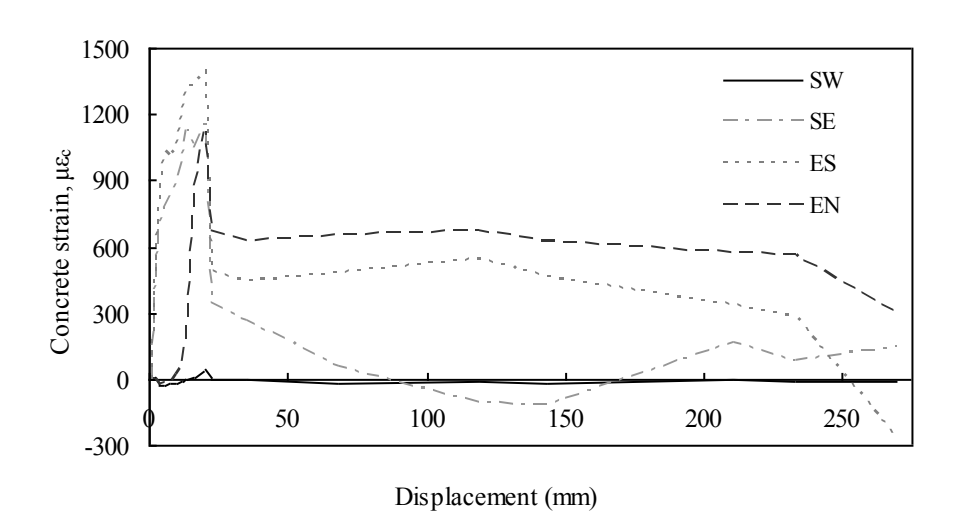


Figure 3.21 Strain-displacement diagram of concrete at slab edges in specimen S2 (see Figure 2.12 for locations of readings).

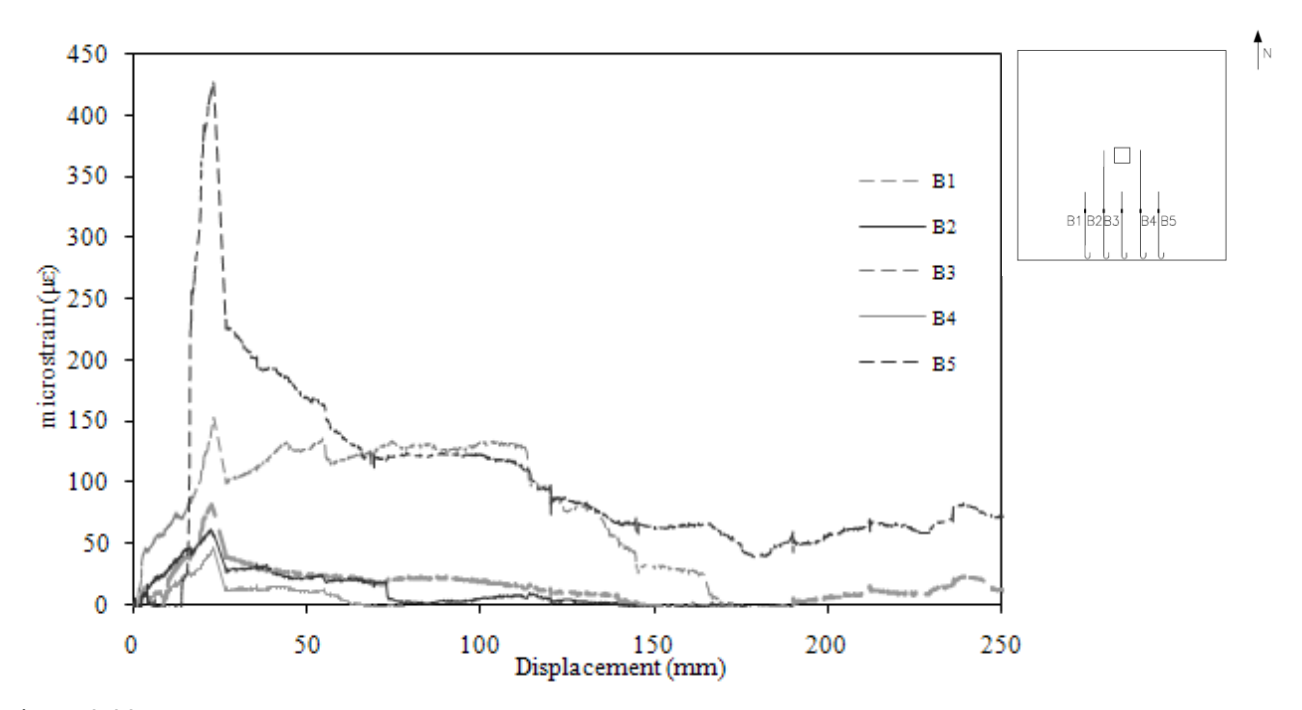


Figure 3.22 Strain-displacement behaviour of bottom reinforcing steel of gauges B1-B5 in specimen S2

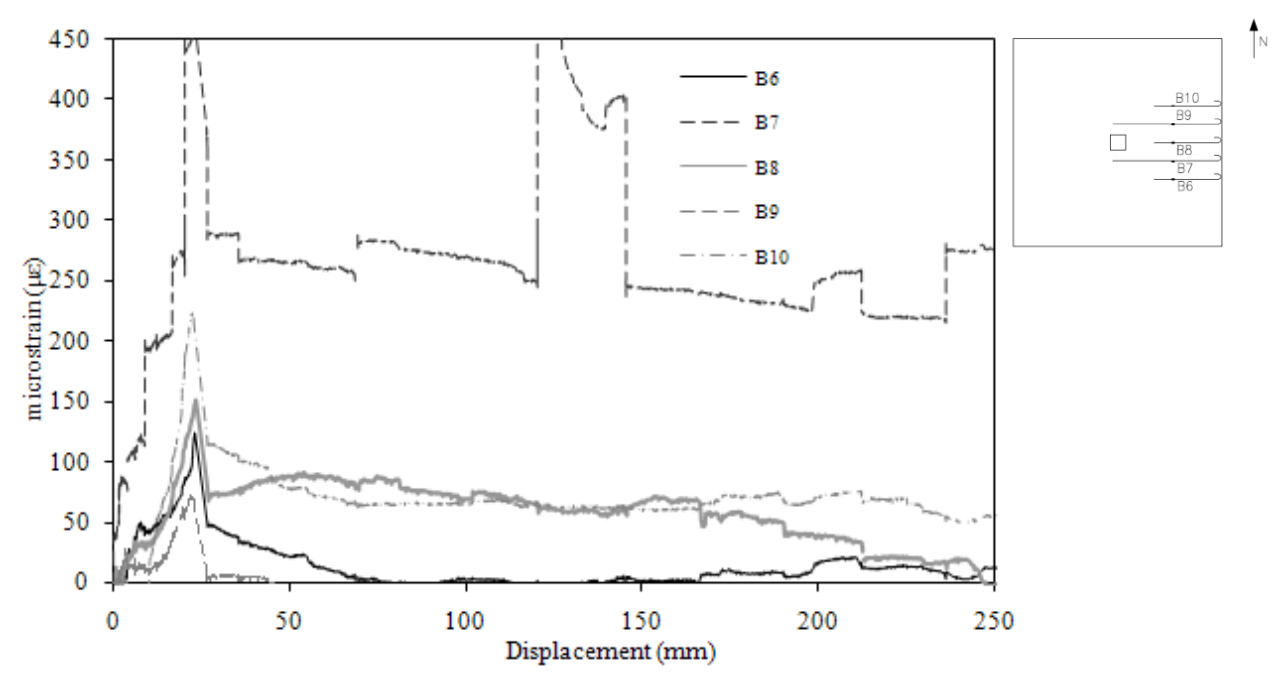


Figure 3.23 Strain-displacement behaviour of bottom reinforcing steel of gauges B6-B10 in specimen S2

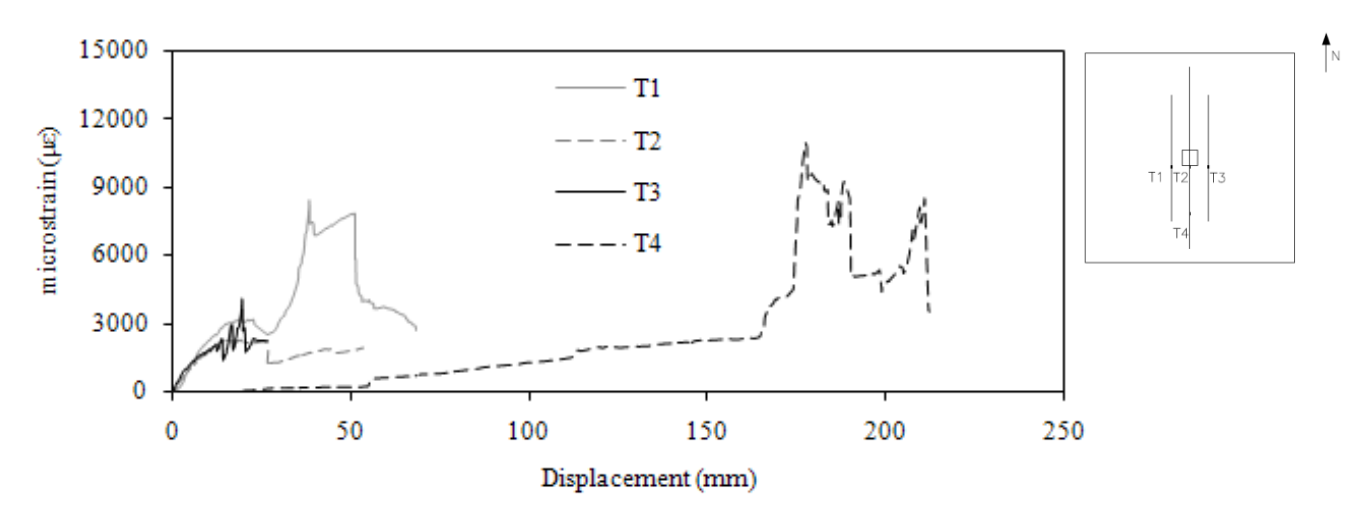


Figure 3.24 Strain-displacement behaviour of top reinforcing steel of gauges T1-T4 in specimen S2

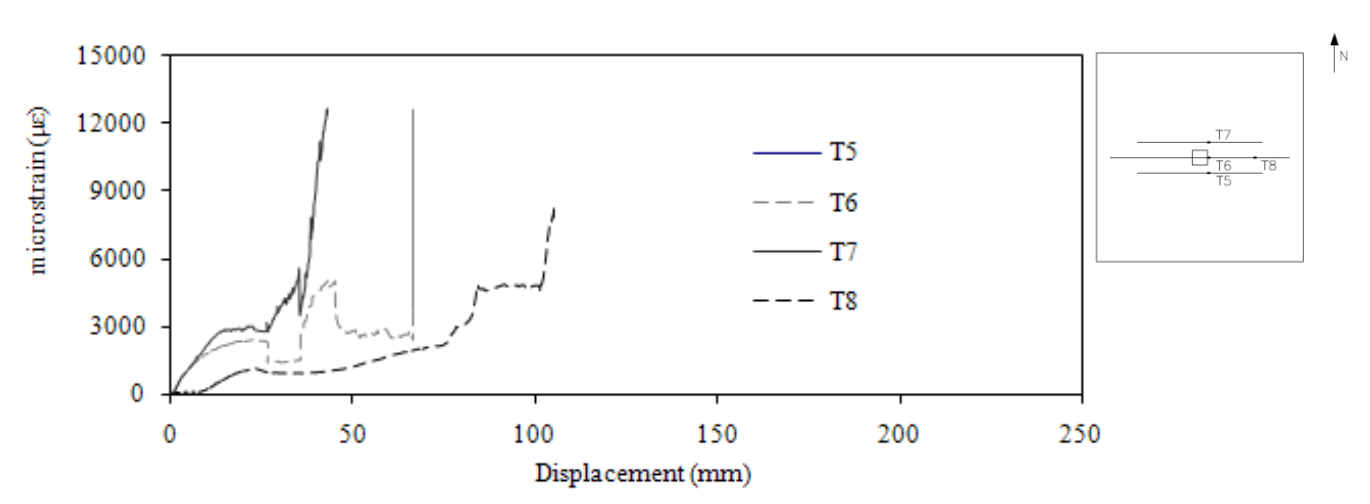


Figure 3.25 Strain-displacement behaviour of top reinforcing steel of gauges T5-T8 in specimen S2

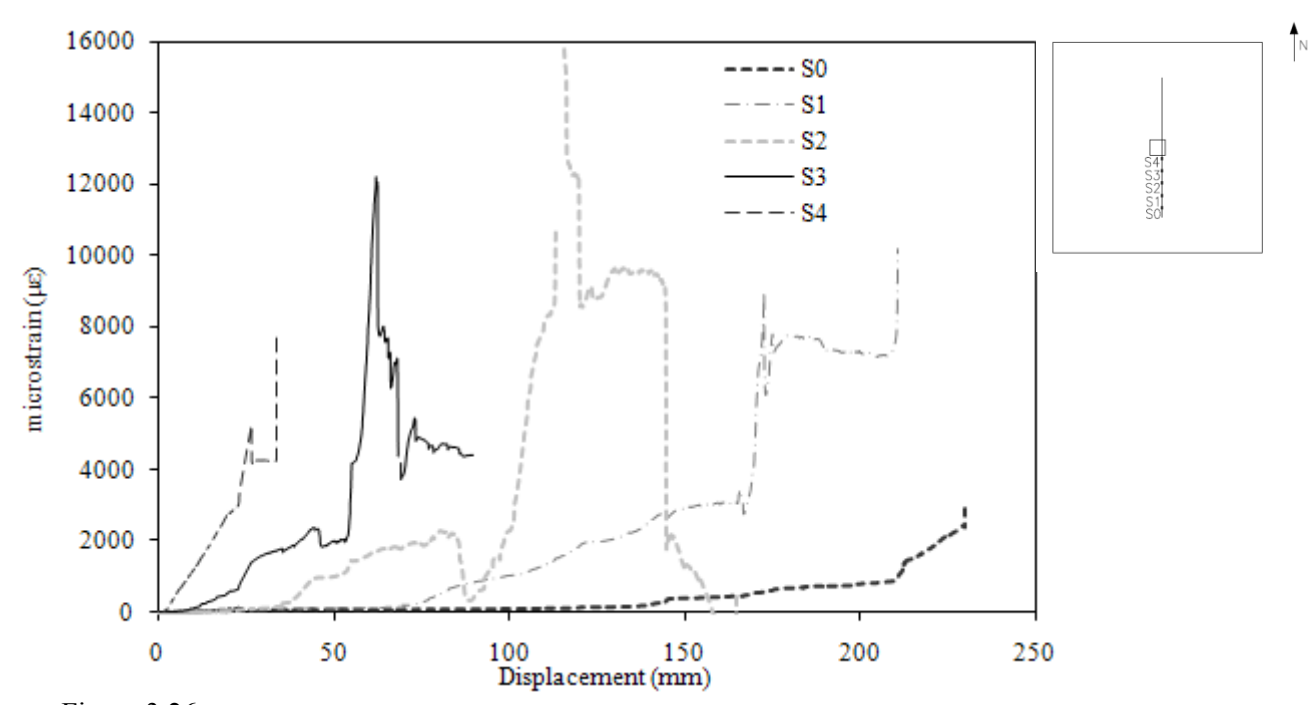


Figure 3.26 Strain-displacement behaviour of structural integrity reinforcing steel of gauges S0-S4 in specimen S2

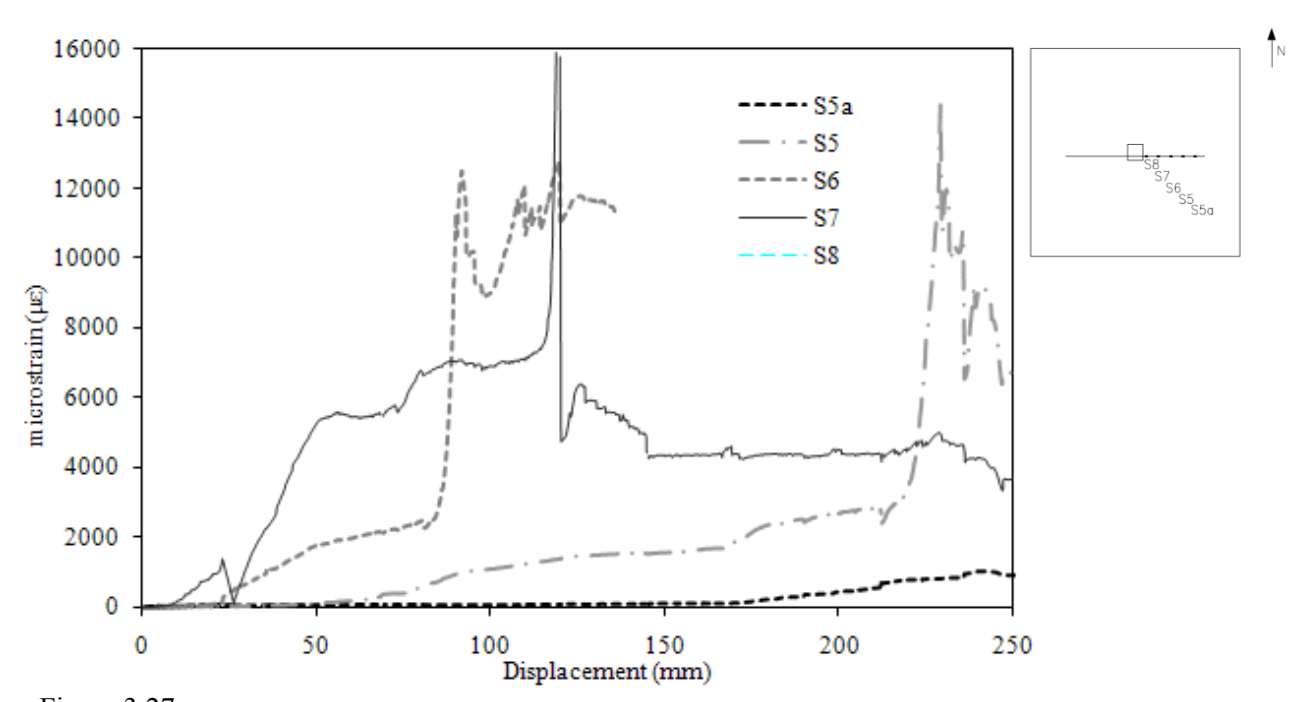


Figure 3.27 Strain-displacement behaviour of structural integrity reinforcing steel of gauges S5a-S8 in specimen S2

# **Chapter 4**

# **Comparison of Test Results and Predictions**

### 4.1 Introduction

The testing results of the two specimens are used to discuss the post-punching response mechanism of flat plate slab-column connections. The discussion considers three possible failure modes – yielding of reinforcing steel; pullout bond failure; and breakout concrete failure – as well as the contribution of top reinforcing steel to the post-punching failure resistance. Also, a comparison is made between the experimental results and the failure loads predicted by current design standard CSA A23.3-04 (2004) for punching shear failure and post-punching failure response. Then, the experimental results are compared to the post-punching failure resistance predicted by Melo and Regan (1998), and the experimental results of Ghannoum (1998) are discussed.

## 4.2 Comparison of Test Results of Specimens S1 and S2

#### *4.2.1 Load-deflection response*

Figure 4.1 presents the shear-displacement behaviour of the two slab-column specimens S1 and S2. The shape of the responses suggest that both specimens developed a post-punching resisting mechanism, as punching failure was followed by a sudden drop, then a gradual increase in load. Specimen S2 resisted greater shears at both punching failure and peak post-punching resistance. Specimen S2 also displayed greater ductility, as the specimen achieved significantly greater displacements. Table 4.1 summarizes the shear and the average deflection of the key load stages of the specimen tests.

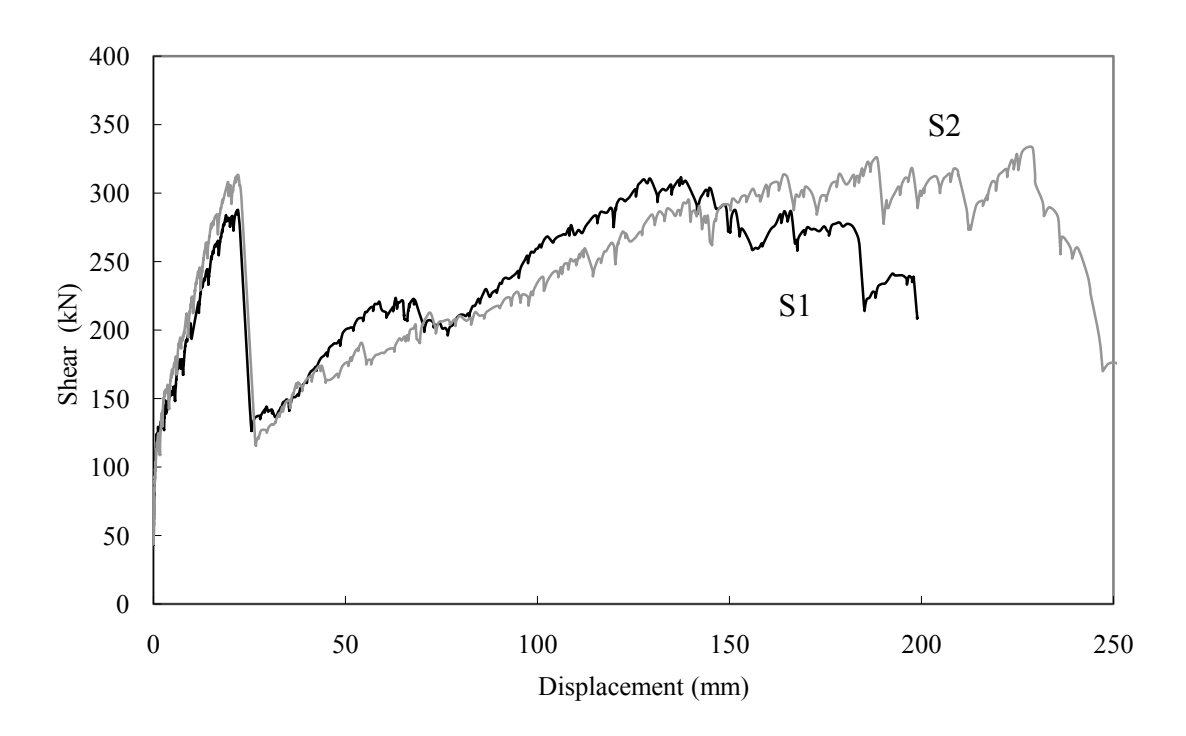


Figure 4.1 Shear-displacement behaviour of specimens S1 and S2

Table 4.1 Summary of shear-displacement behaviour of specimens S1 and S2

	Shear	: (kN)	Deflection (mm)	
	<b>S1</b>	S2	<b>S</b> 1	<b>S2</b>
First Cracking	123	103	0.9	0.2
First Yield 193 (Top Reinforcement)		212	9	9
First Yield (S.I. Reinforcement)			12	15
Punching Failure	289	314	22	22
Post-Punching Peak Shear	314	333	138	228

#### 4.2.2 Punching failure

First cracking was observed earlier in specimen S2 than in S1. In both specimens, cracking initiated at the corners of the column.

Data collected by the strain gauges showed that top reinforcement first yielded at a load level 10% higher in specimen S2 than in specimen S1. First yielding of structural integrity reinforcement was recorded at a load level 26% higher in S2.

Punching shear failure occurred at shears of 289 kN and 314 kN, in specimens S1 and S2, respectively. The increase was 9% for specimen S2. A slightly higher punching shear failure load was expected in specimen S2, as the concrete strength given by materials testing shows slightly higher strength.

### 4.2.3 Post-punching response

The peak shears achieved by specimens S1 and S2 during the post-punching failure response were 314 kN and 333 kN, respectively – a difference of 6% (Table 4.1). The test results were more markedly different in the deflection behaviour of the specimens, and the increased ductility of specimen S2 is clearly seen in Figure 4.1. Specimen S2 supported its peak shear at a deflection of 228 mm while S1 reached its peak shear at 138 mm. In addition, the test of specimen S2 was terminated when the carried shear suddenly dropped as the column split under local stresses of the structural integrity reinforcing steel; the post-punching resistance was not yet limited by the structural integrity reinforcement.

Table 4.2 presents data from the test of specimen S2 suggesting that the structural integrity reinforcing steel was yielding at the peak shear. If the peak shear and the average measured angle of 21 degrees are used in Eq. 1.7, taken from CSA A23.3-04 (2004), the stress in the steel is calculated as 580 MPa, which is greater than the yield strength of 457 MPa, but still less than the ultimate strength of 594 MPa. It is clear from the measured strains in the structural integrity reinforcement that this reinforcement yielded. These predictions assumed that the top reinforcement was not contributing to the post-punching shear resistance.

Table 4.2 Calculated stress of structural integrity reinforcement of specimen S2

Test Specimen	Load Stage	Average Angle (degrees)	Shear (kN)	Calculated stress of steel f <sub>s</sub> (MPa)
<b>S2</b>	20	21	333	580

Park (1964), Hawkins and Mitchell (1979), and Mitchell and Cook (1982) described tensile membrane action or the post-punching behaviour of slabs such that resistance is limited by the yield strength of the reinforcement. Similarly, Melo and Regan (1998) proposed an equation to explain their experimental results that relied upon the ultimate strength of the reinforcement.

Testing of specimen S1 was terminated when bond pullout failure occurred. Structural integrity reinforcing steel was slipping during loading, ensuring that reinforcement would no longer carry its yield stress and that higher shears would not be supported by the slab-column connection. Inspection at the end of the test showed that bars on the south and west sides of the column had lost all bond. In contrast, there was no slipping of bars during the testing of specimen S2, and at the completion of the test, none of the bars showed evidence of bond loss. The increased length of structural integrity reinforcing steel in S2, over which stress is transferred from steel to concrete, prevented bond failures in testing of specimen S2. Consequently, in the post-punching failure response, specimen S2 achieved a slightly greater peak shear at a considerably larger deflection than specimen S1.

Park (1964), Hawkins and Mitchell (1979), Mitchell and Cook (1982), and Melo and Regan (1998) also emphasized the necessity of properly anchoring reinforcement to achieve the desired post-punching resisting mechanism, which is limited by the yielding of reinforcement. To achieve proper anchorage, Mitchell and Cook recommended that structural integrity reinforcing steel extend a minimum of  $2l_d$  immediately outside the support reaction area, where  $l_d$  is the tension development length. Specimen S1 was detailed to this recommendation. Melo and Regan suggested that the anchorage of bottom bars starts at a location approximately 2d, or 2 times the effective depth of the slab, away from the support reaction area, where 2d is an estimate of the radius of the area of damaged concrete. Specimen S2 was therefore detailed with structural integrity

reinforcing steel extending a length of  $2l_d + 2d$  away from the column face. A sufficient length of reinforcement within intact concrete allows tensile forces to transfer from steel to concrete, thus allowing the reinforcing steel to develop its yield stress rather than failing by bond pullout.

Throughout the post-punching failure response, both specimens experienced significant concrete failure around the column. As shown in Figure 4.2, the concrete cracked and spalled, starting near the column and then radiating outward. Specimen S2 experienced greater disintegration of concrete around the column at a similar deflection and lower shear than specimen S1. This observation corresponds with the slightly lower stiffness of specimen S2 during the post-punching failure response (Figure 4.1). Despite its lower stiffness, specimen S2 achieved a slightly higher post-punching peak shear at a considerably larger deflection. The increased ductility of specimen S2 may be attributed to the increased length of structural integrity reinforcing steel.

A number of researchers, including Hawkins and Mitchell (1979), Mitchell and Cook (1982), Pan and Moehle (1992) and Ghannoum (1998), generally described this disintegration of concrete around the column as the "tear out" of top reinforcing bars. Melo and Regan (1998) suggested that bottom reinforcing bars also tear out due to the vertical resultant of the bars' tensile stresses, and Melo and Regan referred to ACI 349-76 Code Requirements for Nuclear Safety Related Concrete Structures (ACI 1978) to describe the failure mechanism resembling the breakout of embedments in which the tensile strength of concrete is a critical factor. Melo and Regan acknowledged that this breakout-type concrete failure is an alternative failure mode that may govern the post-punching failure response, if a large enough area of reinforcing steel is provided.

It is also noted that, at the loading locations on the slab surface, the applied load confined the concrete, reduced tensile stress within the concrete and thus reduced failure by breakout or loss of bond. However, the loading points were not located over structural integrity reinforcing steel. Also, concrete slabs are normally subjected to uniform loading, which would provide some confinement to all of the reinforcing steel. Consequently, it is felt that the experimental design provided a conservative test.

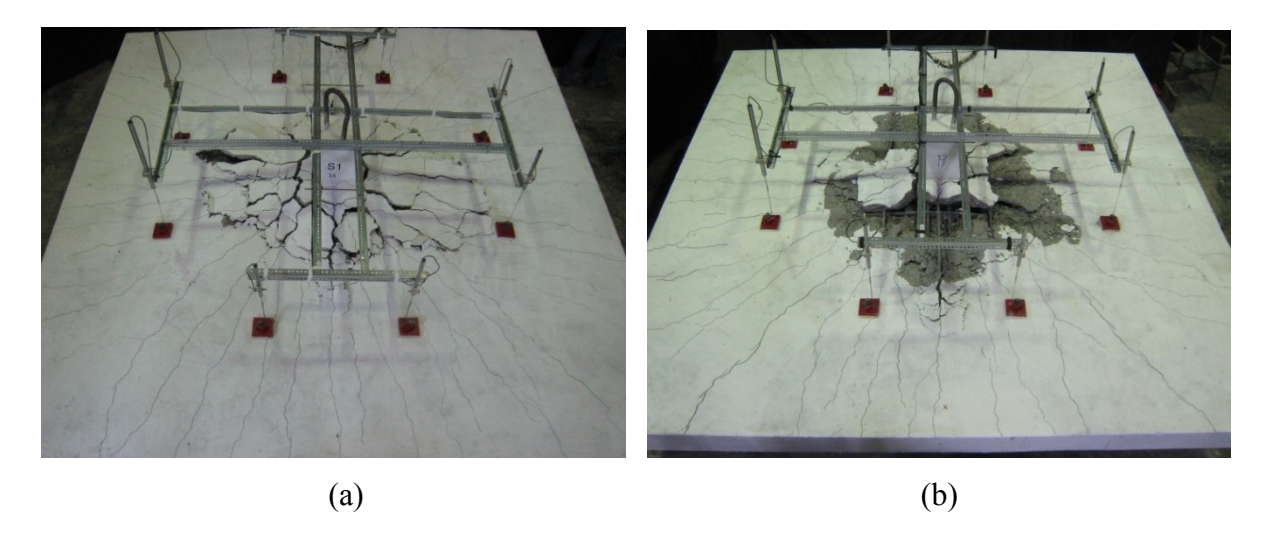


Figure 4.2 Breakout failure of reinforcement extends further from column in S2 than in S1 at similar deflection and lower shear value.

(a) S1. Shear = 288 kN. Deflection = 119 mm (b) S2. Shear = 263 kN. Deflection = 119 mm. (Concrete was removed from S2 to expose structural integrity reinforcement).

#### 4.2.4 Tensile membrane action

The shape of the responses shown in Figure 4.1 suggests that both specimens developed a post-punching resisting mechanism comparable to tensile membrane action, a behaviour that has been presented by a number of researchers, including Park (1964), Hawkins and Mitchell (1979), and Cook (1982), as a characteristic of reinforced concrete slabs (Fig. 1.1). Strain gauge data from testing confirms that the structural integrity reinforcement in the vicinity of the column developed tensile forces during the post-punching failure response. Cracks in the concrete near the edges of the slab specimen widened before punching failure and closed up during the post-punching failure response (Figs. 3.5 and 3.20). Strain measurements from concrete surface targets on specimen S2 near the edges of the slab specimen increased before punching failure and decreased during the post-punching failure response (Fig. 3.21). These observations suggest that during the post-punching failure response, concrete near the edges of the slab specimen was in compression, forming a compressive ring around the area of tension. The same self-equilibrating system, shown in Figure 4.3, was observed by Cook (1982) in his experimental program on slabs with small amounts of edge restraint. The

results of these experiments and Cook's experiments suggest that even unrestrained slabs are capable of developing tensile membrane action, a behaviour which Hawkins and Mitchell (1979) suggested allowed for an effective way to prevent progressive collapse. It is noted that for actual flat plate structures some restraint is usually provided by adjacent slab panels or edge beams.

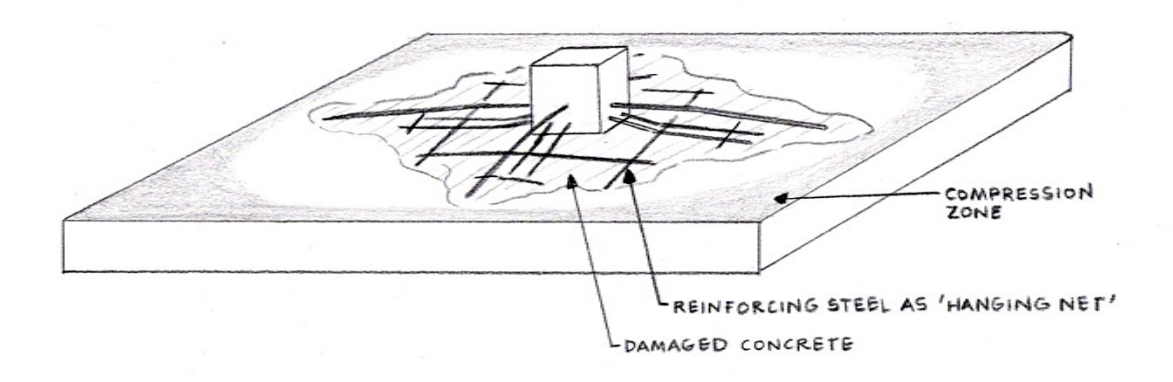


Figure 4.3 Reinforced concrete slab with unrestrained edges develops tensile membrane action

#### 4.2.5 Contribution of top reinforcing steel

A number of researchers have suggested that top reinforcement contributes to the tensile membrane action or the post-punching failure behaviour of reinforced concrete slabs. Park (1964) reported that, in slabs with full flexural and axial load restraint at the edges, top steel at the edges strengthened the slab, and, thus, contributed to tensile membrane action. Cook (1982) developed a computer program to predict the tensile membrane action of reinforced concrete panels, assuming that discontinuous top reinforcement at panel edges negligibly affected the development of tensile membrane action. He found that the program corresponded best with the test results in which only bottom reinforcement was present, thereby indicating that top reinforcement contributed

to tensile membrane action. Mitchell and Cook (1984) stated that top reinforcement tears out of the slab surface during punching and is thus ineffective during post-punching failure response. Therefore, they presented a design equation that relies on bottom reinforcement only. However, Mitchell and Cook acknowledged that, away from the column face where top bars had not torn out, top bars participated by transferring tension to overlapping bottom reinforcement. Pan and Moehle (1992) found that reinforced concrete slabs subjected to gravity loads after failing in punching shear due to lateral loading had greater post-punching resistance than predicted by Mitchell and Cook's equation (Eq. 1.3), and they attributed the additional resistance to the top reinforcement passing through the column, acting in tension.

Observations from the testing of specimens S1 and S2 suggest that top reinforcing bars contributed to the post-punching resisting mechanism. The inner layer of top reinforcement developed angles similar to the structural integrity reinforcement (Table 4.3) and developed strains greater than yield strain suggesting that these bars transferred significant shear to the column (Figs. 3.8, 3.9, 3.24, 3.25). The upper-most layer of top reinforcement developed significantly smaller angles than the structural integrity reinforcement on the same sides of the column, but still developed very high strains during the post-punching response. Top bars passing through the column in both directions tore out completely, or nearly so; however, at the time of peak post-punching shear, top bars remained sufficiently embedded in concrete to carry shear and, thus, contribute to the post-punching resistance.

Also, top reinforcement in the slab exterior to the column indirectly contributed to the post-punching failure resistance of the slab by transferring load to perpendicular underlying reinforcement passing through the column – either structural integrity or top bars – and thus indirectly transferred load to the column. The transfer of load from top reinforcement to perpendicular underlying reinforcement is evident in Figure 4.7 (a) and (b), as the photos show the distinct change in angle in the structural integrity reinforcement or top bar at the location of overlap. Table 4.3 provides the angles measured from specimen S2 at its peak post-punching resistance, where two angle measurements are provided for those bars receiving load from perpendicular top bars.

The change in angle in the structural integrity reinforcing steel varies from 2 to 6 degrees due to the interaction with the perpendicular top reinforcement. While angle measurements were not taken at the peak post-punching shear of specimen S1, test photos show that a similar effect occurred in specimen S1 as in S2.

Table 4.3 Angle below the horizontal of reinforcing steel of specimen S2 at peak post-punching shear

		Angle at Peak Post- Punching Shear
		(degrees)
	NW	18
	NE	21
Structural	EN	19   17
Integrity	ES	22   16
Reinforcement	SE	18
	SW	20
	WS	27   24
	WN	26   24
	N	19
Top Reinforcement	Е	9
	S	19   18
	W	15

Because the top reinforcement in the slab exterior to the column contributes to post-punching failure resistance of the slab-column connection, the area of concrete resisting failure by a mode similar to breakout of embedments, as described by Melo and Regan (1998), is greater than just that area at the ends of the structural integrity bars. Figure 4.8 indicates the locations on specimen S2 where concrete is contributing to the post-punching failure resistance. During this mode of failure, the top reinforcing steel acts only against the 25 mm of top concrete cover, while structural integrity reinforcing steel has a much greater cover to the top surface of the slab, and hence, a much higher concrete breakout resistance.

Top reinforcement exterior to the column also contributed to post-punching resistance by reducing the tear-out of perpendicular underlying reinforcement. Consequently, the damage to concrete around the column was reduced. In Figure 4.4, it can be seen that tear-out of structural integrity reinforcing steel stopped at the location

where it is crossed by perpendicular reinforcement. In contrast, the top-most layer of top reinforcement tore out completely or nearly so (Fig. 4.5), as it was not restrained by a perpendicular layer of reinforcement.

The test results suggest that the description of reinforcing steel as a "hanging net" during tensile membrane action is suitable for this post-punching resisting mechanism. The behaviour of a net is more efficient than cables in tension, as the perpendicular system of a net carries load in two dimensions to the support, minimizes deflections of the system, and is intrinsically redundant. In the experimental program, minimized deflections of reinforcing steel reduced the damage to the concrete. Undamaged concrete is crucial to keeping bars fully anchored and, thus, functional.



Figure 4.4
Top reinforcement exterior to the column reduced the tear-out of perpendicular underlying reinforcement

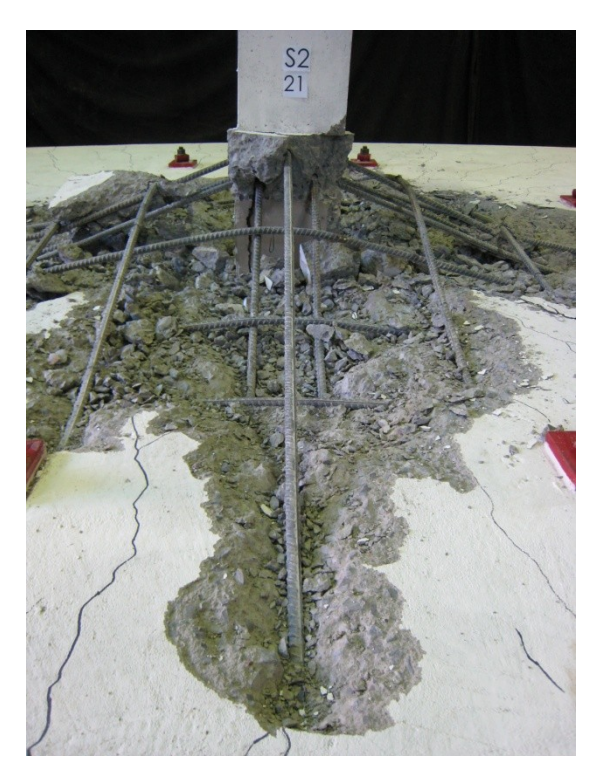


Figure 4.5
Top centre reinforcement, which was not restrained by perpendicular top reinforcement, tore out of the slab nearly completely



Figure 4.6 Contribution of top reinforcing steel.

- (a) Perpendicular top bars cause change in angle of structural integrity reinforcing steel;
- (b) Perpendicular top bars cause change in angle of top reinforcement.
- (Photos taken at end of test of specimen S1).

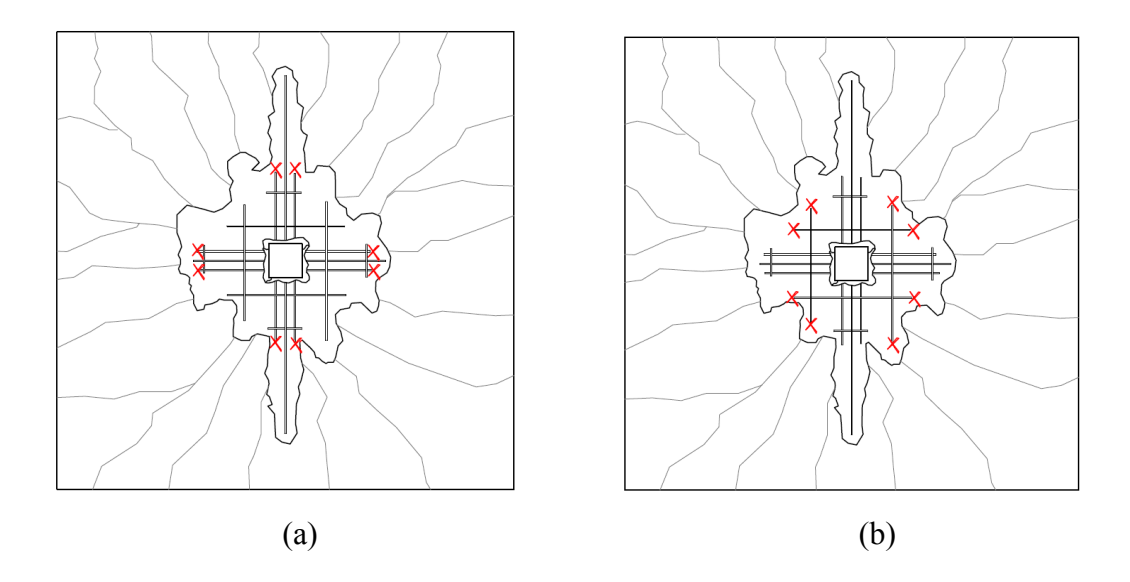


Figure 4.7 Locations where concrete resists breakout failure is at the ends of all bars transferring significant load into the column. Locations are marked with an X. Drawing represents slab at end of testing. (a) Ends of structural integrity reinforcing steel; (b) Ends of top reinforcing steel.

# 4.3 Comparison with Predictions of Design Standard CSA A23.3-04

A comparison is made between the experimental results of the slab-column specimen tests and the failure loads predicted by current design standard CSA A23.3-04 (2004). The analysis considers both the punching shear failure of the slabs and the post-punching failure response of the slab, i.e. the resistance provided by the structural integrity reinforcement.

#### 4.3.1 Punching shear failure

Table 4.4 provides the predicted punching shear resistance and the experimental results of testing specimens S1 and S2. The predicted resistance is the nominal punching shear strength given by CSA A23.3-04 in the equation:

$$V_n = 0.33 \sqrt{f_c'} b_o d$$
 (Eq. 4.1)

where  $f_c$ ' is the specified compressive strength of concrete,  $b_o$  is the width of the slab, and d is the effective depth of the slab. As shown in the table, the differing concrete compressive strengths  $f_c$ ' affects both the predicted and the experimental behaviour. The predictions were reasonable and conservative, as the tests achieved 104% and 110% of the predicted resistance to punching shear failure.

Table 4.4 Predicted and experimental values for punching shear failure

				<b>Punching Shear Resistance</b>				
Test Specimen	Concrete Strength	Effective Depth	Critical Perimeter	CSA A23.3-04 and ACI 318M-08	Experimental Result	$ m V_{exp}/V_{pred}$		
	f <sub>c</sub> ' (MPa)	d (mm)	b <sub>o</sub> (mm)	$V_{pred}(kN)$	$V_{exp}(kN)$			
S1	28.0	110	1440	277	287	1.04		
<b>S2</b>	29.8	110	1440	285	314	1.10		

### 4.2.2 Peak post-punching shear

Table 4.5 provides the predicted post-punching failure resistance and the experimental results of testing specimens S1 and S2. The predicted resistance,  $V_{se}$  is derived from the design equation presented by Mitchell and Cook (1984) and later modified for CSA A23.3-04 (2004) and included in Clause 13.10.6 Structural integrity reinforcement. The resistance predicted by CSA A23.3-04 is:

$$V_{se} = \frac{\sum A_{sb} f_y}{2}$$
 (Eq. 4.2)

where  $\sum A_{sb}$  is the summation of the area of bottom reinforcement on all sides of the column, and  $f_y$  is the specified yield strength of the reinforcement. The design equation implicitly assumes that (1) only structural integrity reinforcing steel contributes to the post-punching failure resistance; (2) structural integrity reinforcing steel is properly anchored to achieve "effective continuity" and thus allow the reinforcement to yield in tension; (3) structural integrity reinforcing steel deforms to an angle of 30 degrees below the horizontal; and (4) the resistance is not a function of the concrete strength, other than affecting the development length of the structural integrity reinforcing steel.

Table 4.5 Predicted and experimental values for peak post-punching shear

				Post-Pun	ching Failure Re	sistance
Test Specimen	Protruding Length of Structural Integrity Steel (mm)		f <sub>y</sub> (MPa)	CSA A23.3- 04 V <sub>pred</sub> (kN)	Experimental Result V <sub>exp</sub> (kN)	$ m V_{exp}$ / $ m V_{pred}$
S1	$2l_d$	780	400	320	314	0.98
31	$2\iota_d$	700	400	320	314	0.70
<b>S2</b>	$2l_d+2d$	1000	400	320	333	1.04

Specimen S1 achieved 98% of the post-punching failure resistance predicted by Eq. 4.2. The peak post-punching shear was 314 kN, and the predicted value was 320 kN (Table 4.5). Specimen S2 achieved the resistance predicted by Eq. 4.2. The peak post-punching shear was 333 kN, or 104% of the predicted resistance.

The angles of structural integrity reinforcing steel in specimen S2 at peak shear varied from 18 to 27 degrees, with an average of 21 degrees (Table 4.3). This observation suggests that the assumption of Eq. 4.2, where the angle of the structural integrity reinforcing steel is taken as 30 degrees, is un-conservative.

Also, two of the four top bars passing through the column deformed to an angle similar to that of the structural integrity reinforcing steel, and the measured strains in all four top bars passing through the column were greater than the yield strain. These observations suggest that top bars transferred load into the column and, consequently, that the assumption of Eq. 4.2, where top reinforcement is considered "ineffective" during the post-punching response, is conservative.

Table 4.6 presents the values of peak post-punching shear, punching failure shear, and design service load for comparison. It is noted that, in both tests S1 and S2, the peak post-punching shear was greater than the shear causing punching failure. Park (1964), Hawkins and Mitchell (1979), and Mitchell and Cook (1984) identified the ability of tensile membrane action to support a shear load greater than that causing initial failure of a slab, and proposed that tensile membrane action may be relied upon to prevent progressive collapse.

The peak post-punching shear was also greater than the design service load for the prototype structure of 215 kN, which is the shear transmitted to the slab-column connection due to specified loads, but not taken less than two times its self-weight. In

the design of the test specimens, the area of structural integrity reinforcing steel required to support the design service load was rounded up to provide a whole number of reinforcing bars, as well as providing a minimum of 2 bars in each direction. This common practice of rounding up in design is inherently conservative.

Table 4.6 Comparison of punching failure shear, peak post-punching shear, and design service load

				Experimen	tal Results				
Test Specimen	Protruding Length of Structural Integrity Steel		of Structural		of Structural Service		Peak Post- Punching Shear	V <sub>exp</sub> / V <sub>se</sub>	$egin{array}{c} V_{ m exp}  / \ V_{ m punch} \end{array}$
		(mm)	$V_{se}(kN)$	V <sub>punch</sub> (kN)	$V_{exp}(kN)$				
<b>S1</b>	$2l_d$	780	215	277	314	1.46	1.13		
<b>S2</b>	2 <i>l</i> <sub>d</sub> +2 <i>d</i>	1000	215	285	333	1.55	1.17		

Other reasons that the design of structural integrity reinforcing steel as specified by CSA A23.3-04 (2004) may be considered conservative include:

- 1. punching shear failure often occurs at a shear less than the predicted value, when deterioration or misplaced top steel, etc. has reduced the strength of the slab-column connection. In this experimental program, punching shear failure occurred at a shear greater than the predicted value;
- 2. punching shear failure of a slab-column connection creates a pin connection at the location of failure. Consequently, load is re-distributed away from the failed connection, and post-punching loads will be smaller than the load causing punching shear failure. In this experimental program, load was not re-distributed away from the failed connection after punching failure; and
- 3. the most severe load case often occurs during construction. Consequently, for the majority of the service life of a structure, the expected shear is less than the design load for structural integrity reinforcing steel.

## 4.4 Comparison with Predictions of Melo and Regan (1998)

The experimental results of the slab-column specimen tests are compared to the post-punching failure resistance predicted by Melo and Regan (1998) and to the experimental program reported by Melo and Regan. Table 4.7 provides the values of the test results and of the two modes of failure proposed by Melo and Regan. Both of these failure modes rely on structural integrity reinforcing steel that is fully anchored in tension.

### 4.4.1 Concrete failure

The first mode of failure is termed here "concrete failure" and is similar to the breakout failure of embedments. Based on ACI 349-76 *Code Requirements for Nuclear Safety Related Concrete Structures* (ACI 1978), Melo and Regan proposed the equation:

$$P_u = 0.33\sqrt{f_c'} \frac{\pi d^2}{2}$$
 (Eq. 4.3)

This equation suggests that the post-punching response of the slab depends on the concrete tensile strength which is estimated by  $0.33\sqrt{f_c}$ , and a cone-shaped failure surface of area depicted in Figure 4.8. The calculation of the area must be adjusted for closely spaced bars where the failure surfaces intersect.

Melo and Regan's prediction of concrete failure underestimates the post-punching resistance of specimens S1 and S2. Specimen S1 achieved 155% of the predicted resistance, and S2 achieved 160%. However, the calculation of the area of concrete resisting failure includes only the concrete at the ends of the structural integrity reinforcing steel. And, as discussed in Section 4.1 and as shown in Figure 4.7, top reinforcement contributes in transferring load to the column. The concrete at the ends of these top bars, with a depth equal to the top cover, could be included. Table 4.8 gives the additional post-punching failure resistance. When the contribution of top bars is included in the calculation, specimen S1 achieved 132% of the predicted resistance, and S2 achieved 136%. Consequently, the prediction which includes the contribution of the top bars is more accurate but still underestimates the post-punching resistance. Details of the calculations are provided in Appendix B.

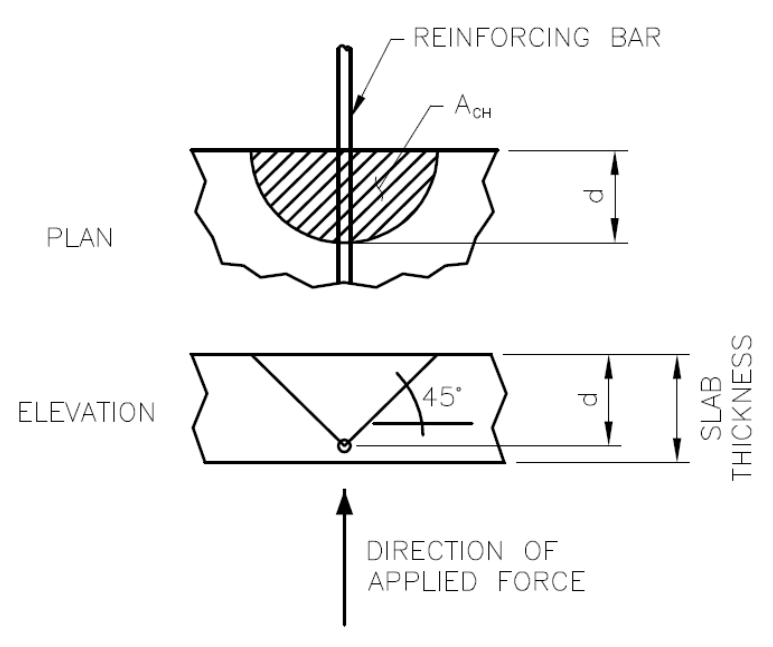


Figure 4.8 Area A<sub>CH</sub> determined from cone-shaped failure surface for breakout failure of embedments (Adapted from Melo and Regan 1998)

## 4.4.2 Reinforcement failure

The second mode of failure assumes that the reinforcement will fracture. The equation proposed by Melo and Regan is:

$$P = 0.44\Sigma A_s F_u \tag{Eq. 4.4}$$

where  $A_s$  is the total area of structural integrity reinforcing steel, and  $F_u$  is its ultimate tensile strength. The factor 0.44 is an experimental value that represents the angle below the horizontal developed by the structural integrity reinforcing steel.

As shown in Table 4.7, Melo and Regan predicted that, for the given specimen design, rupture of the reinforcement will not govern the post-punching resistance. The experimental results of specimens S1 and S2 indicate that there was no fracture of structural integrity reinforcing steel. The peak post-punching shear of the specimen was limited in specimen S1 by loss of bond. In S2, the peak post-punching shear was limited by the splitting of the column under the local stresses of the structural reinforcing steel. However, it has been shown that the structural integrity steel developed stresses much greater than the yield stress.

The value of the design service load is also provided in Table 4.8. If the area of structural integrity reinforcing steel provided in the design just satisfied that required to support the design service load, the structural integrity reinforcing steel would yield before the concrete failed substantially around the column. Consequently, a sufficient length of reinforcement would remain within intact concrete to allow the transfer of tensile stresses from steel to concrete and to allow the yielding of the steel.

Table 4.7 Comparison of experimental results with post-punching failure resistance predicted by Melo and Regan (1998).

	Protruding			Post-	Post-Punching Failure Resistance					
Test Specimen	Length of Structural Integrity Steel	f <sub>c</sub> ' (MPa)	F <sub>u</sub> (MPa)	Predicted Concrete Failure 0.33√f <sub>c</sub> ' A <sub>ch</sub> (kN)	Predicted Reinforcement Failure 0.44ΣΑ <sub>s</sub> F <sub>u</sub> (kN)	Experimental Result V <sub>exp</sub> (kN)	${ m V_{exp}}$ / ${ m V_{pred}}$			
S1	$2l_d$	28.0	594	202	418	314	1.55			
S2	2l <sub>d</sub> +2d	29.8	594	208	418	333	1.60			

Table 4.8 Comparison of experimental results with post-punching failure resistance predicted by Melo and Regan (1998) accounting for contribution of top reinforcement

			Post-Punching Failure Resistance						
Test Specimen	Protruding Length of Structural Integrity Steel			Top Reinf. V <sub>Top</sub> (kN)	Predicted Total V <sub>pred</sub> (kN)	Experimental Result $V_{\rm exp}$ (kN)	$rac{ m V_{exp}}{ m V_{pred}}$		
<b>S1</b>	$2l_d$	215	202	36	238	314	1.32		
S2	$2l_d+2d$	215	208	37	245	333	1.36		

#### 4.4.3 Discussion of experimental program reported by Melo and Regan (1998)

The experimental program reported by Melo and Regan (1998) was similar to the experimental program of this thesis in that the test specimen was a slab-column connection with surrounding slab. However, the specimen was supported both at the column and at the slab edges, which would have affected the load-deflection response of the specimen and the break-out behaviour of the structural integrity reinforcing steel.

Also, the dimensions and reinforcing details of the test specimens differed from those of the experimental program of this thesis. In particular, Melo and Regan provided structural integrity reinforcing steel of high yield strength (759 MPa) and of a protruding length less than  $2l_d$ .

Melo and Regan (1998) have used this test data to support their proposed equation (Eq. 4.3) identifying breakout of concrete as a failure mode. As shown in Table 4.9, the equation predicted the test specimens' post-punching resistance accurately. The four tests achieved between 94% and 103% of the predicted resistance. Table 4.9 also shows that the structural integrity reinforcing steel was specified in these tests so that the failure would definitely be governed by breakout of concrete and not by yielding or fracture of steel.

In contrast, Melo and Regan's equation (Eq. 4.3) greatly underestimated the post-punching failure resistance of specimens S1 and S2 (Table 4.7). These test specimens were unsupported at the edges of the slab, and therefore would be expected to experience larger deflections than Melo and Regan's test specimens. However, because Melo and Regan's test specimens with supported edges un-conservatively represent a slab's deflections, the prediction of breakout concrete failure is conservative. Real flat plate slab systems would undergo deflections somewhere between the cases of supported and unsupported edges.

Table 4.9 Post-punching failure resistance of test specimens reported by Melo and Regan (1998)

				Post-Punching Failure Resistance					
Test Specimen	f <sub>c</sub> ' (MPa)	f <sub>u</sub> (MPa)	$\Sigma A_{sb}$ (mm <sup>2</sup> )	Predicted Concrete Failure 0.33√f <sub>c</sub> ' A <sub>ch</sub> (kN)	Predicted Reinforcement Failure 0.44ΣA <sub>s</sub> F <sub>u</sub> (kN)	Experimental Result V <sub>exp</sub> (kN)	${ m V_{exp}}$ / ${ m V_{pred}}$		
Melo and R	egan (1998)	l							
2	27.3	759	226	68	> 75	64	0.94		
3	34.1	759	453	85	> 151	81	0.95		
4	30.6	529	402	65	> 134	66	1.02		
5	28.8	529	402	63	> 134	65	1.03		

# 4.5 Comparison with Experimental Results of Ghannoum (1998)

The experimental program by Ghannoum at McGill University (1998) used a test set-up very similar to the test set-up of the experimental program of this thesis. A single slab-column connection with surrounding slab 150 mm thick was supported only at the column and was loaded by hydraulic jacks at 8 locations around the column.

The significant variations of the tests performed by Ghannoum from the experimental work of this thesis include: (1) concrete strength was varied and included higher strengths; (2) top reinforcement was either uniformly spaced or banded near the column; (3) the structural integrity reinforcing steel was continuous, as it extended the full width of the slab; and (4) three 10M bars were used as structural integrity reinforcing steel at each face of the column for a total of 1200 mm<sup>2</sup>.

As seen in Table 4.10, all six test specimens supported a peak post-punching shear greater than the resistance predicted by CSA A23.3-04 (2004). The peak shear values varied from 102% to 142% of the predicted resistance. With the exception of specimen S1-B, the specimens with banded top reinforcement and with higher concrete strength achieved higher peak shears during the post-punching failure response. It is expected that banded top reinforcement and higher concrete strength would result in less disintegration of concrete around the column, a stiffer test specimen, and a greater contribution of top bars to the post-punching resistance.

Ghannoum's test specimens achieved higher peak post-punching shears than did specimens S1 and S2. For one, this improved performance may be attributed to the continuous structural integrity reinforcing steel which extended the full width of the specimen to a protruding length greater than  $2l_d + 2d$ . In contrast, the structural integrity reinforcing steel of specimen S1 suffered bond pullout failure; its protruding length of  $2l_d$  was too short for tensile stresses to transfer from steel to concrete. Also, the breakout type concrete failure described by Melo and Regan (1998) was not the governing failure mode in Ghannoum's tests (Table 4.11). This is due to higher concrete strength and to a smaller total area and smaller bar sizes of structural integrity reinforcing steel. The yielding of the reinforcing steel was the governing failure mode, and the concrete would have remained intact such that the yield stress could be developed.

Table 4.10 Comparison of post-punching failure resistance to test specimens reported by Ghannoum (1998)

		-		•				Post-Punching Failure Resistance			
Test Specimen	of Stru	ng Length uctural ty Steel (mm)	Slab Thickness (mm)	Column Dimension (mm x mm)	<i>f</i> <sub>c</sub> ' (MPa)	f <sub>y</sub> (MPa)	$\sum A_{sb}$ (mm <sup>2</sup> )	Design Service Load V <sub>se</sub> (kN)	Predicted by CSA A23.3-04 V <sub>pred</sub> (kN)	Experimental Result $V_{exp}(kN)$	${ m V_{exp}}$ / ${ m V_{pred}}$
Redl (2009)	)										
<b>S</b> 1	$2l_d$	780	150	250 x 250	28.0	400	1600	215	320	314	0.98
<b>S2</b>	$2l_d + 2d$	1000	150	250 x 250	29.8	400	1600	215	320	333	1.04
Ghannoum	(1998)										
S1-U	> 21 <sub>d</sub>	1025	150	225 x 225	37.2	400	1200	215	240	273	1.14
S1-B	> 21 <sub>d</sub>	1025	150	225 x 225	37.2	400	1200	215	240	245	1.02
S2-U	> 21 <sub>d</sub>	1025	150	225 x 225	57.2	400	1200	215	240	266	1.11
S2-B	> 21 <sub>d</sub>	1025	150	225 x 225	57.2	400	1200	215	240	298	1.24
S3-U	> 21 <sub>d</sub>	1025	150	225 x 225	67.1	400	1200	215	240	281	1.17
S3-B	> 21 <sub>d</sub>	1025	150	225 x 225	67.1	400	1200	215	240	340	1.42

Table 4.11
Post-punching failure resistance of test specimens by Ghannoum (1998), as predicted by Melo and Regan (1998)

	Protrudin	a I enath				Post-Pu	nching Failure Resi	stance
Test Specimen	Protruding Length of Structural Integrity Steel (mm)		f <sub>c</sub> ' (MPa)	f <sub>u</sub> (MPa)	$\Sigma A_{sb}$ (mm <sup>2</sup> )	Predicted Concrete Failure 0.33√f <sub>c</sub> ' A <sub>ch</sub> (kN)	Experimental Result V <sub>exp</sub> (kN)	$ m V_{exp}$ / $ m V_{pred}$
Ghannoum (	1998)							
S1-U	$> 2l_d$	1025	37.2	676	1200	283	273	0.96
S1-B	> 21 <sub>d</sub>	1025	37.2	676	1200	283	245	0.87
S2-U	> 21 <sub>d</sub>	1025	57.2	676	1200	352	266	0.76
S2-B	> 21 <sub>d</sub>	1025	57.2	676	1200	352	298	0.85
S3-U	> 21 <sub>d</sub>	1025	67.1	676	1200	380	281	0.74
S3-B	> 21 <sub>d</sub>	1025	67.1	676	1200	380	340	0.89

# **Chapter 5**

## **Conclusions**

The purpose of this thesis was to study and describe the post-punching resisting mechanism that develops in flat plate slab-column connections detailed with structural integrity reinforcing steel. Based on the experimental results of two test specimens, an analysis of the predicted resistance by CSA A23.3-04 (2004) and Melo and Regan (1998), and experimental results by Ghannoum (1998), the following conclusions were drawn:

- (1) CSA A23.3-04 accurately and conservatively predicts the punching failure resistance of flat plate slab-column connections. Specimens S1 and S2 achieved 104% and 110%, respectively, of the predicted nominal shear resistance;
- (2) The detailing of structural integrity reinforcing steel to a length such that it protrudes a distance of  $2l_d$  or greater from the column face allows for this steel to develop its yield during the post-punching response. Measured strains from the strain gauges showed that structural integrity reinforcing steel was yielding;
- (3) Increasing the protruding length of structural integrity reinforcing steel prevents pullout bond loss and results in greater ductility in the post-punching response. Specimen S1 achieved a peak post-punching shear of 314 kN at a deflection of 138 mm, and specimen S2 achieved a peak post-punching shear of 333 kN at a deflection of 228 mm. The increase in shear was 6% and the increase in deflection was 65%;
- (4) Top reinforcement contributes to the post-punching response. Top reinforcement passing through the column was carrying shear and developed strains greater than yield strain before tearing out of the top surface of the slab. Top reinforcement exterior to the column contributed to the post-punching response by reducing the tear out of underlying perpendicular bars and by transferring load to underlying perpendicular bars passing through the column. The interaction between the top bars and the underlying structural integrity reinforcing steel resulted in a localized

- change in angle of 2 to 6 degrees in the structural integrity reinforcing steel at the location of overlap.
- (5) CSA A23.3-04 accurately predicts post-punching resistance based on the assumptions that structural integrity reinforcing steel yields in tension and deforms to an angle of 30 degrees below the horizontal. Specimens S1 and S2 achieved 98% and 104%, respectively, of the predicted resistance. Additional conservatism was identified in the experimental program because the specimen edges were entirely unrestrained, no bottom reinforcement passed through the column, top reinforcement was uniformly spaced (rather than concentrated close to the column), the slab thickness was relatively small for the specified design loads, and 15M bars were used as structural integrity reinforcing steel. Also, the total area of structural integrity reinforcing steel was overdesigned by 48%, and there was, thus, an unnecessarily high expectation for post-punching resistance in the slab as compared to the design service load.
- (6) ACI 318M-08 does not specify a design equation to calculate the required area of structural integrity reinforcing steel, requiring only that 2 bars or wires pass through the column. Consequently, a flat plate reinforced concrete slab designed according to ACI 318M-08 cannot reasonably be expected to develop a post-punching resisting mechanism that is able to prevent progressive collapse after punching shear failure.
- (7) The equation for breakout failure of concrete proposed by Melo and Regan (1998) underestimates the strength of slab-column connections. Specimens S1 and S2 achieved 155% and 160%, respectively, of the predicted resistance for concrete breakout.
- (8) Higher concrete strength, banded reinforcement near the column, and continuous structural integrity reinforcing steel improves the post-punching resisting mechanism. The six test specimens by Ghannoum (1998) achieved between 102% and 142% of the predicted resistance, where higher concrete strength and banded reinforcement improved the post-punching resistance.

(9) The post-punching resisting mechanism developed by the slab-column connection is comparable to the tensile membrane action described by Park (1964), Hawkins and Mitchell (1979), and Mitchell and Cook (1984). Specimens S1 and S2 were completely unrestrained at the edges, but measurements of crack widths and concrete strains near the edges of the specimen showed that compression was developed at the edges of the specimen to equilibrate the tension in the structural integrity reinforcing steel.

#### References

ACI 1978. "Proposed Addition to: Code for Nuclear Safety Related Concrete Structures (ACI 349-76)," *American Concrete Institute Journal*, Title No. 75-35, Aug 1978, pp 329-335.

ACI 2008. Building Code Requirements for Structural Concrete and Commentary, American Concrete Institute, Farmington Hills, MI, USA, 436 pp.

Cook, W.D., 1982. "Tensile Membrane Action in Reinforced Concrete Slabs," thesis presented to McGill University at Montréal, Canada, in 1982, in partial fulfillment of the requirements for the degree of Master of Engineering.

CSA 1984. CSA A23.3-M84, *Design of Concrete Structures for Buildings*, Canadian Standards Association, Rexdale, Ontario, 281 pp.

CSA 2004. CSA A23.3-04, *Design of Concrete Structures*, Canadian Standards Association, Mississauga, Ontario, 232 pp.

Ghannoum, C.M., 1998. "Effect of High-Strength Concrete on the Performance of Slab-Column Specimens," thesis presented to McGill University at Montréal, Canada, in 1998, in partial fulfillment of the requirements for the degree of Master of Engineering.

Hawkins, N.M. and Mitchell, D., 1979. "Progressive Collapse of Flat Plate Structures," *American Concrete Institute Journal*, Technical Paper Title No. 76-34. Vol. 76, No. 7, July 1979, pp 775-807.

King, S, and Delatte, N.J., 2004. "Collapse of 2000 Commonwealth Avenue: Punching Shear Case Study," *Journal of Performance of Constructed Facilities*, ASCE, February 2004, pp 54-61.

Lew, H.S., Carino, N.J., and Fattal, S.G., 1982. "Cause of the Condominium Collapse in Cocoa Beach, Florida," *Concrete International: Design and Construction*, American Concrete Institute, Vol. 4, No. 8, August 1982, pp 64-73.

Leyendecker, E.V., and Fattal, S.G., 1973. "Investigation of the Skyline Plaza Collapse in Fairfax County, Virginia," Report BSS 94, Centre for Building Technology, Institute for Applied Technology, National Bureau of Standards, Washington, D.C., June 1973, 57 pp.

Melo, G.S.S.A, and Regan, P.E., 1998. "Post-punching resistance of connections between flat slabs and interior columns," *Magazine of Concrete Research*, Vol. 50, No. 4, December 1998, pp 319-327.

Mitchell, D. and Cook, W.D., 1984. "Preventing Progressive Collapse of Slab Structures," *Journal of Structural Engineering*, Vol. 110, No. 7, July 1984, pp 1513-1532.

Mitchell, D., 1993. "Controversial Issues in the Seismic Design of Reinforced Concrete Frames," *Recent Developments in Lateral Force Transfer in Buildings*, as part of the Thomas Paulay Symposium at La Jolla, California: September 20-22, 1993.

NBCC 2005. *National Building Code of Canada*, National Research Council of Canada - Institute for Research in Construction, Ottawa, 1167 pp.

Pan, A.D., and Moehle, J.P, 1992. "An Experimental Study of Slab-Column Connections," *American Concrete Institute Structural Journal*, Technical Paper Title No. 89-S59, Vol. 89, No. 6, Nov-Dec 1992, pp 626-638.

Park, R., 1964. "Tensile membrane behaviour of uniformly loaded rectangular reinforced concrete slabs with fully restrained edges," *Magazine of Concrete Research*, Vol. 16, No. 46, March 1964, pp 39-44.

# Appendix A

# **Design of Prototype Structure and Test Specimens**

## A.1 Introduction

The design of the prototype flat plate structure and the test specimens is detailed below. Chapter 2 describes the design philosophy of the prototype and provides detailed drawings of the test specimens.

# A.2 Details of Design

- based on CSA A23.3-04
- flat plate structure
- 4.75 m square panels
- 250 mm x 250 mm square columns
- $f_c' = 30$  MPa, specified concrete compressive strength
- $f_y = 400$  MPa, specified reinforcing steel yield strength

tension development length of reinforcement

- 25 mm cover, top and bottom

# A.3 Symbols

а	depth of equivalent rectangular stress block
$A_{g}$	gross area of section
$A_s$	area of longitudinal reinforcement on the flexural tension side of the member
$A_{sb}$	minimum area of bottom reinforcement crossing one face of the periphery of a column and connecting the slab to the column or support to provide structural integrity
$b_o$	perimeter of critical section for shear in slabs
$b_s$	width of support reaction
C	width of column
d	effective depth of slab; distance from extreme compression fibre to centroid of longitudinal tension reinforcement
$d_b$	diameter of bar
$\tilde{D}$	dead load, per unit area
$f_c$ '	specified compressive strength of concrete
$f_{y}$	specified yield strength of reinforcing steel
$h_s$	overall thickness of slab
-	

- $l_n$  clear span, in the direction being considered, measured face-to-face of supports  $l_{2a}$  average  $l_2$  for the adjacent spans transverse to  $l_1$ ; where  $l_2$  and  $l_1$  are lengths of the spans measured from centre-to-centre of supports, and  $l_1$  is the span in the direction that moments are being determined
- L live load, per unit area
- $M_f$  moment due to factored loads
- $M_o$  total factored static moment
- $M_r$  factored moment resistance
- $V_f$  factored punching shear force
- $V_n$  nominal punching shear resistance
- $V_r$  factored punching shear resistance
- $V_{se}$  shear transmitted to column due to specified loads, but not less than shear corresponding to twice the self-weight of the slab
- $w_D$  factored dead load per unit area
- $w_f$  factored load per unit area
- $w_L$  factored live load per unit area
- $\alpha_s$  factor that adjusts  $\nu_c$  for support dimensions
- $\alpha_1$  ratio of average stress in rectangular compression block to the specified concrete strength
- $\beta_c$  ratio of long side to short side of concentrated load or reaction area
- $\phi_c$  resistance factor for concrete
- $\phi_s$  resistance factor for non-prestressing reinforcing bars

# A.4 Loading

- based on NBCC 2005
- superimposed dead load: 1.2 kPa
- live load: 4 8 kPa
- load combination: 1.4D or 1.25D +1.5L

# A.5 Design for Shear

#### A.5.1 Slab thickness

§13.2

- $l_n = 4750 \text{ mm} 250 \text{ mm column} = 4500 \text{ mm}$
- $h_s \ge \frac{l_n(0.6 + f_y/1000)}{30} \ge \frac{4500(0.6 + 400/1000)}{30} \ge 150 \text{ mm}$
- $h_s = 150 \text{ mm}$

#### A.5.2 Critical shear section

\$13.3.3

- 
$$d = h_s - \text{cover} - d_b = 150 \text{ mm} - 25 \text{ mm cover} - 15 \text{M bar} = 110 \text{ mm}$$

-  $b_o = 4 (d + c) = 4 (110 + 250) = 1440$ mm, where c is the width of the column

#### A.5.3 Maximum shear stress resistance

\$13.4

- For a square interior column,  $\beta_c = 1$  and  $\alpha_s = 4$
- Therefore, for the stated dimensions, the limiting shear stress resistance is:

NOMINAL: 
$$V_n = 0.33\sqrt{f_c}'b_od = 0.33\sqrt{30}$$
MPa $(1440$ mm $)(110$ mm $) = 286$  kN Factored:  $V_r = 0.38\varphi_c\sqrt{f_c}'b_od = 0.33(0.65)\sqrt{30}$ MPa $(1440$ mm $)(110$ mm $) = 214$  kN

#### A.5.4 Factored shear stress

- Tributary area =  $(4750 \text{ mm})^2$   $(250 \text{ mm} + 110 \text{ mm})^2$  = 22.4 m<sup>2</sup>
- Self-weight =  $(150 \text{ mm thick slab})(23.5 \text{kN/m}^3) = 3.5 \text{kPa}$
- Factored loads:  $w_f = 1.25w_D + 1.5w_L = 1.25(3.5 + 1.2) + 1.5(4.8) = 13.1$ kPa
- Shear stress:  $V_f$  = tributary area  $\times w_f = (22.4 \text{ m}^2)(13.1 \text{kPa}) = 294 \text{ kN}$

Note:  $V_f > V_n$ 

This design of the column with dimensions of 250 mm x 250 mm leaves no doubt that failure will occur by punching shear.

# A.6 Design for Moment

A.6.1 Applied factored moments – using direct design method

§13.9.2.2

- $w_f = 13.1 \text{kPa}$
- $M_o = \frac{w_f l_{2a} l_n^2}{8} = \frac{(13.1 \text{ kPa})(4750 \text{mm})(4500 \text{mm})^2}{8} = 158 \text{ kN} \cdot \text{m}$
- Negative factored moment at face of support =  $0.65M_o = 102 \text{ kN} \cdot \text{m}$  §13.9.3.1
- Positive factored moment at midspan =  $0.35M_o = 56 \text{ kN} \cdot \text{m}$
- Reinforcement will be placed uniformly, so column and middle strips need not be considered

A.6.2 Negative moment reinforcing steel (top reinforcement)

\$13.9.2.2

- 
$$\alpha_1 = 0.85 - 0.0015 f_c^{'} = 0.805 \le 0.67$$

- d = 150mm thick slab - 25 mm cover -  $\frac{3}{2}$  15M bar = 102.5 mm (for inner layer)

$$- a = \frac{\varphi_s A_s f_y}{\alpha_1 \varphi_c f_c b_s}$$

- 
$$M_r = \varphi_s A_s f_y (d - \frac{a}{2})$$
  
=  $0.85 A_s (400 \text{MPa}) (102.5 \text{mm} - \frac{0.85 A_s (400 \text{MPa})}{2(0.805)(0.65)(30 \text{MPa})(4750 \text{mm})})$ 

- If  $A_s = 3600 \text{ mm}^2$ ,  $M_r = 115 \text{ kN} \cdot \text{m}$  and  $M_r > M_f$
- Minimum reinforcement requirement:  $0.002A_q = 0.002(150)(4750) = 1425 \text{ mm}^2$
- Spacing of reinforcement = 4750 mm/18 15 M bars = 264 mm spacing

#### Note:

To ensure that similar negative moment resistance is provided each way, top reinforcing steel will be spaced at 250 mm on the outer layer and at 300 mm on the inner layer

## A.6.3 Positive moment reinforcing steel (bottom reinforcement)

- d = 150mm thick slab 25 mm cover  $\frac{3}{2}$  10M bar = 110 mm (for inner layer)
- $M_r = 0.85A_s(400\text{MPa})(110\text{mm} \frac{0.85A_s(400\text{MPa})}{2(0.805)(0.65)(30\text{MPa})(4750\text{mm})})$
- If  $A_s = 1600 \text{ mm}^2$ ,  $M_r = 58 \text{ kN} \cdot \text{m}$  and  $M_r > M_f$
- Minimum reinforcement requirement:  $0.002A_g = 0.002(150)(4750) = 1425 \text{ mm}^2$
- Spacing of reinforcement= 4750 mm/16 10 M bars = 297 mm spacing
- Bottom reinforcing steel will be spaced at 300 mm each way

## A.6.4 Curtailment of reinforcement

\$13.10.8

- Because reinforcement will be placed uniformly, all cut-offs are considered to be in the "column strip"
- Top reinforcement: 50% extends  $0.3l_n = 1350$  mm away from column face 50% extends  $0.2l_n = 900$  mm away from column face
- Bottom reinforcement: 50% extends 75 mm over the column centreline 50% terminates  $0.125l_1 = 590$  mm from column centreline

# A.7 Structural Integrity Reinforcing Steel

§13.10.6

# $A.7.1 \sum A_{sb}$

- Specified loads:  $V_{se} = (3.5 + 1.2 + 4.8) \text{ kPa} \times (4.75 \text{ m})^2 = 215 \text{ kN}$
- $\sum A_{sb} = \frac{2V_{se}}{f_y} = \frac{2(215 \text{ kN})}{400 \text{ MPa}} = 1075 \text{ mm}^2$
- $\frac{\sum A_{sb}}{4 \text{ sides}} = 270 \text{ mm}^2/\text{side}$  therefore, use 2 15M bars each way
- Total structural integrity reinforcing steel provided is  $\sum A_{sb} = 1600 \text{ mm}^2$

## A.7.2 Effective continuity

- To achieve effective continuity of bottom reinforcement through the column, structural integrity reinforcement will be provided of length  $2l_d$  on each side of the column face
- $l_d = 390$  mm for a 15M bar with yield strength of 400 MPa in 30 MPa concrete
- $2l_d = 780 \text{ mm}$

# Appendix B

# Post-Punching Failure Resistance Governed by "Concrete Failure"

### **B.1 Details of Calculation**

The equation proposed by Melo and Regan (1998) is:

$$P_u = 0.33\sqrt{f_c'}A_{CH}$$

- $0.33\sqrt{f_c'}$  estimates the tensile strength of the concrete
- $A_{CH}$  is the horizontal projection of the conical failure surface, and is equal to

$$\frac{\pi d^2}{2}$$

where d is the depth of concrete above the reinforcing bar

- when bars are closely spaced (s < 2d), failure surfaces will intersect and:

$$A_{CH} = \frac{\pi d^2}{2} - A_1$$

$$A_1 = \frac{\varphi \pi}{360} d^2 - \frac{s}{4} d \sin \varphi$$

$$\varphi = \cos^{-1} \frac{s}{2d}$$

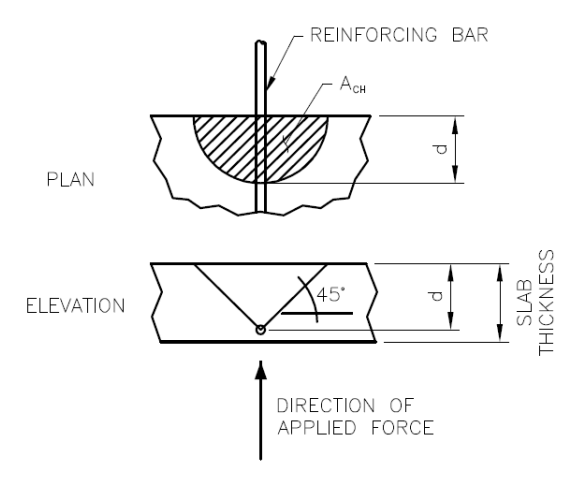


Figure D.1 Conical failure surface of a reinforcing bar, as proposed by Melo and Regan (1998).

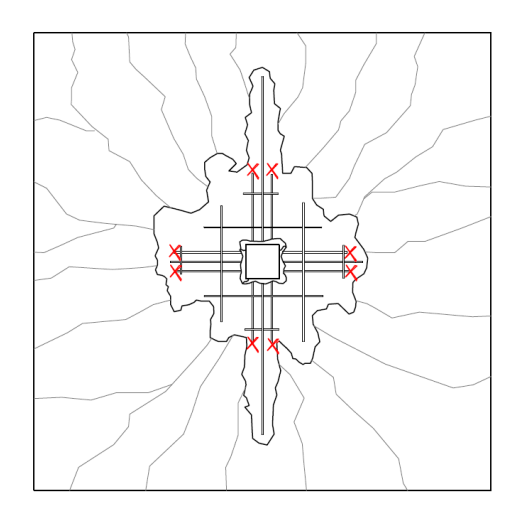


Figure D.2 Locations where concrete provides resistance against break-out – structural integrity steel

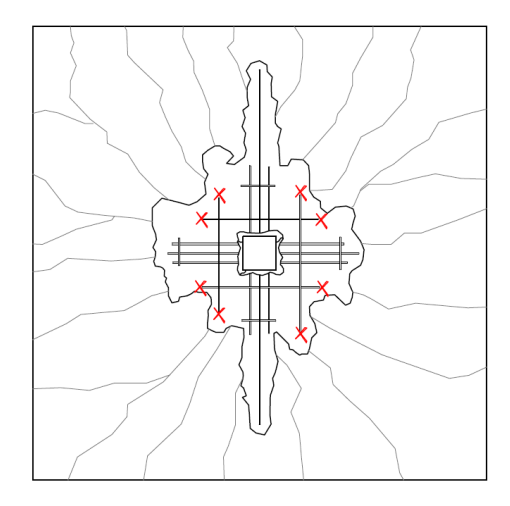


Figure D.3 Locations where concrete provides resistance against break-out – top reinforcing steel

# **B.2 Specimens S1 and S2**

(Redl 2009)

# B.2.1 Area of failure surface

## **Lower Structural Integrity Reinforcing Steel:**

d = 150 mm slab - 25 mm bottom cover - 10 M bar - 0.5 (15 M bar) = 107.5 mm

$$s = 250 \text{ mm column} - 2(20 \text{ mm side cover}) - 2(10 \text{M hoop}) - 2(15 \text{M vertical bar}) - 15 \text{M}$$
  
bar = 145 mm

Because 
$$s < 2d$$
:  $\varphi = 47.5$  °
$$A_1 = 1922 \text{ mm}^2$$

$$A_t = 16230 \text{ mm}^2 / \text{bar}$$

## **Upper Structural Integrity Reinforcing Steel:**

# of bars = 4

d = 150 mm slab - 25 mm bottom cover - 10 M bar - 1.5 (15 M bar) = 92.5 mm

$$s = 250 \text{ mm column} - 2(20 \text{ mm side cover}) - 2(10 \text{M hoop}) - 2(15 \text{M vertical bar}) - 15 \text{M}$$
  
bar = 145 mm

Because 
$$s < 2d$$
:  

$$\phi = 38.3^{\circ}$$

$$A_1 = 788 \text{ mm}^2$$

$$A_t = 12652 \text{ mm}^2 / \text{bar}$$

$$\# \text{ of bars} = 4$$

# **Lower Top Reinforcing Steel:**

$$d = 25 \text{ mm top cover} + 1.5 (15 \text{M bar}) = 47.5 \text{ mm}$$

s = 250 mm minimum

Because 
$$s > 2d$$
:  $A_t = 3544 \text{ mm}^2 / \text{bar}$   
# of bars = 4

# **Upper Top Reinforcing Steel:**

$$d = 25 \text{ mm top cover} + 0.5 (15 \text{M bar}) = 32.5 \text{ mm}$$

s = 250 mm minimum

Because 
$$s > 2d$$
:  $A_t = 1659 \text{ mm}^2 / \text{bar}$   
# of bars = 4

# B.2.2 Concrete resistance – structural integrity reinforcing steel only **Specimen S1:**

$$f_c' = 28.0 \text{ MPa}$$

$$f_{ct}$$
' =  $0.33\sqrt{f_c}$ ' = 1.746 MPa

$$P_u = (4 \text{ bars}) \text{ x} (16230 \text{ mm}^2 / \text{bar} + 12652 \text{ mm}^2 / \text{bar}) \text{ x} (1.746 \text{ MPa}) = 202 \text{ kN}$$

#### **Specimen S2:**

$$f_c' = 29.8 \text{ MPa}$$

$$f_{ct}$$
' = 0.33 $\sqrt{f_c}$ ' = 1.801 MPa

$$P_u = (4 \text{ bars}) \text{ x } (16230 \text{ mm}^2 / \text{bar} + 12652 \text{ mm}^2 / \text{bar}) \text{ x } (1.801 \text{ MPa}) = 208 \text{ kN}$$

# B.2.3 Concrete resistance – structural integrity and top reinforcing steel **Specimen S1:**

$$f_c' = 28.0 \text{ MPa}$$

$$f_{ct}$$
' = 0.33 $\sqrt{f_c}$ ' = 1.746 MPa

$$P_{u(additional)} = (4 \text{ bars}) \text{ x } (3544 \text{ mm}^2 / \text{bar} + 1659 \text{ mm}^2 / \text{bar}) \text{ x } (1.746 \text{ MPa}) = 36 \text{ kN}$$

$$P_{u(total)} = 202 \text{ kN} + 36 \text{ kN} = 238 \text{ kN}$$

#### **Specimen S2:**

$$f_c' = 29.8 \text{ MPa}$$

$$f_{ct}$$
' = 0.33 $\sqrt{f_c}$ ' = 1.801 MPa

$$P_{u(additional)} = (4 \text{ bars}) \times (3544 \text{ mm}^2 / \text{bar} + 1659 \text{ mm}^2 / \text{bar}) \times (1.801 \text{ MPa}) = 37 \text{ kN}$$

$$P_{u(total)} = 208 \text{ kN} + 37 \text{ kN} = 245 \text{ kN}$$

# B.3 Specimens S1-U, S1-B, S2-U, S2-B, S3-U, S3-B (Ghannoum 1998)

# B.3.1 Area of failure surface

### **Lower Structural Integrity Reinforcing Steel:**

d = 150 mm slab - 25 mm bottom cover - 10 M bar - 0.5 (10 M bar) = 110 mms = 87.5 mm (specified in drawings)

Because 
$$s < 2d$$
:  $\varphi = 66.6$  °
$$A_I = 4821 \text{ mm}^2$$

$$A_{t(outer\ bars)} = \frac{\pi d^2}{2} - A_1 = 14186 \text{ mm}^2/\text{ bar}$$

$$\# \ of\ bars = 4$$

$$A_{t(middle\ bar)} = \frac{\pi d^2}{2} - 2A_1 = 9365 \text{ mm}^2/\text{ bar}$$

$$\# \ of\ bars = 2$$

## **Upper Structural Integrity Reinforcing Steel:**

d = 150 mm slab - 25 mm bottom cover - 10 M bar - 1.5 (10 M bar) = 100 mms = 87.5 mm (specified in drawings)

Because 
$$s < 2d$$
:  $\varphi = 64.1^{\circ}$ 

$$A_{1} = 3623 \text{ mm}^{2}$$

$$A_{t(outer\ bars)} = \frac{\pi d^{2}}{2} - A_{1} = 12085 \text{ mm}^{2}/\text{ bar}$$

$$\# \ of \ bars = 4$$

$$A_{t(middle\ bar)} = \frac{\pi d^{2}}{2} - 2A_{1} = 8462 \text{ mm}^{2}/\text{ bar}$$

$$\# \ of \ bars = 2$$

# B.3.2 Concrete resistance – structural integrity reinforcing steel only Specimen S1-U and S1-B:

# $f_c' = 37.2 \text{ MPa}$

$$f_{ct}' = 0.33 \sqrt{f_c'} = 2.013 \text{ MPa}$$

$$P_u = [(4 \text{ bars}) \text{ x} (14186 \text{ mm}^2 / \text{bar} + 12085 \text{ mm}^2 / \text{bar}) + (2 \text{ bars}) \text{ x} (9365 \text{ mm}^2 / \text{bar} + 8462 \text{ mm}^2 / \text{bar})] \text{ x} (2.013 \text{ MPa}) = 283 \text{ kN}$$

### Specimen S2-U and S2-B:

$$f_c' = 57.2 \text{ MPa}$$

$$f_{ct}' = 0.33 \sqrt{f_{c}'} = 2.496 \text{ MPa}$$

$$P_u = [(4 \text{ bars}) \text{ x} (14186 \text{ mm}^2 / \text{bar} + 12085 \text{ mm}^2 / \text{bar}) + (2 \text{ bars}) \text{ x} (9365 \text{ mm}^2 / \text{bar} + 8462 \text{ mm}^2 / \text{bar})] \text{ x} (2.496 \text{ MPa}) = 352 \text{ kN}$$

## Specimen S3-U and S3-B:

$$f_c' = 67.1 \text{ MPa}$$

$$f_{ct}$$
' =  $0.33\sqrt{f_c}$ ' = 2.703 MPa

$$P_u = [(4 \text{ bars}) \text{ x} (14186 \text{ mm}^2 / \text{bar} + 12085 \text{ mm}^2 / \text{bar}) + (2 \text{ bars}) \text{ x} (9365 \text{ mm}^2 / \text{bar} + 8462 \text{ mm}^2 / \text{bar})] \text{ x} (2.703 \text{ MPa}) = 380 \text{ kN}$$